Master Thesis

Development of engineering tools to evaluate deliquification measures for gas wells

Written by:
David List, BSc
01235037

Advisors:
Dipl.-Ing. Dipl.-Ing. Dr.mont. Clemens Langbauer
Dipl.-Ing. Bernd Kometer

Leoben, 05.09.2018

EIDESSTATTLICHE ERKLÄRUNG

Ich erkläre an Eides statt, dass ich die vorliegende Diplomarbeit selbständig und ohne fremde Hilfe verfasst, andere als die angegebenen Quellen und Hilfsmittel nicht benutzt und die den benutzten Quellen wörtlich und inhaltlich entnommenen Stellen als solche erkenntlich gemacht habe.

AFFIDAVIT

I hereby declare that the content of this work is my own composition and has not been submitted previously for any higher degree. All extracts have been distinguished using quoted references and all information sources have been acknowledged.

Kurzfassung

Für gewöhnlich wird Erdgas von geringen Mengen Flüssigkeit begleitet, die entweder aus der Lagerstätte stammt oder durch Kondensation im Steigrohr verursacht wird. Diese werden bei Neubohrungen einfach durch das geförderte Gas aus dem Bohrloch gehoben. Wenn jedoch mit der Zeit die Förderrate natürlich abfällt, sinkt auch die in-situ Flussgeschwindigkeit. Dadurch werden anfallende Flüssigkeiten nicht mehr zu Tage gefördert, sondern sammeln sich im Bohrloch. Dies ist gemein hin als „liquid loading“ bekannt und verursacht eine Flüssigkeitssäule, die hydrostatischen Druck auf die Perforationen ausübt. Dadurch wird die Förderung der Gassonde stark geschwächt oder im Extremfall sogar gestoppt. Dementsprechend wird Förderung aus diesem Horizont unwirtschaftlich was in weiter Folge den erzielbaren Gewinnungsfaktor stark einschränkt.

Obwohl es zahlreiche technische Ansätze gibt um diesem Problem Abhilfe zu schaffen, sind nur einige davon operativ und wirtschaftlich tragbar, wenn man bedenkt, dass sich diese Sonden typischerweise dem Ende ihrer Lebensdauer nähern. Vor einigen Jahren, wurden innerhalb der OMV Austria Versuchsprojekte mit vier ausgewählten Methoden zum künstlichen Flüssigkeitsaustrag durchgeführt. Die Ergebnisse reichten von einwandfreier bis unzureichender Funktion für die verschiedenen Versuchssonden. Ziel dieser Arbeit ist es sowohl detailliertes, theoretisches Grundwissen als auch Verständnis der zu Grunde liegenden Mechanismen zu erarbeiten, um eine Reihe an Hilfsprogrammen zu entwickeln, mit denen die Versuchsprojekte untersucht und die verschiedenen Methoden evaluiert werden können.

Die Arbeit beginnt mit einer detaillierten Literaturrecherche, in der die wichtigsten „liquid-loading“ Kriterien, wie z. B. das Turner- oder das Coleman-Kriterium vorgestellt und deren Schwächen und Einschränkungen erklärt werden. Danach werden die vier ausgewählten Methoden, nämlich Velocity String, Obertage-Verdichtung, Schäumer und Plunger Lift vorgestellt und erläutert. Im praktischen Teil wird zuerst die Entwicklung der drei Hilfsprogramme gezeigt. Dabei dient das erste als einfacher Einheiten-Umrechner für einen Vorgabewert für PROSPER, einem Programm das häufig zur Steigrohr oder Velocity String Auslegung verwendet wird. In dieser Arbeit wird gezeigt, dass der Standardwert zu hoch angesetzt ist. Deshalb ist es ratsam Literaturwerte zu verwenden, was diese besonders fehleranfällige Einheitenumrechnung nötig macht. Ein weiteres Programm wurde speziell für Machbarkeitsstudien von Plunger Lift Einrichtungen entwickelt. Damit konnte die Grundursache des misslungenen Plunger Lifts nachvollziehbar identifiziert werden. Das dritte, weitaus aufwändigere Programm basiert auf Visual Basic for Excel und sollte die Effektivität der verschiedenen Methoden direkt vergleichen. Das ist insbesondere von Bedeutung da Gassonden mit Flüssigkeitsproblemen, gewöhnlich niedrige Förderraten aufweisen und eine Auswahl deshalb auf Basis von Wirtschaftlichkeit und nicht technischer Machbarkeit erfolgen sollte.

Schlussendlich werden alle Ergebnisse ausgewertet und Empfehlungen für die Anwendung der entwickelten Programme, PROSPER als auch die angeführten Literaturmodelle werden

erarbeitet. Diverse Auslegungsüberlegungen der Versuchsprojekte werden untersucht und Ideen sowie Vorschläge für zukünftige Projekte werden angeführt. Schlussendlich kamen die entwickelten Programme zu übereinstimmenden Ergebnissen mit z. B. PROSPER und bereits bekannten Messdaten. Gleichzeitig bieten diese Programme eine gesteigerte Transparenz, mehr Flexibilität und können zusätzlich mühelos erweitert werden.

Abstract

Most of the produced natural gas is accompanied by small amounts of free liquids which originate from either the reservoir or condensation in the production tubing. At the beginning of a gas well's lifecycle, these are lifted out of the well by the gas stream itself. However, when the productivity of a well declines, the in-situ gas velocity drops, the liquids are no longer transported by the gas stream and start to collect in the well. This phenomenon, which is called liquid loading, results in a liquid column exerting hydrostatic pressure on the perforations and thus drastically reducing the productivity of the well or killing it all together. Subsequently, it renders these horizons uneconomical and hence also deteriorates the achievable recovery factor.

Although there exist numerous technical approaches to remedy this problem, only a few of them are operational sustainable and economically viable, considering that the wells near the end of their lifecycle. A few years ago, four selected deliquification methods were piloted in OMV Austria with results reaching from successful to unsatisfactory for the different pilot wells. This thesis aims to establish not only the theoretical knowledge but also an understanding of the underlying principles or governing mechanisms, to develop a set of engineering tools to evaluate and troubleshoot these selected deliquification methods.

The thesis starts with a detailed literature review describing popular liquid loading criteria, like for example Turner's or Coleman's critical velocity criterion as well as their limitations and shortcomings. This is followed by elaborating on the four selected methods, velocity string, surface compression, foam lift, and plunger lift. In the practical part, three different computer-based engineering tools are created. The first one has the purpose of basic unit conversion of the critical liquid loading related input parameter, for PROSPER, a nodal analysis program which is widely used for tubing size and velocity string design. The default value is considered too conservative by experts, which is also indicated by data evaluated in this thesis. Therefore, it is advisable to use values provided by the literature which make this particularly error-prone unit conversion inevitable. Secondly, a separate tool was built, dedicated to evaluating the feasibility of plunger lift and subsequently analyzing the disappointing performance of the pilot. Using this tool, the root cause can be identified and hopefully avoided in the future. The third is a much larger, more sophisticated Excel-based Visual Basic program with the aim to compare said, selected deliquification measures by their performance. This is especially valuable because liquid loading is usually a problem of low producing wells and thus the selection of deliquification measures should be based on their economics rather than just feasibility.

Finally, all the results are interpreted, several recommendations for the application of these developed tools are made, PROSPER and implementation of the discussed models from the literature are stated. Different design choices from the pilots are investigated, discussed, and ideas, as well as advice for the future, is given. Ultimately the tools proofed valuable by yielding

results consistent with e. g. PROSPER as well as measurements while offering additional transparency, flexibility, and adaptability to a great extent.

List of Tables

List of Figures

Abbreviations

AL	Artificial lift
AOF	Absolute open flow potential
API	Application programming interface
API	American Petroleum Institute
BHP	Bottomhole pressure
BPV	Back pressure valve
CFM	Cubic feet per minute
CT	Coiled tubing
EOS	Equation of state
ESP	Electrical submersible pump
GLR	Gas-liquid ratio
ICPT	Institutului de Cercetare și Proiectare Tehnologică
ID	Inside diameter
IFT	Interfacial tension
IPR	Inflow performance relationship
LGR	Liquid gas ratio
MEG	Mono-Ethylenglycol
OGR	Oil gas ratio
PCP	Progressive cavity pump
PDA	Phase Doppler anemometry
PDF	Probability density function
PLT	Production logging tool
PVT	Pressure, volume, temperature
PVT	Pressure volume temperature
RF	Recovery factor
SPF	Shots per foot, shot density
SRP	Sucker rod pump
TPC	Tubing performance curve
TVD	True vertical depth
VBA	Visual Basic for Applications
VLP	Vertical lift performance
WGC	Water gas contact
WGR	Water gas ratio
WHC	Wellhead compressor
WHFP	Wellhead flowing pressure

Nomenclature

ΔH_g	gas holdup change between iterations	-
Δp_i	pressure loss in component i	bar
$\Delta p_{i(downstream)}$	pressure loss in the downstream component i	bar
$\Delta p_{i(upstream)}$	pressure loss in the upstream component i	bar
Δp_{sys}	total pressure loss in the system	bar
Δq_g	difference of formation flowrates between iterations	m³/s
A	pipe inside cross-sectional area	m²
a	constant from 0.5 to 0.6	-
A_{ann}	crossectional area of the casing-tubing annulus	m²
$A_{csg,ID}$	casing inside cross section area	m²
A_p	reference area	m²
A_{tbg}	inside crossectional area of the tubing	m²
$A_{tbg,ID}$	tubing inside cross section area	m²
$A_{tbg,OD}$	tubing outside cross section area	m²
API	oil API gravity	API
B_o	oil formation volume factor	m³/Sm³
B_w	water formation volume factor at a specified pressure and temperature	-
C	velocity profile factor	-
C	performance coefficient	Sm³/(s Pa² ⁿ)
C_d	drag coefficient	-
C_E	minimum effective concentration	%
C_f	future performance coefficient	Sm³/(s Pa² ⁿ)
C_{max}	maximum cycles per day	-
C_p	present performance coefficient	Sm³/(s Pa² ⁿ)
C_s	surface concentration	%
c_{sw}	water salt molality	mol/kg
D	depth of the plunger stop	m
D_1	outside diameter of the inner tube	m
D_2	inside diameter of the outer tube	m
D_H	hydraulic diameter	m
d_i	pipe inside diameter at the point of evaluation	m
$d_{i,t}$	critical pipe inside diameter at point of evaluation	m
d_l	liquid droplet diameter	m
d_m	maximum liquid drop diameter	m
D_{packer}	packer setting depth	m
D_{perf}	mid perforation depth	m
D_{tbg}	depth of the end of the tubing	m
dh	height differential	m

dp	pressure drop differential	Pa
f	Darcy friction factor	-
f_f	Darcy friction factor for foam	-
f_g	Darcy Weisbach friction factor for the gas	-
F_{gs}	Foss and Gaul slippage factor	-
f_l	Darcy Weisbach friction factor for the liquid	-
f_o	producing oil fraction	-
$F_{pl,f}$	plunger sidewall friction	N
$F_{pl,g}$	weight of the plunger	N
f_w	producing water fraction	-
Fr	Froude number	-
g	gravitational acceleration	m/s²
g	gravitational acceleration	m/s²
h	reservoir height	-
H_g	gas holdup	-
$H_{g,i}$	gas holdup of the previous iteration	-
$H_{g,i+1}$	gas holdup of the next iteration	-
H_l	liquid holdup	-
k	number of iteration step	-
K	constant	m
k_g	effective gas permeability	m²
L_l	chemical injection rate	m³/d
L_p	liquid production rate	m³/d
m	exponent	-
M_a	apparent molecular weight	g/mol
m_g	mass of gas dissolved in one m³ of oil	kg
m_o	mass oil in one m³ of oil	kg
m_w	mass of water in which the salt is dissolved in	kg
n	exponent	-
n	amount of substance	mol
N_D	nominal diameter	-
n_s	amount of salt dissolved in water	mol
N_V	velocity number	-
p	pressure	bar
P	wetted perimeter	m
$\overline{p}$	average pressure in the casing	Pa
$\overline{p}_f$	future average reservoir pressure	Pa
$\overline{p}_{max}$	average pressure in the wellbore at the end of the build	s
$\overline{p}_R$	average reservoir pressure	bar
p_1	initial pressure	Pa

p_2	final pressure	Pa
$p_{bd,min}$	minimum bottomhole pressure during blowdown	Pa
p_{bh}	(casing) pressure at bottom hole	Pa
p_c	capillary pressure	Pa
p_{csg}	casing pressure at the surface	Pa
$p_{csg,max}$	shut in casing/build pressure	Pa
$p_{csg,min}$	casing pressure at the surface when plunger arrives	Pa
p_d	dew point pressure	Pa
$p_{g,f,ann}$	friction pressure loss of the gas in the annulus	Pa
$p_{g,f,tbg,1}$	friction pressure loss of the gas under the plunger	Pa
$p_{g,f,tbg,2}$	friction pressure loss of the gas above the plunger	Pa
$p_{g,h,ann}$	hydrostatic pressure of the gas column in the annulus	Pa
$p_{g,h,tbg,1}$	hydrostatic pressure of the gas column in the tubing under the plunger	Pa
$p_{g,h,tbg,2}$	hydrostatic pressure of the gas column in the tubing above the plunger	Pa
$p_{l,f}$	friction pressure loss of the liquid slug	Pa
$p_{l,h}$	hydrostatic pressure of the slug	Pa
$p_{l,max}$	maximum flow line pressure	Pa
$p_{l,prod}$	pressure to account for produced liquids underneath the plunger	Pa
p_{node}	pressure at the node	bar
p_{pc}	pseudo critical pressure	Pa
p_{pr}	pseudo reduced pressure	-
p_{sc}	pressure at standard conditions (usually 101350 Pa)	Pa
p_{sep}	separator pressure	bar
p_{shutin}	average pressure in the wellbore at the start of the build	s
p_{tbg}	tubing pressure at the surface	Pa
p_{wf}	well flowing pressure	Pa
$p_{wf,0}$	bottomhole pressure at the start of the blowdown	Pa
$q_{ann,i+1}$	gas flowrate from the annulus	m³/s
q_g	volumetric gas flow rate	m³/s
$q_{g,f}$	future gas flow rate	Sm³/s
$q_{g,i}$	gas flowrate from the formation	m³/s
$q_{g,i+1}$	gas flowrate from the formation for the next iteration	m³/s
q_l	volumetric liquid flow rate	m³/s
q_o	volumetric oil flow rate	m³/s

q_{sc}	given/desired volumetric gas flow rate at standard conditions	Sm^3/d
$q_{t,g}$	volumetric gas flow rate	Sm^3/d
$q_{tbg,i}$	gas flowrate through the tubing	m^3/s
$q_{tbg,i+1}$	new gas flowrate through the tubing	m^3/s
$q_{tbg,i+1}$	gas flowrate through the tubing	m^3/s
q_w	volumetric water flow rate	m^3/s
R	superficial liquid to gas ratio	-
R	universal gas constant, 8.3144598	J/(mol K)
R_1, R_2	principle radii of the surface curvature	m
r_e	reservoir drainage radius	m
R_s	gas solubility	Sm^3/Sm^3
r_w	wellbore radius	m
Re	Reynolds number	-
Re_f	Reynolds number for foam	-
s	skin factor	-
s	liquid slug volume	m^3
S_o	specific gravity of the oil	-
S_p	surface of the particle, here droplet	m^3
S_s	surface of a sphere with the same volume as the particle	m^3
T	temperature	K
t	inverse of the reduced temperature	-
$\bar{T}$	average temperature in the wellbore	K
t_{build}	build up time	s
T_{pc}	pseudo critical temperature	K
T_{pr}	pseudo reduced temperature	-
T_{sc}	temperature at standard conditions (usually 288.71 K)	K
v	gas stream velocity	m/s
v	fluid velocity	m/s
V_1	initial volume	m^3
V_2	final volume	m^3
V_{ann}	volume in the annulus (below packer)	m^3
V_{end}	volume beneath the plunger when it has arrived at the surface	m^3
v_g	actual gas velocity	m/s
V_g	require gas volume per cycle	m^3
V_{ideal}	volume of an ideal gas at same conditions	m^3
v_l	actual liquid velocity	m/s
$V_{o,p,T}$	volume of oil at actual conditions	m^3
$V_{o,sc}$	volume of oil at standard conditions	Sm^3
V_p	particle volume	m^3

V_{real}	real gas volume	m³
v_s	slippage or slip velocity	m/s
v_{sg}	superficial gas velocity	m/s
v_{sl}	superficial liquid velocity	m/s
v_{sm}	(superficial) mixture velocity	m/s
v_{so}	superficial oil velocity	m/s
V_{start}	volume beneath the plunger before it starts	m³
v_{sw}	superficial water velocity	m/s
v_t	terminal velocity	m/s
V_t	tubing volume above the liquid slug	m³
$v_{t,condensate}$	critical velocity for condensate	m/s
$v_{t,water}$	critical velocity for water	m/s
V_{ta}	volume of open annulus and tubing	m³
w_s	water salinity as a mass fraction	-
Y	reduced density	-
z	compressibility factor at p and T	-
z_f	future compressibility factor	-
z_p	present compressibility factor	-
z_{sc}	compressibility factor at standard conditions (~1)	-
α	critical velocity factor	$ft^{0.25}\,lbm^{0.25}\,cm^{0.25}\,s\,dyne^{0.25}$
Γ	foam quality	-
γ_g	specific gas gravity (relative to air = 1)	-
ε	pseudo wall roughness	m
ε_g	pipe wall roughness to gas	m
λ_g	no-slip gas holdup	
λ_l	no-slip liquid holdup	
μ_f	foam viscosity	Pa s
μ_g	dynamic gas viscosity	Pa s
$\mu_{g,f}$	future gas viscosity	Pa s
$\mu_{g,p}$	present gas viscosity	Pa s
μ_l	liquid viscosity	Pa s
μ_n	mixture viscosity neglecting slip	Pa s
μ_o	oil viscosity	Pa s
μ_{od}	dead oil viscosity	Pa s
μ_s	mixture viscosity considering slip	Pa s
$\mu_{s.p.}$	dynamic gas viscosity at standard pressure	Pa s
μ_w	water viscosity	Pa s
ρ	fluid density	kg/m³
ρ_g	gas density	kg/m³

ρ_g	gas density	kg/m³
ρ_k	fluid density for Re and friction calculations	kg/m³
ρ_l	liquid density	kg/m³
ρ_n	fluid density neglecting slip	kg/m³
ρ_o	oil density	kg/m³
$\rho_{o,sc}$	density at standard conditions	kg/m³
ρ_p	particle density	kg/m³
ρ_s	fluid density considering slip	kg/m³
ρ_w	water density	kg/m³
$\rho_{w,sc}$	water density at standard conditions, 999.55	kg/m³
$\rho_{w,sp}$	water density at standard pressure and specified temperature	kg/m³
σ	liquid-gas interfacial tension	N/m
σ	surface tension, IFT	N/m
σ_l	liquid surface tension	N/m
σ_o	oil surface tension	N/m
σ_{od}	dead oil-gas interfacial tension	N/m
σ_w	water surface tension	N/m
σ_w	interfacial tension of brine and gas	N/m
σ_w^0	interfacial tension of sweet water and gas	N/m
Ψ	sphericity	-
$\overline{p_{csg}}$	average casing pressure	Pa
$\overline{T_g}$	absolute average gas Temperature	K
$\overline{v_{fg}}$	average plunger falling velocity trough gas	m/s
$\overline{v_{fl}}$	average plunger falling velocity trough liquid	m/s
$\overline{v_r}$	average plunger rise velocity	m/s
$\left(\frac{p_{l,h}+p_{l,f}}{s}\right)$	hydrostatic and friction pressure of the slug per volume	Pa/m³
Δq_{tbg}	change in gas flowrate through the tubing	m³/s
Δt_i	time step	s

Table of content

Page

1 Introduction

The majority of gas wells produce small quantities of liquids along with the natural gas. Over a well's lifetime the overall pressure regime as well as the gas flow rate decline. Depending on the design of the well's completion, at some point, these liquids are no longer lifted out of the wellbore by the gas stream and start collecting downhole. This phenomenon, called liquid loading, has severe, detrimental implications on the performance of the well and subsequently the recovery factor that can be economically reached for the perforated horizon.

Due to the fact that in addition to specialized deliquification methods also most conventional artificial lift systems can be adapted for deliquification use, a myriad of options is available. The majority of the respective publications focus on either one specific system in great detail or on the selection of a system based on feasibility. However, many gas wells with liquid loading problems only yield low production rates and thus choosing the most economic deliquification method is critical. In addition to that, some deliquification methods might not be feasible due to very specific operational issues or the setup of the downhole completion which is usually not captured in conventional selection criteria. OMV Austria has so far implemented four selected methods: wellhead compression, velocity string, foam lift, and plunger lift. Their performance reached from successful to unsatisfactory.

The goal of this thesis is to first establish a thorough understanding of all mechanisms as well as theoretical models related to liquid loading or one of the four selected deliquification methods that are widely accepted by industry professionals. Secondly, it should present some novel ideas and recent research results which challenge said accepted models or address their shortcomings. Thirdly based on this theoretical knowledge a set of computer-based engineering tools are developed which can be facilitated to troubleshoot, compare and ultimately select deliquification measures. Finally, the failed, as well as the successful implementations of deliquification methods in OMV Austria, should be investigated to find the root failure cause and evaluate their performance. Based on these results, conclusions should be drawn in order to provide recommendations for future implementations of deliquification measures.

2 What is liquid loading?

Liquid loading refers to a situation where the gas phase in the wellbore does not deliver enough energy to continuously produce the liquid phase to surface. Thus, the liquids are not or only partially produced and accumulate in the wellbore. The backpressure of this liquid column on the perforations will reduce the gas well's production performance and eventually kill the well. [1, p. 369]

2.1 Multiphase flow regimes

When a liquid phase is produced along with the gaseous phase, the flow characteristics become rather complex. Depending on the relative volumes of gas and liquid and their respective velocities we can distinguish between four characteristic flow regimes as depicted in Figure 1. At any point in the lifetime of a gas well, it produces under one or more of these flow regimes. [2, p. 2]

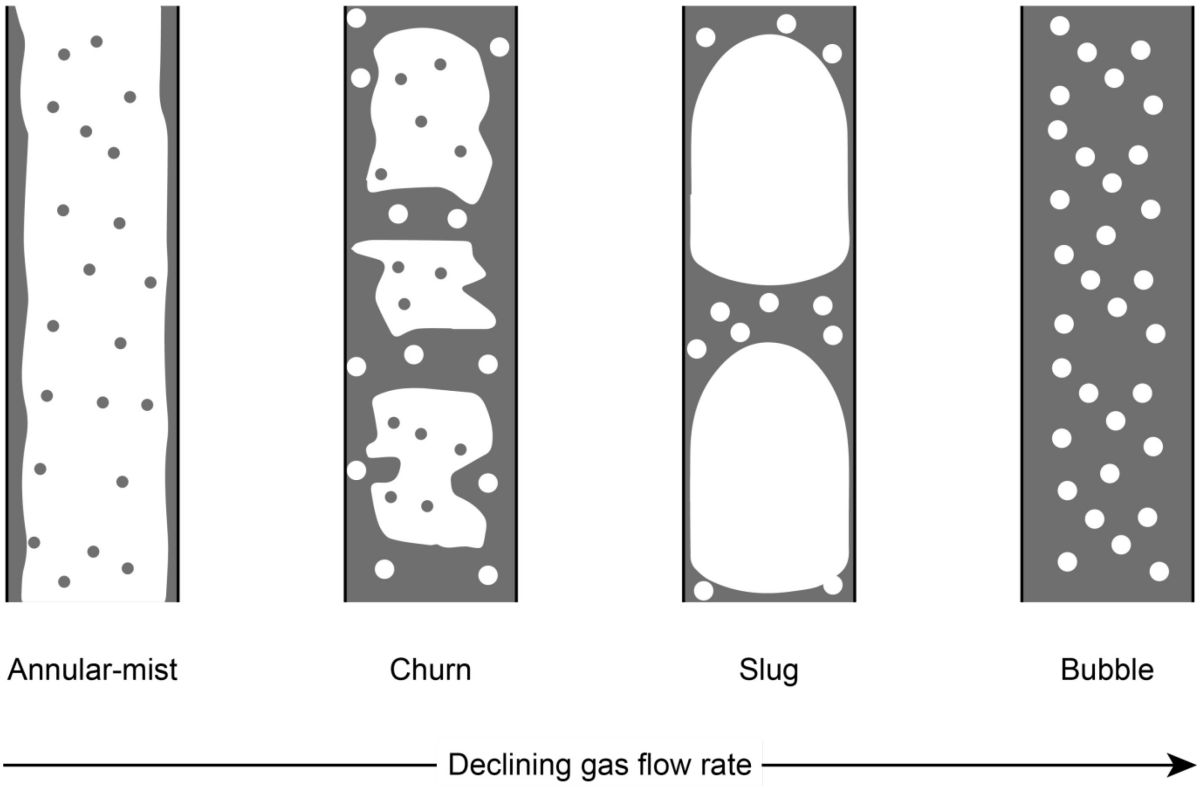

Figure 1: Vertical multiphase flow regimes with declining gas flow rate [2, p. 2]

Annular-mist flow develops when the volumetric gas flow rate is high compared to the liquid flow rate. The gaseous phase is continuous and the bulk of the liquid is entrained in the gas stream as mist. A small part of the liquid also forms a continuous phase which coats the pipe walls. However, the pressure losses are primarily governed by the gas flow. [2, p. 3]

Churn flow occurs when there is only one continuous phase formed by the liquid phase. In this case, compared to the previous, the liquid flow rate is higher and the gas flow rate lower. Smaller quantities of liquid form droplets in the gaseous phase, while gas bubbles are

dispersed throughout the continuous liquid phase. Pressure losses are now influenced considerably by the liquids. Nevertheless, they are still largely controlled by the gas flow. [2, p. 3]

Slug flow establishes when larger gas bubbles expand under the reducing pressure during the rise in the wellbore and eventually merge with their neighbors. These expanding and coalescing gas bubbles, called slugs are enclosed by a liquid film, which can fall back down the hole. The liquid phase is continuous while the gas phase is not. The pressure drop along the pipe is strongly affected by both, the gaseous as well as the liquid phase. [2, p. 3]

Bubble flow appears when most of the pipe's volume is occupied by liquids, which therefore form the continuous phase. Gas rises through the liquid in form of small bubbles. The pressure gradient is now mainly defined by the liquid and the gas only reduces the average density of the liquid column. [2, p. 2]

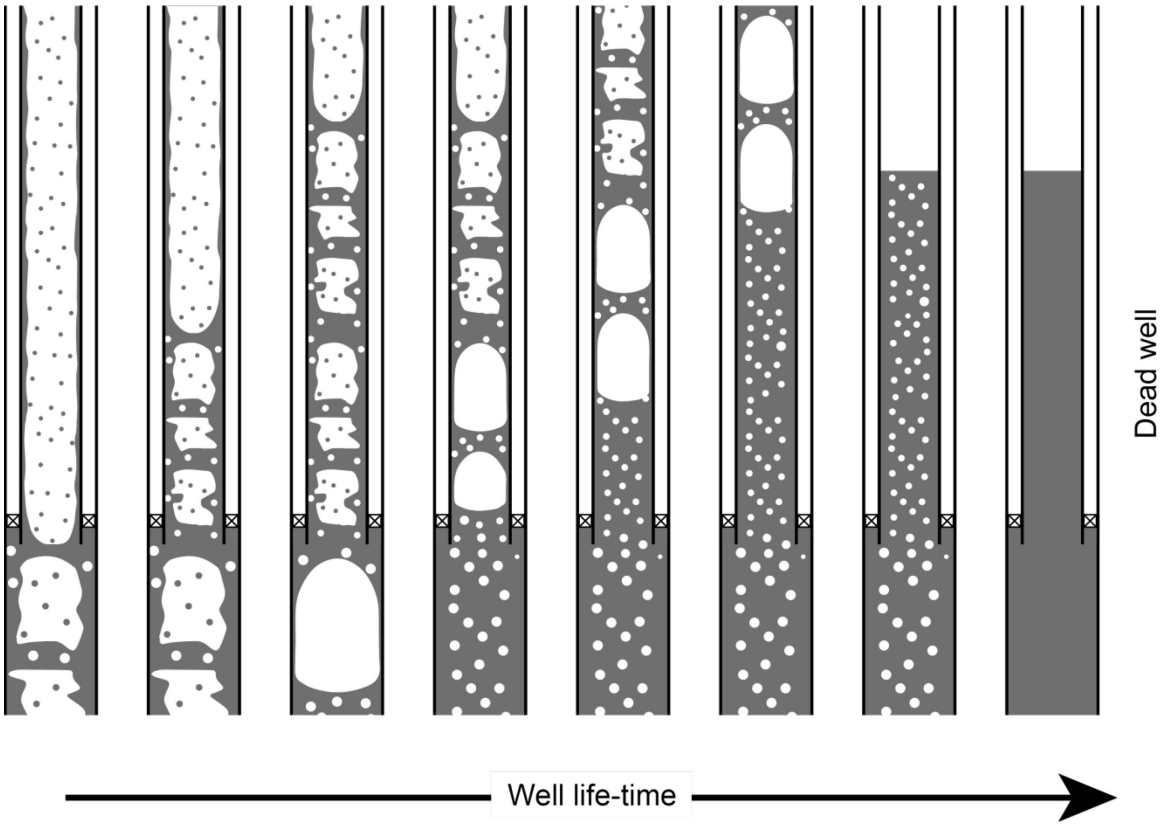

Figure 2: Flow regimes during the lifetime of a gas well [2, p. 3]

Figure 2 shows the advancement of liquid loading from the start of production until the well is finally killed by the accumulated liquid. It has to be noted that in the illustrated example the production tubing ends some distance above the perforations. After perforating (Figure 2 – left) the gas flow rate is so high compared to the liquid rate that a mist flow regime develops. However, due to the larger inside diameter of the casing compared to the tubing and thus lower gas velocity, slug, transition or bubble flow can develop below the end of the tubing. As time moves on the gas production typically declines and the flow regimes change accordingly. In addition to the reduced gas flow rate, the amount of produced liquids may grow. The production

at the surface can stay stable and in mist flow although transition and slug flow regimes are developing. At some point, the transitional regime will reach the surface followed by slug flow. Usually, this transition is also noticeable by a distinct increase in the gas production decline rate. At this time the overall production behavior of the well is often described as irregular and erratic. The gas production rate will decline further until it is too low to carry liquids to surface. Gas bubbles through the stationary liquid column at a fairly stable and constant, but low rate. The well might produce for a long time under this loaded by liquid conditions until it finally dies. [2, pp. 3, 4]

2.2 Type and sources of liquids in a gas well

Generally, two types of liquid may be encountered in a gas well: liquid hydrocarbons, water or both. They either enter the wellbore through the perforations or form in the wellbore somewhere on the way to surface. Some phenomena that induce liquids to appear in a gas wellbore are described in the following. [2, p. 8]

2.2.1 Condensation of hydrocarbons

Generally natural gas is a mixture of large amounts of very light hydrocarbons, primarily methane, small fractions of higher alkanes and impurities. As long as the reservoir temperature stays above the cricondentherm, or at least above the dewpoint at pressures found in the reservoir, no hydrocarbon liquids will enter the wellbore from the reservoir. However, due to the loss in temperature and pressure during the way to the surface, hydrocarbons may condense, or drop out in the wellbore. [2, p. 9]

2.2.2 Condensation of water

A liquid substance, for instance, water, that is in contact with a gas is constantly evaporating and at the same time condensing. At equilibrium, the rate of evaporation equals the rate of condensation. This equilibrium is reached when a certain amount of the substance, which is defined by the vapor pressure, is in the gaseous phase and thus dissolved in the gas. The vapor pressure and thus the amount that is dissolved in the gas are highly dependent on pressure and temperature. In a similar way, natural gas usually contains some amount of gaseous water, which might condense when pressure or temperature change. This can either happen already in the reservoir or later somewhere in the wellbore. The general trends of water solubility in natural gas are illustrated in Figure 3 for two temperatures. [2, p. 9]

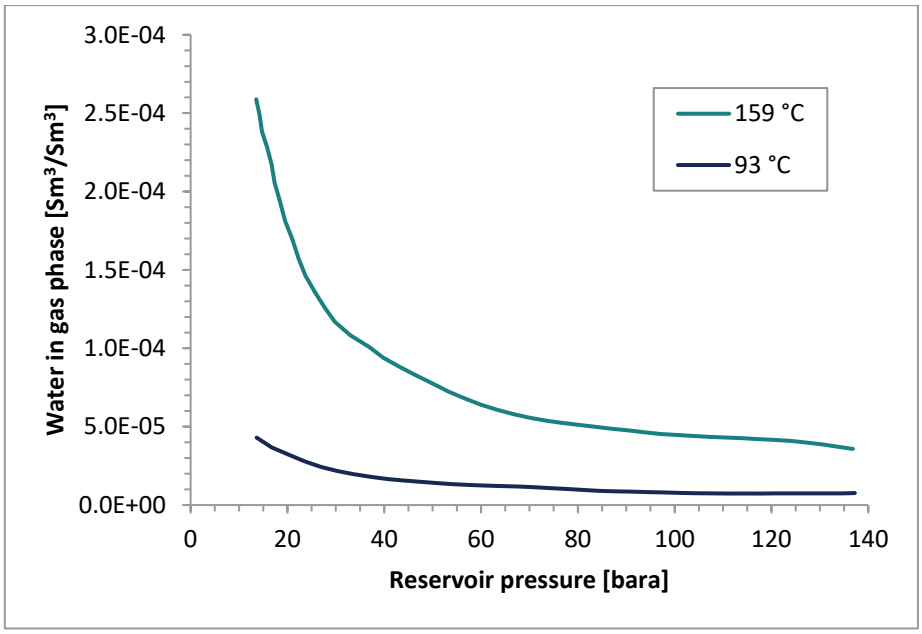

Figure 3: Water solubility in natural gas [2, p. 10]

2.2.3 Water from another zone

When the well has an open hole completion and the well penetrates through water-bearing layers, naturally, water is produced alongside the gas. However, also in a cased hole scenario, water might be produced from other layers because these intervals were perforated unintentionally. Other possible sources for water are very small water-bearing layers in the gas reservoir interval. These are hard to isolate because they are too thin and there are usually many of them. [2, p. 8]

2.2.4 Water from aquifer

Some gas reservoirs rely on the pressure support from an adjacent aquifer. As the reservoir is depleted, the interface between reservoir and aquifer, known as water gas contact (WGC) begins to move. When the water gas contact reaches the perforated section, significant amounts of water will enter the wellbore. [2, p. 8]

2.2.5 Water coning

When gas is produced at a high rate the pressure drop near the wellbore can become large due to radial flow effects. So even though the water gas contact is not in the perforated interval, water from nearby zones might be drawn into the reservoir layer and subsequently through the perforations into the wellbore. [2, p. 8]

2.3 Consequences of liquid loading

Liquid loading is a problem that can affect almost all gas wells. Even wells producing very dry gases, gases with a low gas-liquid ratio (GLR), can accumulate liquids and load up when the gas velocity in the tubing is not high enough. The low gas velocity is either caused by a too

large tubing or an inherently low volumetric gas flow rate due to a low permeability reservoir or high skin.

The hydrostatic pressure of the accumulating liquid column can increase the bottom hole pressure (BHP) significantly. This increased backpressure reduces the gas production rate according to the inflow performance relationship (IPR). On the one hand, when the reservoir pressure is high enough, slugging will occur which can cause many difficulties due to its erratic nature. On the other hand, a low pressure well might be entirely killed by the accumulating liquids.

When the liquid level has risen far above the perforations, the backpressure is so high that the gas only bubbles through the liquid column. At this point, no slugging occurs and no liquid is produced to surface. Then the gas production rates are very low but fairly constant and stable such that one could mistake this well for a not loaded but just very bad gas producer. [2, pp. 5, 6]

2.4 Modeling liquid loading

The main goal of modeling liquid loading is to determine the minimum gas flowing velocity that is necessary to lift all liquids out of a specific wellbore. Conversely one could, for a given gas well, predict whether it will load up or not.

2.4.1 Turner model

In order to keep wells unloaded Vitter [3] and Duggan [4] suggested to look at the velocities at the wellhead. Meanwhile, Dukler [5] and Jones [6] proposed analytically derived equations to determine, a critical flow rate for lifting the liquids. These developments suggest two primary mechanisms responsible for lifting the liquids in a gas well. The first one is called continuous film model and the other one entrained drop model. During the development of the Turner model, these two effects were dealt with separately granting that in reality liquid is exchanged between the film and the mist in the gaseous core continuously. [7, p. 1]

2.4.1.1 The continuous film model

Liquid drops transported by the gas stream constantly collide with the pipe wall. Furthermore, often, especially in the case of gas production wells, the borehole wall is cooler than the transported gas. Thus the dissolved liquids condense on the tubing or casing. Therefore, the accumulation of a continuous liquid phase at the borehole wall in the form of a film is very likely. So with regards to liquid removal from the wellbore, the movement of the liquid film has to be considered. With the description of the velocity profile inside the liquid film a critical or minimum flow rate could be derived, that ensures that the liquid film is moving upwards. However, a comparison of the behavior predicted by this model and test data didn’t show a good correlation between suitable and too low flow rates. The model also suggests a dependence on the gas-liquid ratio which is not seen from the field data at liquid rates associated with usual gas wells. So for example in several field tests, the wells were unloading although according to the continuous film model the gas velocity would be too low. This

suggests that the entrained drop movement alone is sufficient and mainly responsible for continuous liquid removal from the wellbore. [7, pp. 1475,1479]

2.4.1.2 Entrained drop model

Assuming this liquid removal mechanism the main goal is to calculate a minimum gas flow rate which is capable of lifting the liquid droplets out of the wellbore. The first simplification that has to be made is to consider the liquid drops as particles. These particles have a relative velocity to the surrounding gas and are exposed to a gravitational field.

Since only the relative velocity is of importance one could think of it as a freely falling particle through a stagnant gas. Mathematically this implies a simple transformation of coordinates. Freely falling particles reach a terminal velocity at which the buoyancy- and drag forces balance the gravitational force. Since the resulting force is zero a free falling particle at terminal velocity doesn't accelerate any further. A gas velocity that is high enough to keep a particle (the liquid drop) floating is the analog to the terminal velocity in the other coordinate space. If the gas velocity is slightly higher the drops will move upwards, against the direction of gravity instead of just floating stationary. The terminal velocity of a particle falling freely in a fluid is determined by **eq. 1**. The reference Area (A_p) is usually the projected cross-sectional area in direction of movement, or against the fluid flow. [7, p. 1476]

$$v_t = \sqrt{\frac{2gV_p(\rho_p - \rho_g)}{\rho_g A_p C_d}} \qquad (1)$$

v_t terminal velocity [m/s]
g gravitational acceleration [m/s^2]
V_p particle volume [m^3]
ρ_p particle density [kg/m^3]
ρ_g gas density [kg/m^3]
A_p reference area [m^2]
C_d drag coefficient [-]

It is customary to express **eq. 1** in terms of a particle or liquid droplet diameter in order to combine volume (V_p) and reference area (A_p), which results in **eq 2**. According to Turner, this is reasonably applicable here because the surface tension of the liquid draws the drop into a spheroidal shape. For consistency the particle density (ρ_p) is renamed liquid density (ρ_l). [7, p. 1476]

$$v_t = \sqrt{\frac{4gd_l(\rho_l - \rho_g)}{3\rho_g C_d}} \qquad (2)$$

ρ_l liquid density [kg/m^3]
d_l liquid droplet diameter [m]

It seems natural that for larger liquid drops a higher gas velocity is needed. This is confirmed by **eq. 2** the terminal velocity grows with the square root of the droplet diameter. Thus to make sure all liquid droplets are removed from the borehole, the diameter of the largest droplets that may form, must be determined. Hinze [8] showed that the maximum size a droplet in a gas stream can reach before it shatters into several smaller drops depends on two counteracting pressures. One is caused by the velocity of the gas and the other one by the surface tension of the liquid. The effect of both of these pressures can be captured with the Weber number, **eq. 3**. [7, p. 1476]

$$N_{We} = \frac{v^2 \rho_g d_l}{\sigma} \qquad (3)$$

N_{We} Weber number [-]
v gas stream velocity [m/s]
σ liquid-gas interfacial tension [N/m]

Testing indicates a Weber number of 20 to 30 for free-falling drops. Inserting the larger one into **eq. 3** and rearranging results in **eq. 4** for the maximum droplet diameter. [7, p. 1476]

$$d_m = \frac{30\sigma}{\rho_g v^2} \qquad (4)$$

d_m maximum liquid drop diameter [m]

Setting the gas velocity (v) of **eq. 4** to the terminal velocity (v_t) of **eq 2** and inserting **eq. 4** for the diameter (d_l) into **eq. 2** results in **eq. 5**. [7, p. 1476]

$$v_t = \sqrt[4]{\frac{40 g \sigma (\rho_l - \rho_g)}{{\rho_g}^2 C_d}} \qquad (5)$$

The value for the interfacial tension can be retrieved from tables or handbooks with adequate precision. Turner suggested that a constant drag coefficient (C_d) of 0.44 is applicable for the whole range of his test data. Inserting this and the gravitational acceleration results in **eq. 6**. [7, p. 1476]

$$v_t = 5.46 \sqrt[4]{\frac{\sigma (\rho_l - \rho_g)}{{\rho_g}^2}} \qquad (6)$$

Comparison with field data performed by Turner, which is plotted in Figure 4, shows a clear separation between loaded and unloaded. To make the drop removal model fit the test data Turner suggested to increase the critical velocity, predicted by the model, by 20% which results in **eq. 7**. [7, p. 1479]

$$v_t = 6.56 \sqrt[4]{\frac{\sigma (\rho_l - \rho_g)}{{\rho_g}^2}} \qquad (7)$$

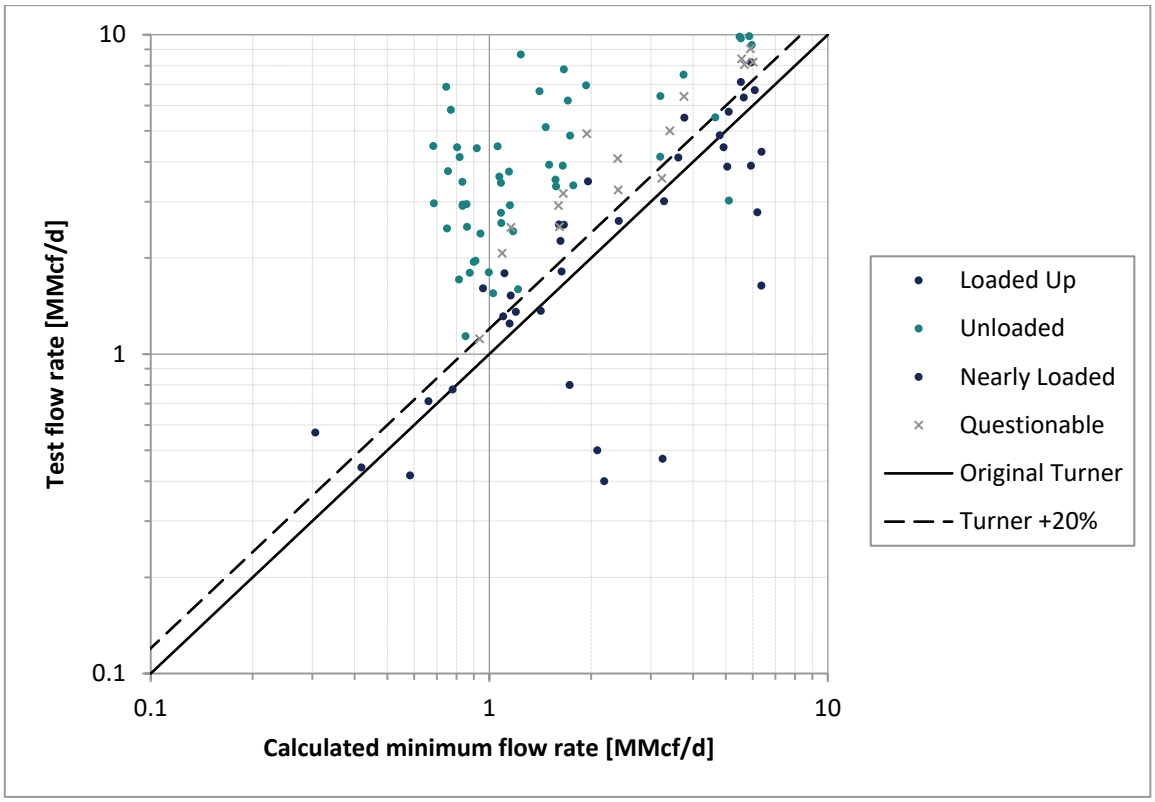

Figure 4: Drop removal model - test data x-plot [7, pp. 1477-1479]

For field application, Turner suggested some further simplifications. Therefore, he assumed a water density of 1073 kg/m^3 and an interfacial tension of 0.06 N/m. Since the effect of pressure on the gas density is much stronger than the one of temperature or specific gas gravity, he assumed fixed values of 49°C and 0.6. This results in **eq. 8** in case the liquid is water. Similarly, for condensate, he assumed 720.8 kg/m^3 and 0.02 N/m resulting in **eq. 9**. When both liquids are present the critical gas velocity should be calculated for water because it is higher and will ensure that both liquids are lifted. Turner also concluded from the test data that the (flow-) conditions at the wellhead were controlling whether liquid loading will occur.

$$v_{t,water} = 3.24\sqrt[4]{\frac{(1073-0.7201p)}{(0.7201p)^2}} \qquad (8)$$

$$v_{t,condensate} = 2.46\sqrt[4]{\frac{(720.8-0.7201p)}{(0.7201p)^2}} \qquad (9)$$

$v_{t,water}$	critical velocity for water [m/s]
$v_{t,condensate}$	critical velocity for condensate [m/s]
p	pressure [bar]

2.4.2 Coleman model

To evaluate the applicability of Turner's critical velocity for gas wells with wellhead flow pressures (WHFP's) below ~35 bar Coleman [9] collected and studied data from two sources. On the one hand, tests were conducted where wells were flowing stable above the critical rate

and the rate was lowered stepwise, by increasing the WHFP, until wells started to load up. On the other hand, data was retrieved from several 8-day long, L-10 production charts, which were inspected for the characteristic rate-decline that indicates load up. Figure 5 plots the data gained from these investigations. [9, p. 330]

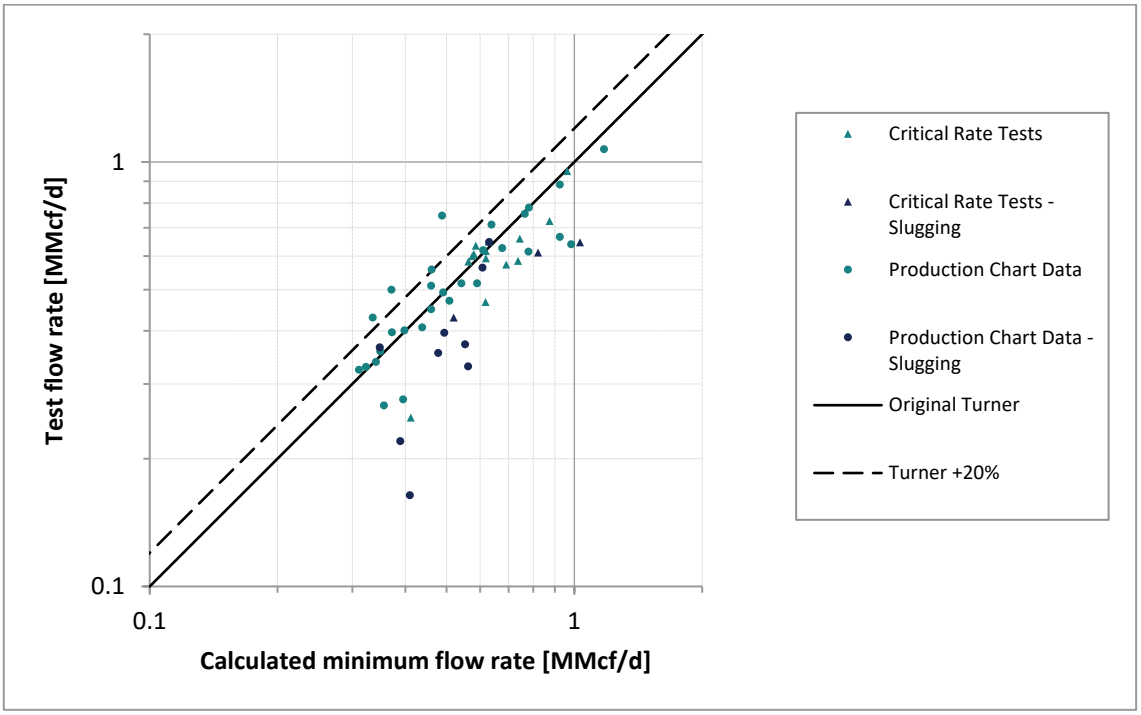

Figure 5: Drop removal model - test data x-plot for low pressures [9, pp. 331,332]

The plot shows that for these low-pressure-gas-wells the unadjusted, original Turner model without the 20% increase, as stated in **eq. 6**, provides a better fit. [9, p. 330] Therefore, eq. 6 is referred to by many as “Coleman Model”. And thus the approximations for condensate and water (**eq. 8-9**) are modified to **eq. 10-11** to be valid for lower pressures. [2, pp. 31, 32]

$$v_{t,water} = 2.69\sqrt[4]{\frac{(1073-0.7201p)}{(0.7201p)^2}} \qquad (10)$$

$$v_{t,condensate} = 2.05\sqrt[4]{\frac{(720.8-0.7201p)}{(0.7201p)^2}} \qquad (11)$$

Further, the following conclusions were drawn by Coleman from analyzing the test data. The assumption that usually wellhead conditions determine the start of liquid loading holds. The start of liquid loading is independent of the GLR, at least for the range tested, which is also in agreement with Turner’s results. Condensing water can be the main source for liquids in gas wells. Turner’s droplet model does not apply for wells under slugging condition. The critical volumetric gas flow rate is strongly influenced by pipe diameter and pressure whereas temperature, liquid- and gas density, as well as the interfacial tension, have no significant impact. Finally, when the tubing and packer are located a considerable distance above the uppermost perforations the wellhead flowing conditions may not be relevant for the critical rate.

Instead, the flowing conditions at the largest diameter, meaning the casing section below the packer must be modeled. [9, pp. 331, 332]

2.4.3 Li model

Li argued that the shape of a liquid droplet in a gas stream would deviate significantly from the spherical shape and approaches a somewhat flat, convex bean type shape shown in Figure 6. [10, p. 2]

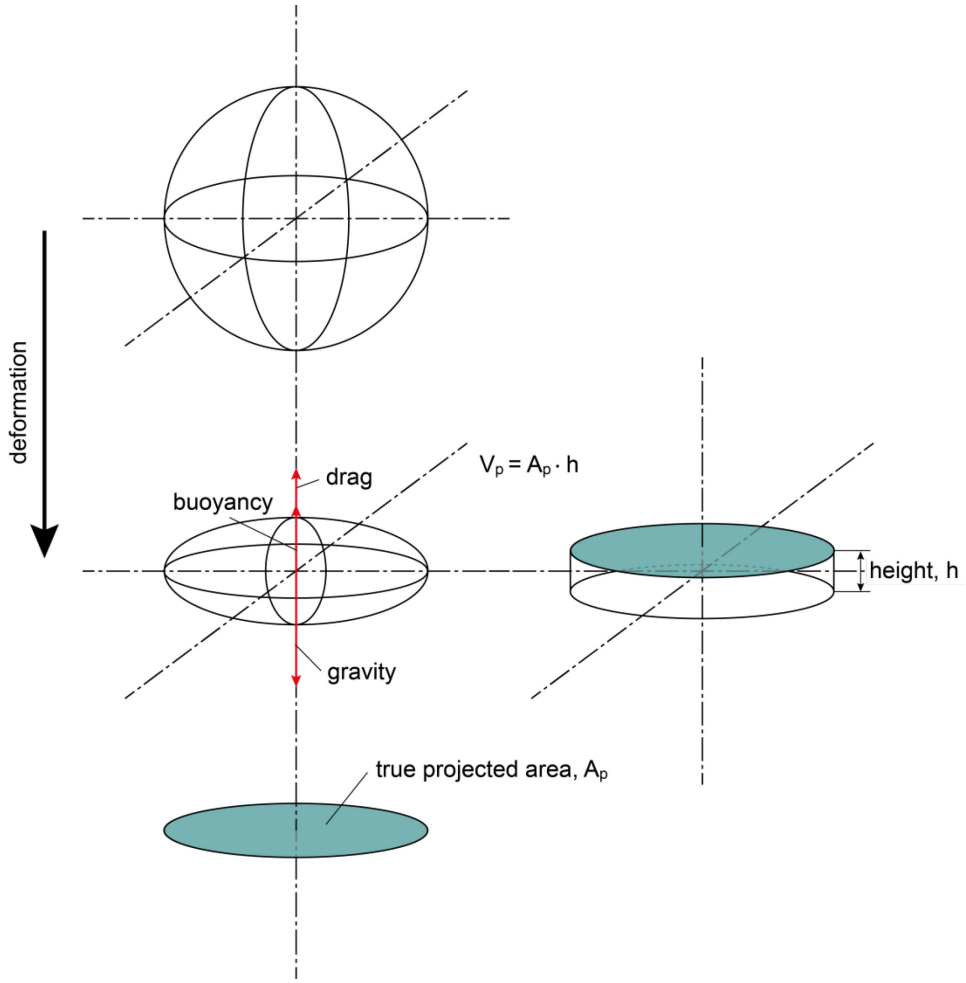

Figure 6: Deformation of a liquid droplet in a gas stream, adapted from [10, p. 5]

He derived a relationship, between the droplet shape, so the ratio of projected area to volume, and the gas velocity. It is given by **eq. 12** and illustrated in Figure 6. Inserting it into **eq. 1** yields **eq. 13**. Further, he suggests that with the droplet being close to a flat shape a drag coefficient (C_d) of 1.0 is reasonable. [10, pp. 2, 4]

$$A_p = \frac{\rho_g v^2 V_p}{2\sigma} \qquad (12)$$

$$v_t = \sqrt[4]{\frac{4g\sigma(\rho_l - \rho_g)}{\rho_g{}^2 C_d}} \qquad (13)$$

This model was tested against field data and showed a better fit for these wells compared to Turner's model. [10, p. 3]

Nonetheless, it is noteworthy that Li used a heavily simplified approach for the shape of the droplets. McDonald [11], [12] showed that the physical processes that govern the shape of falling raindrops, which behave in analog to liquid drops in a gas stream, are much more complex. Instead of the flat bean shape illustrated in Figure 6, larger liquid droplets feature a shape shown in Figure 7 at or near terminal velocity.

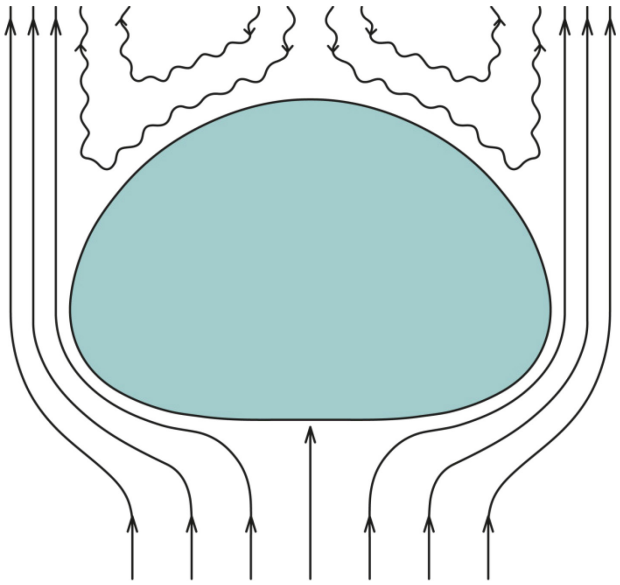

Figure 7: Flow of air around a large falling raindrop adapted from [11, p. 67]

2.4.4 Nosseir model

Nosseir [13] recognized that the original Turner model without the universally accepted +20% adjustment fits the test data from Coleman [9] nicely while it needs the adjustment to fit the Turner data [7]. He also pointed out that the assumption that a drag coefficient (C_d) of 0.44 is applicable because of the Reynolds number being between 1 000 and 200 000, is probably incorrect. The Reynolds number, calculated by **eq. 14**, of most of the Turner data, is above 200 000 where a drag coefficient of 0.2 should be applied. [13, p. 191]

$$Re = \frac{\rho_g v d_l}{\mu_g} \qquad (14)$$

Re Reynolds number [-]

μ_g dynamic gas viscosity [Pa s]

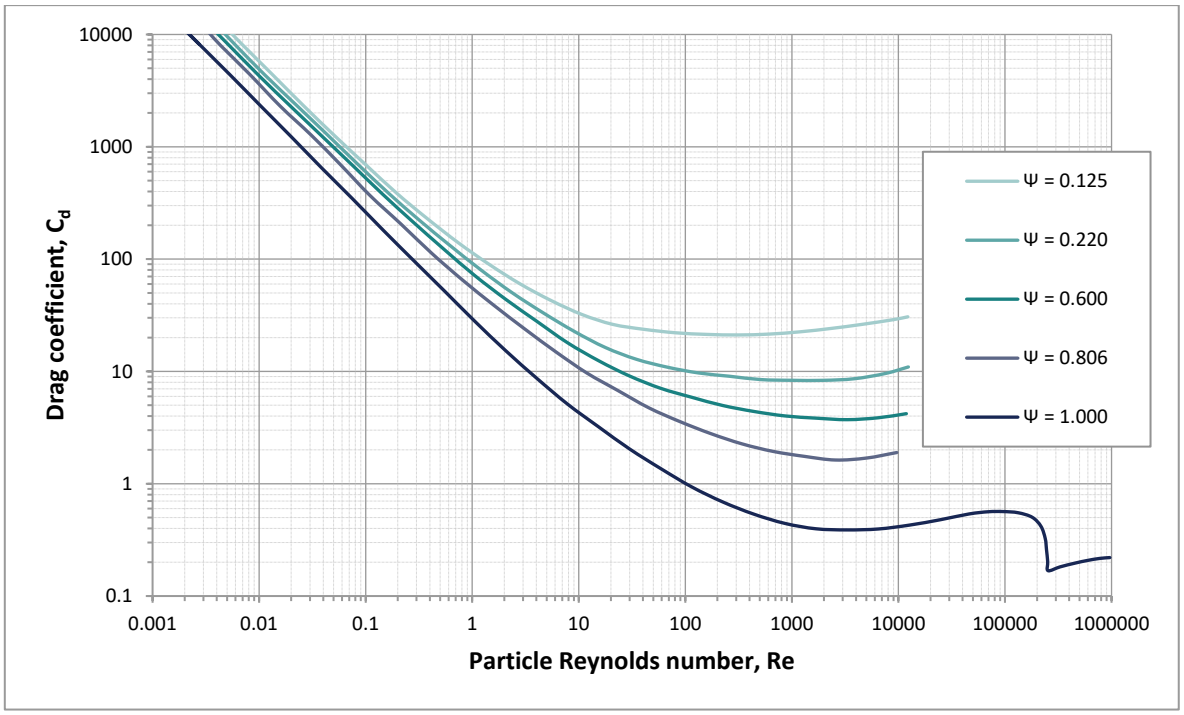

Figure 8: Dependence of drag coefficient on Reynolds number [14, p. 76]

The applicable drag coefficient for different Reynold numbers is shown in Figure 8 where Ψ denotes the sphericity which is calculated by **eq. 15**. For this application d,rops are again approximated as spheres which naturally have a sphericity of 1. [14, p. 77]

$$\Psi = \frac{S_s}{S_p} \qquad (15)$$

Ψ sphericity [-]

S_p surface of the particle, here droplet [m^3]

S_s surface of a sphere with the same volume as the particle [m^3]

Using drag coefficients according to Figure 8, different models for predicting the critical velocity were derived, which are summarized in Table 1. This way Nosseir basically found a way to consolidate the models from Stokes, Turner, and Coleman.

Table 1: Critical velocity estimation for different flow regimes [13]

Laminar	$Re < 1$	$C_d = \frac{24}{Re}$	$v_t = \left(\frac{50\sigma^2(\rho_l - \rho_g)g}{{\rho_g}^2 \mu_g}\right)^{0.200}$ (16)
Transition	$1 < Re < 10^3$	$C_d = \frac{30}{Re^{0.625}}$	$v_t = 1.69\left(\frac{(\rho_l - \rho_g)g}{{\rho_g}^2}\right)^{0.216} \frac{\sigma^{0.351}}{{\mu_g}^{0.135}}$ (17)
Turbulent	$10^3 < Re < 2 \cdot 10^5$	$C_d = 0.44$	$v_t = 3.09\left(\frac{g\sigma(\rho_l - \rho_g)}{{\rho_g}^2}\right)^{0.250}$ (18)
Highly turbulent	$2 \cdot 10^5 < Re < 10^6$	$C_d = 0.2$	$v_t = 3.76\left(\frac{g\sigma(\rho_l - \rho_g)}{{\rho_g}^2}\right)^{0.250}$ (19)

2.4.5 The critical volumetric gas flow rate

Although it is the gas velocity that directly determines whether liquids are lifted out of the wellbore, it is convenient to express it in terms of gas flow rate. For this conversion, the inside diameter of the tubing and a fluid model must be considered. Fluid models could be either black oil correlations or preferably equations of state (EOS) that relate pressure, volume and temperature (hence the term PVT-model). In the following **eq. 20** the ideal gas law corrected for non-ideality by the compressibility factor (z-factor) is utilized. [2, pp. 30, 31]

$$q_{t,g} = 21600 \frac{v_t {d_i}^2 \pi \ p \ T_{sc} \ z_{sc}}{T \ z \ p_{sc}} \qquad (20)$$

$q_{t,g}$ volumetric gas flow rate [Sm³/d]
d_i pipe inside diameter at the point of evaluation [m]
p pressure at the point of evaluation [Pa]
T temperature at the point of evaluation [K]
z compressibility factor at p and T [-]
p_{sc} pressure at standard conditions [Pa], (usually 101350 Pa)
T_{sc} temperature at standard conditions [K], (usually 288.71 K)
z_{sc} compressibility factor at standard conditions [-], (~1)

Inserting **eq. 8** and **eq. 9** for the critical velocity (v_t,) and assuming the usual standard conditions, yields **eq. 21** and **eq. 22** respectively.

$$q_{t,water} = 751.96 \ \frac{\pi \ p}{T \ z} \sqrt[4]{\frac{1073 - 0.7201 \ p}{p^2}} \qquad (21)$$

$$q_{t,condensate} = 570.94 \ \frac{\pi \ p}{T \ z} \sqrt[4]{\frac{720.8 - 0.72 \ p}{p^2}} \qquad (22)$$

2.4.6 Critical tubing inside diameter

From **eq. 20** it is obvious that the tubing inside diameter has a strong influence on the gas velocity for a given gas flow rate. Therefore, it can be useful to rearrange **eq. 20** in order to express the relationship in terms of critical tubing inside diameter, **eq 23**. [2, p. 31]

$$d_{i,t} = \sqrt{\frac{q_{sc}\, T\, z\, p_{sc}}{21600\, \pi\ p\, T_{sc}\, z_{sc}\, v_t}} \qquad (23)$$

$d_{i,t}$ critical pipe inside diameter at point of evaluation [m]

q_{sc} given/desired volumetric gas flow rate at standard conditions [Sm^3/d]

2.4.7 Criticism on droplet flow reversal criteria

Van't Westende [15] studied amongst other things, the transition from annular mist flow to churn flow for vertical pipes. The two flow patterns are illustrated in detail in Figure 9. The term co-current-annular (mist) flow highlights that gas, dispersed liquid droplets and the annular liquid film flow in the same direction. For churn-annular flow the dispersed droplets and the waves on the annular liquid film flow in the direction of the gas. However, the annular liquid film itself flow or drains downwards in the direction of gravity.

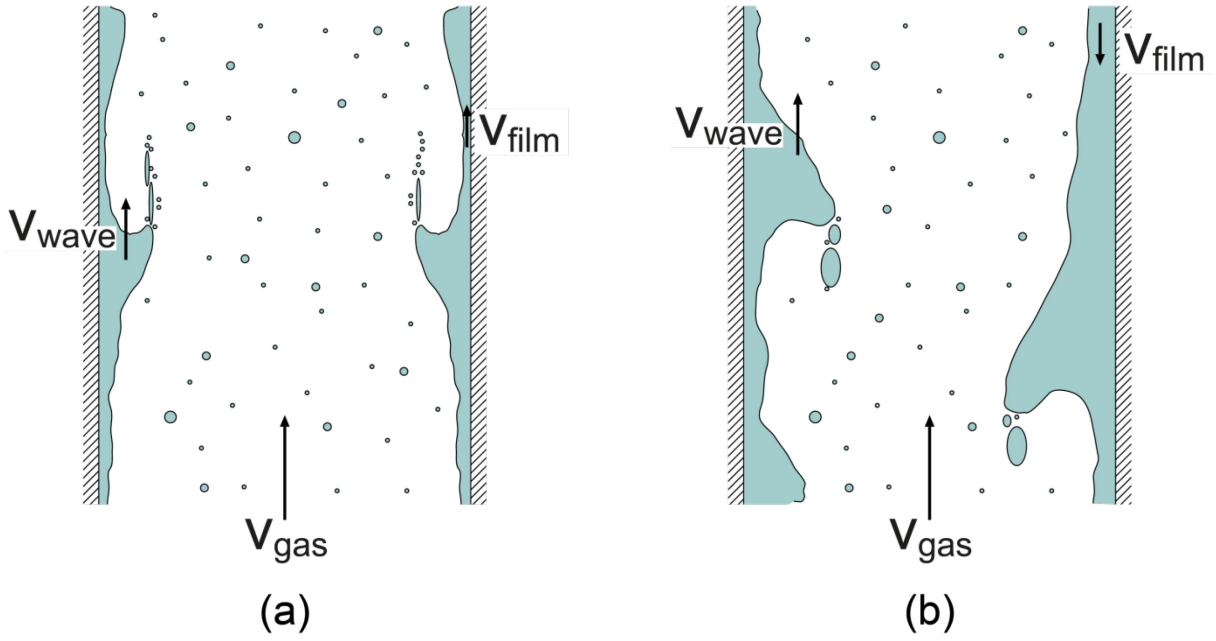

Figure 9: Co-current-annular flow (a) and churn-annular flow, adapted from [15, p. 27]

Additionally, it is stated that neither the popular droplet- nor the film flow reversal models can fully capture the phenomenon of liquid loading. In reality, the flow behavior is much more complex due to the fact that the different phases are interacting with each other. The generally accepted interactions between the three phases (gas-, dispersed- and liquid film phase) are illustrated in Figure 10 and described briefly in the following.

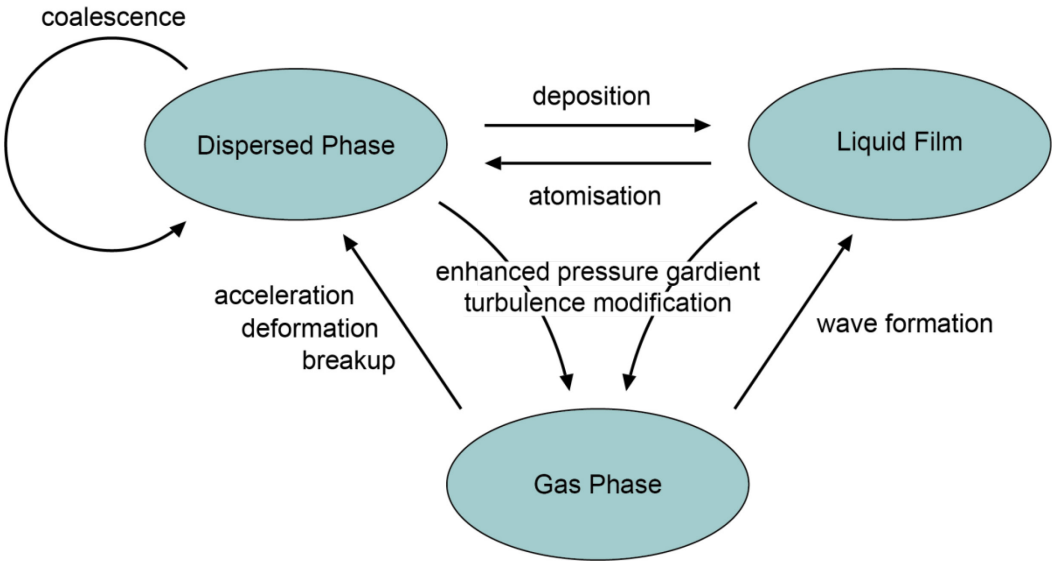

Figure 10: Generally accepted interactions between gas phase, dispersed phase and liquid film [15, p. 16]

Deposition describes liquid droplets from the dispersed phase depositing on the pipe wall or integrating with the annular liquid film. Droplet deposition is mainly governed by the intensity of gas flow turbulence, the angle of gravitational acceleration relative to the flow axis and the droplet relaxation time. [15, p. 16], [16], [17], [18], [19], [20], [21]

Atomization denotes the phenomenon when small amounts of liquid leave the continuous annular film and join the dispersed phase in form of droplets. At both, lower gas- and liquid flow rates, bag break up is the dominant mechanism. Gas undercuts the continuous liquid phase and forms half open bubbles (bags) which due to excessive stretching break up into small droplets. For higher gas flow rates the waves on the liquid film surface start to roll over. These rolling over wave crests are elongated by the gas flow into thin ligaments, which disintegrate and enter the dispersed phase. This second mechanism is therefore called ligament break up. [15, p. 16], [22], [23]

Deformation and breakup of liquid droplets occur when there is a large difference between gas velocity and droplet velocity but also depends on the turbulence of the gas phase. Additionally, when droplets collide, they might also break up into smaller ones. [15, p. 16], [8], [24]

Coalescence is the merging of two colliding droplets into one large droplet. It has been shown that coalescence can be a fast cascaded process also relevant for ligament breakup. [15, p. 17], [25], [23]

Acceleration happens to freshly created (atomized) droplets due to the difference between gas- and liquid film velocity (slip). [15, p. 17], [26]

Wave formation starts with regular, periodic ripple waves for low slip velocity between gas and liquid film. When the gas velocity increases relative to the liquid film, also the gas-shear

at the phase interface increases. This results in irregularly occurring, asymmetric disturbance waves which tend to transport a lot of liquid. [15, p. 17], [27], [28]

Enhanced pressure-gradient and turbulence modification denominate the interdependencies of the pressure gradient and some of the described phenomenon. For instance, the waves on the annular liquid film cause an increased pressure drop in the gas phase similar to increased wall roughness would. However, also the acceleration of atomized droplets needs energy, which comes from the gas phase. This manifests as increased gas pressure drop as well. Subsequently, the increased pressure drop leads to more turbulence. The turbulence itself again influences amongst other mechanisms the droplet dispersion and deposition. [15, p. 17], [29], [26], [30], [31], [32], [33], [34], [35], [36], [37]

To examine some of these mechanisms Van't Westende [15] needed simultaneous information on the probability density function (PDF) of the droplet diameters as well as their velocity. Therefore, he set up measurements for a 50 mm pipe with Phase Doppler Anemometry (PDA). The information from this experiments was then also used to evaluate the assumptions on which the Turner and all following droplet flow reversal models are built.

For an air-water system eq. 5 suggests a terminal or critical velocity (v_t) of 14.5 m/s which corresponds to a maximum droplet diameter (d_m) of 8.5 mm according to eq. 4. However according to previously done studies [38], maximum drop diameters of around 2 mm should be expected for such an air-water system. Furthermore, even the waves which are responsible for creating these droplets are usually smaller. Thus coalescence would be needed to achieve such droplet sizes. Van't Westende [15] concluded, however, that neither droplet breakup nor coalescence is a dominant mechanism in the gas core of the flow conditions of his experiments and drop-size distribution is mainly governed by the atomization process.

When the gas flow rate decreases below a Froude number (Fr) of 1 the flow regime changes to churn-annular flow. The Froude number can be calculated with **eq. 24**. At this point some of the liquid starts flowing downwards in the direction of the gravitational acceleration (g), marking the onset of liquid loading. However, all liquid droplets in the dispersed phase still move upwards, cocurrent with the gas stream under these conditions. This suggests that the physical explanation from Turner is most likely incorrect. [15, p. 125] Also Christiansen [39] observed during his experiments that the onset of liquid loading is most likely governed by annular film flow reversal. Furthermore, Veeken et al. [40] did multiphase flow simulations using the OLGA transient multiphase-flow simulator and reached conclusions in agreement with Christiansen and Van't Westende.

$$Fr = \frac{{v_{sg}}^2}{g\, d_i} \frac{\rho_g}{\rho_l - \rho_g} \qquad (24)$$

v_{sg} superficial gas velocity [m/s]
g gravitational acceleration [m/s^2]
ρ_g gas density [kg/m^3]
ρ_l liquid density [kg/m^3]

d_i pipe inside diameter[m]

2.5 Identifying liquid loading

If a gas well suffers from liquid loading it is important to recognize and diagnose this condition as early as possible in order to minimize the losses in gas production. When the liquid loading of a well is overlooked or misinterpreted for a long period, liquids not only accumulate in the wellbore but also in the near wellbore region of the reservoir rock. This might cause temporary or even permanent damage to the productivity of the well. In the following different symptoms of liquid loading are listed and explained with a focus on the ones using data that is available in the field. [2, p. 13]

2.5.1 Pressure spikes

Liquid loading can be deducted from the data from either digital, automated data collection systems or conventional two pen pressure recorders. In both cases, the pressure drop and the flow rate through an orifice is logged. When a gas well produces its liquids under mist flow condition it has little influence on these kinds of measurements. The measurement device can easily be corrected or calibrated to account for the error caused by the liquid mist. However, when a well starts to accumulate liquids and load up, it sometimes produces bigger liquid drops or slugs to surface. The density of the liquid causes a pressure spike in the recorded data. [2, p. 14]

Figure 11 on the left illustrates a chart recorded by a two pen recorder that is expected for a gas well producing without any problems under mist flow. Figure 11 on the right shows a typical pressure drop recording from a well that starts to accumulate liquids and flows under slug flow condition. Over time as the loading advances, the pressure spikes occur more frequently. At some point, the increased backpressure of liquid column reduces the overall wellhead pressure. Then also the slope of the gas production rate decline starts to become steeper. This fairly quick reduction in gas production combined with the jagged pressure recordings are a strong indication for liquid loading problems. [2, p. 14]

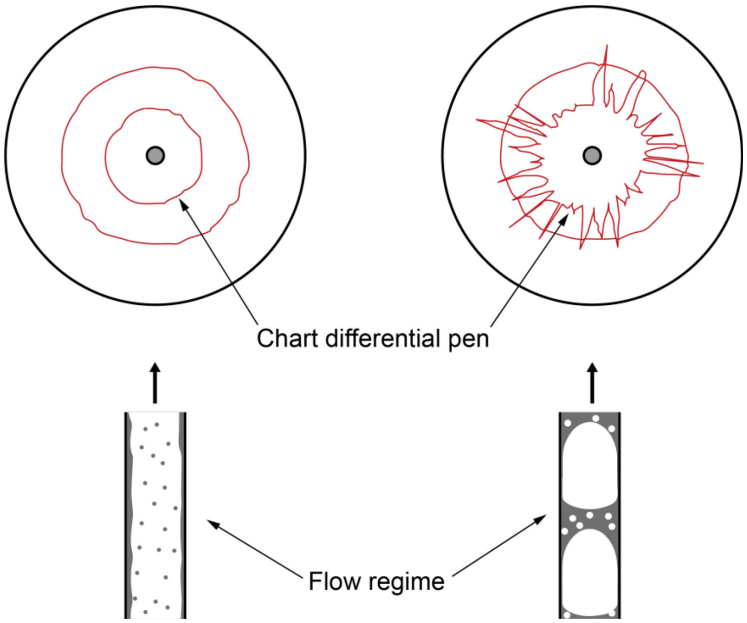

Figure 11: Orifice pressure drop for different flow regimes [2, p. 15]

2.5.2 Decline curve analysis

Liquid loading problems can also be inferred from the shape of the gas production decline curve. Figure 12 shows, on the one hand, a smooth decline curve, of the ideal exponential type. This shape is expected for a gas well producing from a depletion drive gas reservoir without any liquid loading problems. On the other hand, a decline curve is plotted that shows the erratic flow rate fluctuations that are typical for liquid loading. Furthermore, the curve from the loaded well drops off much earlier than predicted by the normal reservoir depletion. This increase in decline is, as already mentioned, caused by the additional hydrostatic back pressure from the accumulated liquid column. The faster pressure decline naturally leads to an earlier abandonment of the well and lower recovery factor. So, in summary, to identify liquid loading problems from the gas rate curve, one should look out for ragged fluctuations and a sudden deviation from the expected decline with a significantly steeper slope. [2, pp. 14, 15]

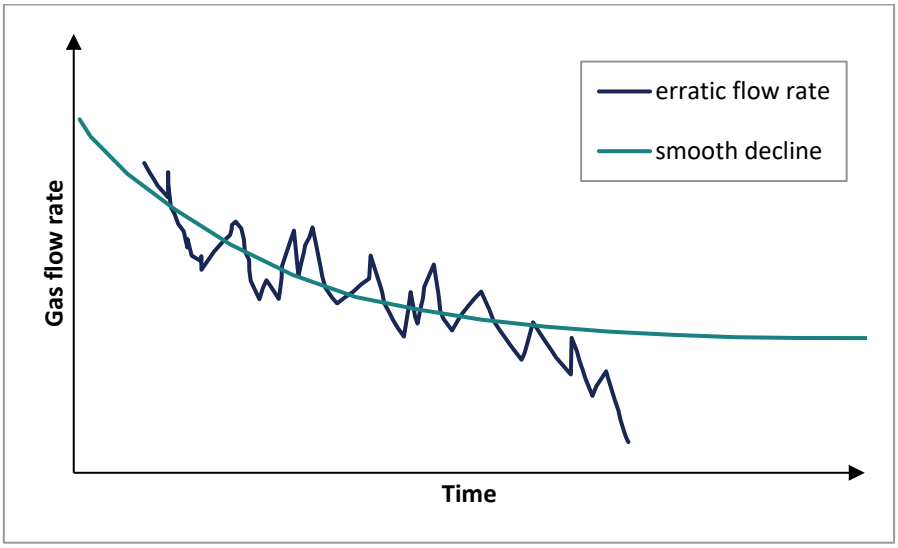

Figure 12: Schematic decline curves with and without liquid loading [2, p. 18]

2.5.3 Increase in the tubing-casing-pressure difference

During the accumulation of liquids, the wellhead flowing pressure decreases because of two reasons. Firstly, the hydrostatic backpressure of the increasing liquid column grows with liquid accumulation. Secondly, the increased liquid production increases the average density of the gas-liquid mist fluid which adds to the tubing pressure losses. These two effects can both lower the wellhead flowing pressure or increase the bottom hole flowing pressure. The higher bottom hole flowing pressure, in case of a packerless completion, causes directly a higher casing pressure. Furthermore, the gas tends to partially percolate into the annulus and accumulates there. Similar to a rising kick bubble during drilling, these gas bubbles carry the reservoir pressure with them and therefore also the casing head pressure increases. Figure 13 tries to illustrate this phenomenon, however for a real well the pressure changes are most likely not linear. Since the tubing pressure declines and casing pressure increases the key indicator is the difference between both pressures, which increases under liquid loading conditions. [2, pp. 15-18]

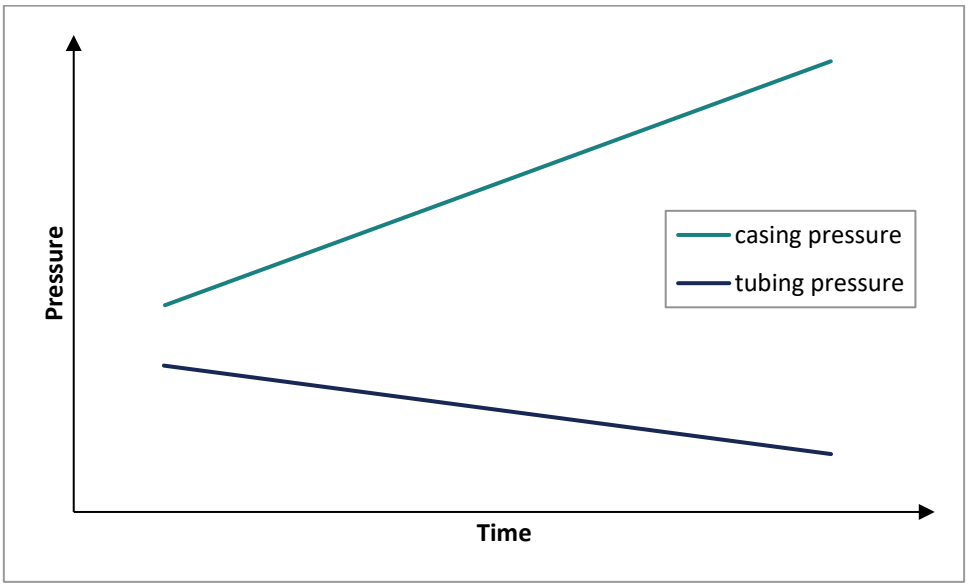

Figure 13: Tubing- and casing pressure with time [2, p. 19]

2.5.4 Pressure gradient survey

Performing a static or flowing pressure survey in the tubing provides typically the most detailed information on how severe the liquid loading is and where the liquid level is located. Under static conditions, the pressure gradient is directly related to the density of the fluid at that depth. For a shut-in well with an incompressible fluid, the pressure gradient is constant, which means that the pressure changes with depth linearly. Since gas has a very low density the pressure only changes slightly with depth, while for liquids like water and condensate the pressure gradient is much higher. Therefore, at the liquid-gas interface, a change in pressure gradient occurs which is visible as a sharp bend in the pressure survey plot. This is schematically illustrated in Figure 14. [2, pp. 18-21]

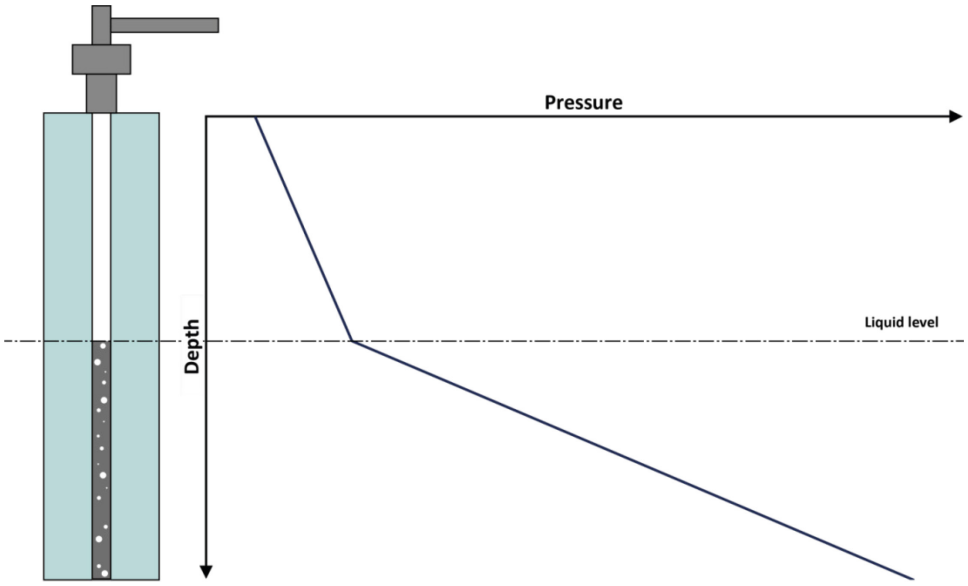

Figure 14: Pressure survey schematic [2, p. 20]

Since the wells under consideration in this context produce gas and liquids, multiphase flow conditions are faced during a dynamic pressure survey. The gradient is now the sum of the hydrostatic pressure caused by the average density of liquid and gas and dynamic pressure losses due to friction. In extreme cases, for instance, at high flow rates through a small tubing, the friction pressure loss will be so substantial that it masks up the pressure gradient change at the liquid level. A tapered tubing string consists of two or more different tubing sizes, thus the inside cross-sectional area available to gas flow changes at several points. When the cross-sectional area changes pressure losses due to velocity change (acceleration head) occur and the losses due to friction also change because of the different velocity. Thus it may also cause a kink in the pressure survey graph which must not be mistaken for the liquid level. [2, pp. 18-21]

2.5.5 Well performance monitoring

Usually, raw well performance data itself is not particularly useful and often doesn't justify the data acquiring cost. However, with certain data processing and visualization techniques, a lot of valuable information becomes available and different problematic well conditions can be identified. One of them is liquid loading. There is a technique to draw a critical rate curve, in this context often referred to as minimum lift curve, directly on the wellhead backpressure curve. When new data is recorded and data points are added to the backpressure curve it will be apparent immediately whether the well approaches liquid loading issues. [41]

2.5.6 Annulus heading

When low rate and or low GLR gas wells are completed packerless, the production can fall into a low-frequency oscillation. These oscillating conditions can reduce the production by more than 40%. [2, p. 21] Figure 15 illustrates the following steps of one annulus heading cycle:

1. When there is no packer installed, part of the produced gas percolates into the tubing-casing annulus where it accumulates. Although there is no flow in the annulus the gas flows, or bubbles, upwards through the liquid, provoked by the density difference. The accumulating gas pushes the liquid into the tubing and thus lowers the liquid level in the annulus.
2. Thus the average density of the two-phase fluid column in the tubing rises and the well produces at a low rate.
3. The liquid level has reached the end of the tubing and no more gas can flow into the annulus. Now all the gas flows into the tubing and the annulus has no more liquids to push into the tubing, thus the tubing has to take only the actual liquids from the formation. Therefore, the GLR in the tubing is increased and the average density lowered significantly, which reduces the intake pressure.
4. The lowered intake pressure finally causes the pressurized gas from the annulus to “blow around” into the tubing and gas lift the well for a short period of time. This reduces the intake pressure even further.
5. After some time most of the annulus gas is spent, the pressures have equalized and the gas expansion ceases. Due to the low intake pressure liquids are drawn into the borehole at a high rate. The large amounts of liquid increase the average density in the tubing and raise the intake pressure.
6. Liquids continue to flow into the wellbore at a rate higher than the rate they are produced with, which leads to accumulation.
7. Eventually the inflow- and outflow rates balance and gas starts to partially flow into the annulus and the whole cycle starts over. [42, p. 136]

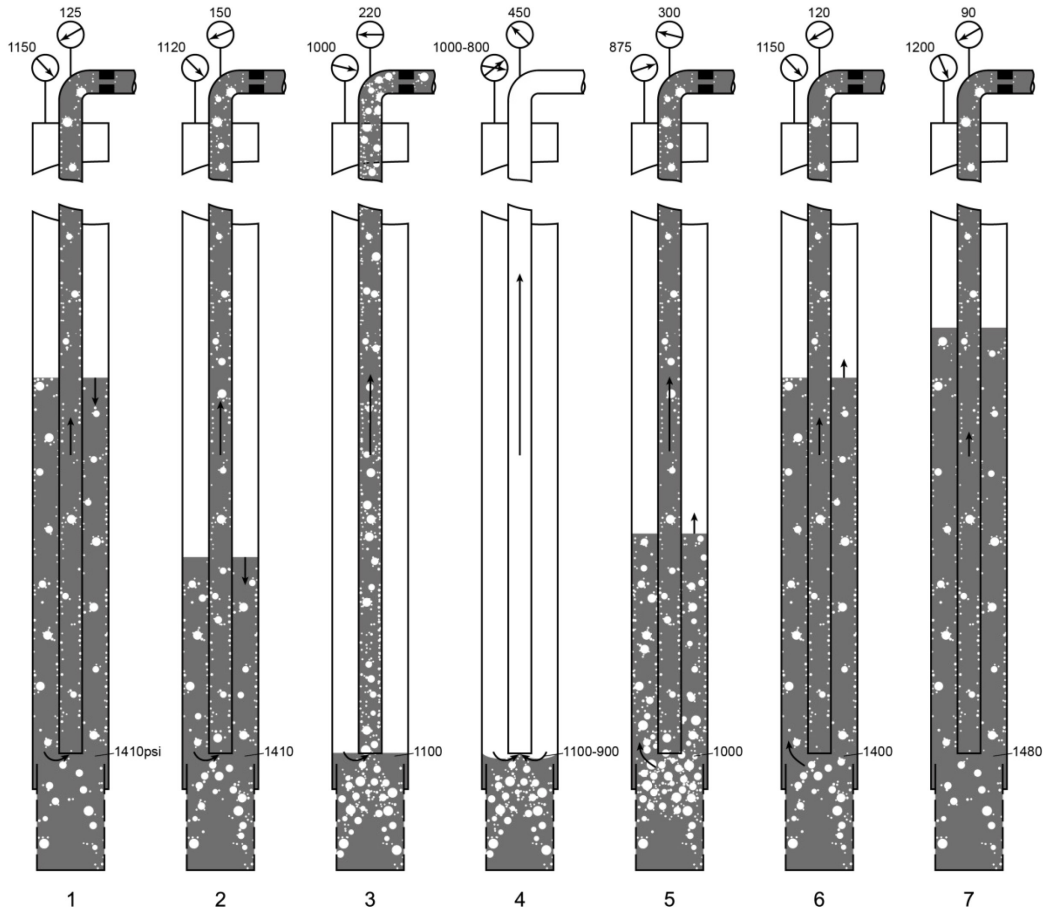

Figure 15: Schematical illustration of the annulus heading cycle [42, p. 136]

As a result of these heading oscillations, most of the liquids are produced with insufficient gas rates and very little liquid is produced under excessive amounts of gas. In other words, this represents a waste of downhole energy and a loss in efficiency. It is often tried to solve this problem by choking down the well, which is normally rather ineffective and costly because of the reduced production. This heading behavior is commonly seen in gas wells in the later stage of their lifetime. However, it can also occur in new wells with low GLR. Of course, a packer installed near the end of the tubing eliminates the problem altogether, but installing a packer in an old well bears the risk of damaging it with the mud or water used for killing it for the intervention. [42, p. 136]

2.5.7 Liquid production stops

When a gas well produces some amounts of liquids and as the gas rate naturally declines at some point liquid production can suddenly stop. This is an indication that the gas production rate has fallen below the critical rate and the liquid is no longer lifted out of the wellbore. This is usually accompanied by an increase in gas rate decline shortly after. The liquid is accumulating downhole and the increased backpressure reduces the gas rate even faster. After some time the gas production either stops completely or slides into gas percolating through the liquid column at a very low rate. [2, p. 25]

2.5.8 Acoustic measurements

Conventionally acoustic liquid level measurement devices are used in a static condition and mostly for oil wells. However, this technology can also be used in gas wells to perform flowing pressure gradient surveys. The main intention is to determine the amount of liquid in the tubing and its distribution. The measurement should give an indication if liquids are transported in the form of finely dispersed mist, under annular flow conditions or are accumulating downhole. Furthermore, it helps to estimate the flowing- and static bottom hole pressures as well as how severely the production is influenced by liquid loading. [43]

3 Nodal analysis

In a very simplified approach, the fluids that are produced in an oil or gas well have to move through the reservoir, into the wellbore, up the tubing through the surface flow lines into the separator. Along this way, pressure losses occur in all these components of the flow path, which are illustrated in Figure 16. The total pressure loss in the system is the difference between the boundary pressures, here average reservoir pressure and separator pressure. Furthermore, is the total pressure loss the sum of all pressure losses in the components, see **eq. 25**. [44, p. 1]

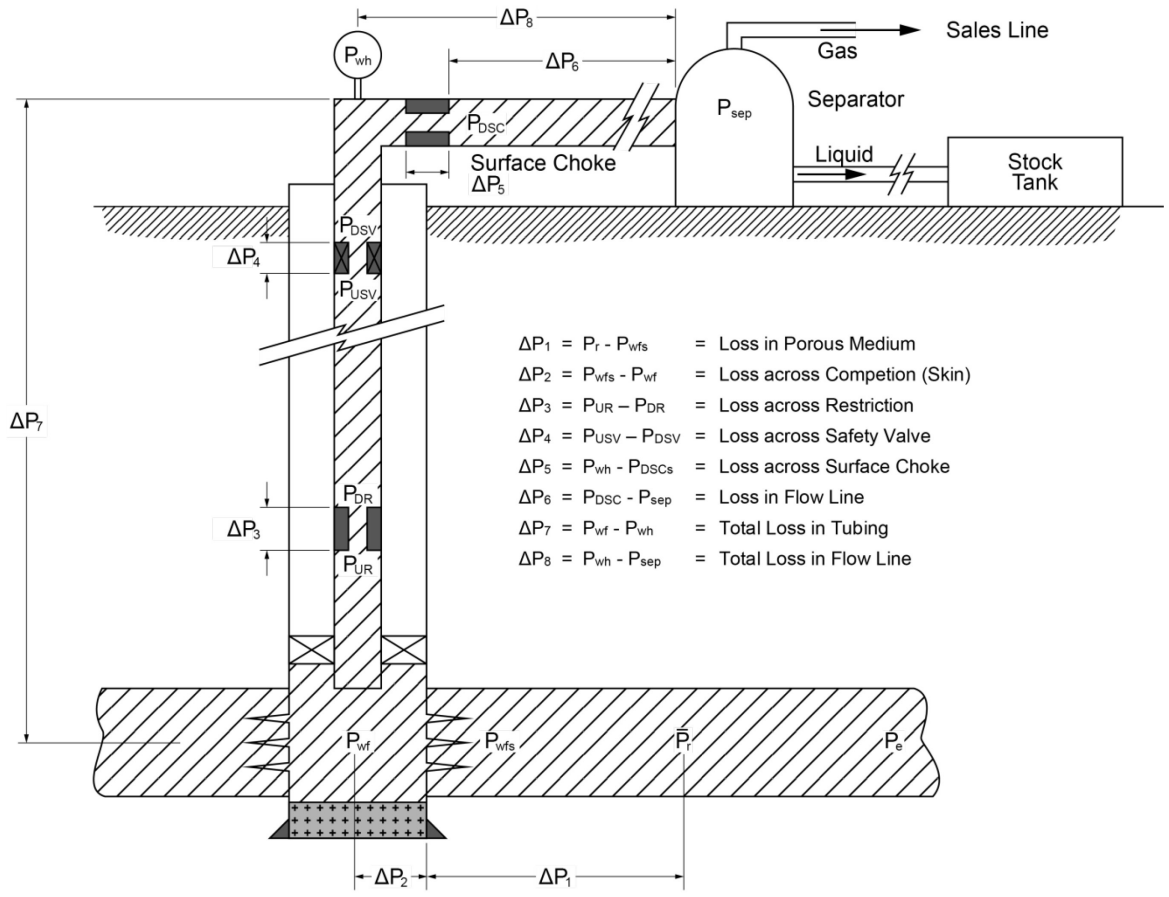

Figure 16: Pressure losses between reservoir and separator [44, p. 2]

$$\Delta p_{sys} = \bar{p}_R - p_{sep} = \sum_{i=1}^{8} \Delta p_i \qquad (25)$$

Δp_{sys} total pressure loss in the system [bar]

$\bar{p}_R$ average reservoir pressure [bar]

p_{sep} separator pressure [bar]

Δp_i pressure loss in component i [bar]

When taking electrical circuits as analogs, the voltage corresponds to the pressure, fluid flow rate corresponds to the electrical current. Similar as all conventional conductors have a resistance to electrical current all components of the flow path, which are in fact hydraulic

conductors, have a resistance to flow which manifests in pressure drops. There are also similar analogies to heat transfer phenomena. [45]

The pressure loss in the components usually depends on the flow rate and the flow rate is driven by the overall pressure drop. Since the fluids are compressible the absolute pressure in one component also influences the pressure losses. As a result, when the pressure drop in one component changes it has an impact on the pressure drops in the other components. Therefore, it is not possible to divide the system into several parts, like the reservoir, the wellbore, and the surface flow lines, analyze or design them separately. The pressure losses in the tubing impact also the flow rate through the reservoir and vice versa. Thus the whole system between the fixed boundary pressures can only be studied as one unit. The system's behavior as such could be described as highly nonlinear. The effect of changing one component, like for instance the tubing diameter, is not clear a priori. A larger tubing diameter could, on the one hand, lower the friction pressure and thus increase the flow rate, if the tubing is too large on the other hand, liquid hold up might increase significantly and the flow rate decreases. [44, p. 1]

The systems analysis approach is often called nodal analysis hence the name of this chapter. Because of the aforementioned analogies, it is self-evident that this technique has been used by electrical engineers and other disciplines for years. Gilbert [42] is considered the first to have brought this concept to the oil and gas industry where it was later popularized by Nind [46] and Brown [47].

First, the system has to be split into two parts and the splitting point is called a node- or nodal point. Theoretically, the node point can be an arbitrary point between the two outer boundaries (usually reservoir and separator). However, it is often useful to divide the system in a way that the influences of different components can be isolated. Typically one would select the wellhead or the mid perforations as the nodal point, these and other occasionally used nodes are illustrated in Figure 17.

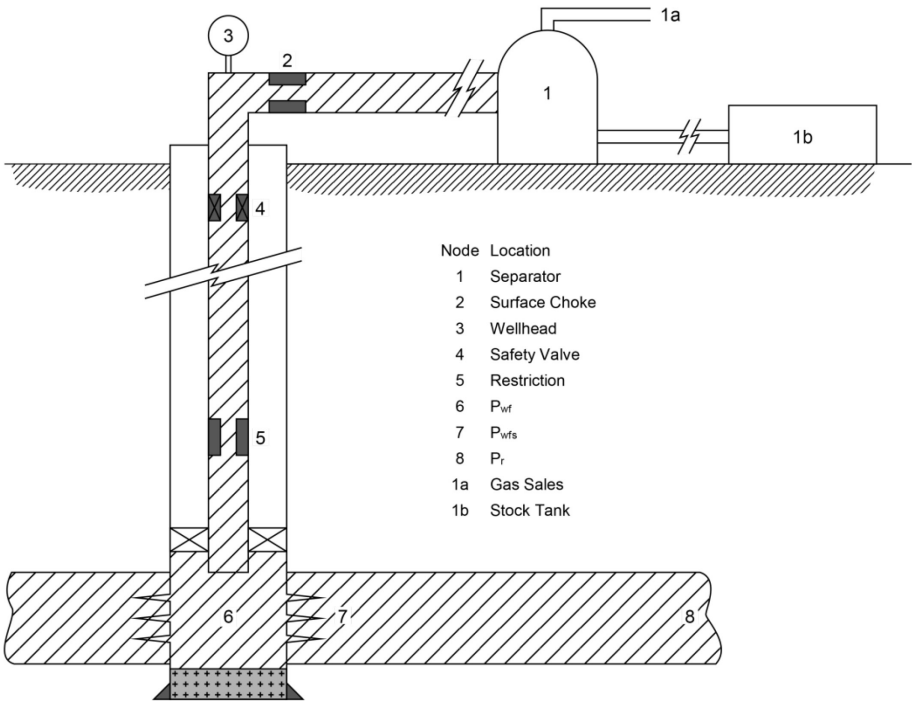

Figure 17: Commonly used nodal points [44, p. 3]

At the selected node the flow rate dependent pressure can be calculated from the inflow or upstream direction and from the downstream or outflow direction, as shown in **eq. 26** and **eq. 27**.

$$p_{node} = \bar{p}_R - \sum_{i=1}^{8} \Delta p_{i(upstream)} \quad (26)$$

$$p_{node} = p_{sep} + \sum_{i=1}^{8} \Delta p_{i(downstream)} \quad (27)$$

p_{node}	pressure at the node [bar]
$\Delta p_{i(upstream)}$	pressure loss in the upstream component i [bar]
$\Delta p_{i(downstream)}$	pressure loss in the downstream component i [bar]

Two rules apply for any nodal point. Firstly the flow rate into the node is the same as the flow out of the node. Secondly, there can only be one pressure at the node, or equivalently the downstream-side node pressure must equal the upstream-side node pressure. This makes it tempting to combine **eq. 26** and **eq. 27**, eliminate p_{node} and solve for the flow rate. However the usual,ly complex pressure loss equations are often not explicit in terms of flow rate and computers with sufficient power for instant numerical solutions were not available at that time. Therefore, the conventional approach is to graphically plot the pressure - flowrate relationship for the upstream as well as the downstream side. The intersection point is the only point where the previously mentioned conditions are met simultaneously. This idea is illustrated in Figure 18. In case the nodal point is selected at the mid perforations, the inflow curve is usually called inflow performance relationship (IPR) and the outflow either tubing performance curve (TPC) or vertical lift performance (VLP). The pressure at the mid perforations is commonly called well flowing pressure (p_{wf}).

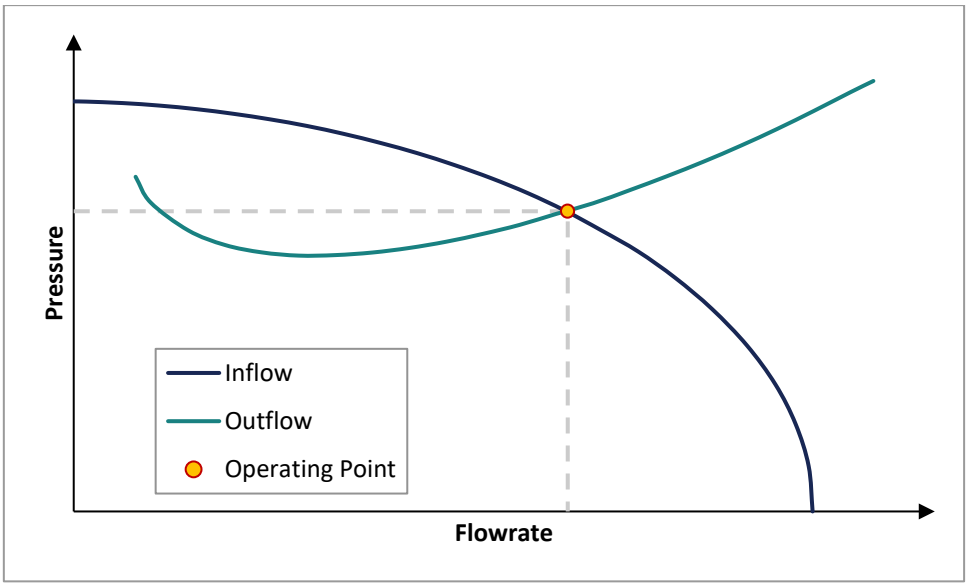

Figure 18: Graphical representation of nodal analysis [2, p. 44]

When any parameters of upstream components vary, the inflow pressure curve changes accordingly. For example, Figure 19 shows that for a nodal point at the mid perforations an increase in shot density (SPF) boosts the inflow performance, by lowering the perforation pressure drop. Since the perforation pressure drop is flow rate dependent, there is no change at zero-flowrate. That's plausible since the pressure at zero-rate resembles the reservoir pressure which is of course not influenced by the shot density. [44, p. 6]

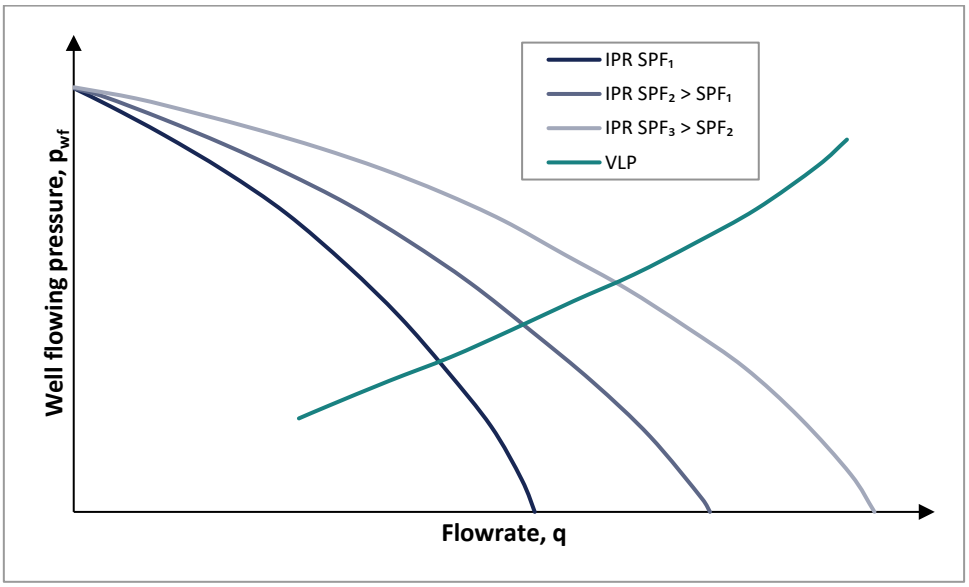

Figure 19: Effect of increasing the shot density [44, p. 6]

If downstream components or the downstream pressure boundary are changed, the outflow pressure curve changes. For example, Figure 20 shows the effect of increasing the tubing size from t_1 to t_2 for a nodal point at the mid perforations. In this case, the increased inside diameter reduces the friction pressure losses and thus the VLP curve is shifted downwards. In

combination with this particular inflow performance, this comes along with a shift of the operating point to a higher flow rate. [44, pp. 4-5]

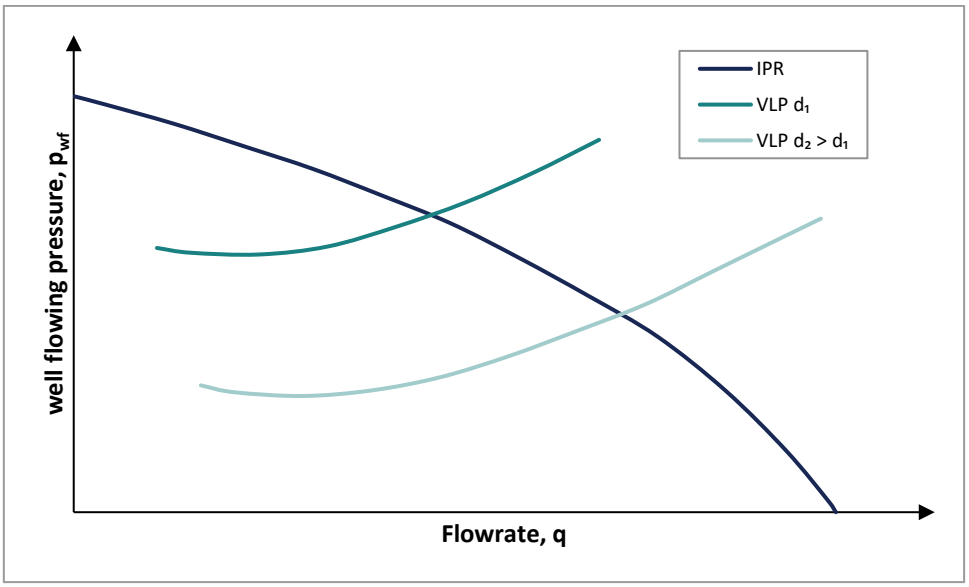

Figure 20: Effect of increasing tubing sizes [44, p. 4]

3.1 Tubing performance curve

When speaking of tubing performance curve the nodal point is assumed at mid perforations otherwise the core principles would be the same. However, the designation would be confusing. The tubing performance curve shows the downstream boundary pressure plus all pressure losses between the nodal point and the downstream boundary in dependence on flow rate. Theoretically it also includes the losses at restrictions or chokes and the surface lines, however often TPC is used synonymously with VLP which only describes the pressure drop in the tubing to the wellhead. In a simplified approach, the VLP comprises of the hydrostatic pressure drop and frictional pressure losses. For gas wells, the hydrostatic pressure drop is determined by the average density of the gas in the tubing and the accumulated liquid called liquid “holdup”. Technically the VLP also contains an acceleration term, which is only significant at very high gas flow rates [2, p. 45], and is zero for constant area incompressible flow. [44, p. 64] Figure 21 illustrates the composition of the tubing performance, or pressure loss in the tubing. This TPC has a minimum, which resembles the flow rate at which the pressure losses in the tubing are the lowest. To the right of this minimum the TPC is dominated by the frictional pressure losses caused by the high flow rate. The flow regime in this range is usually mist flow, which is very effective and efficient in lifting liquids out of the wellbore. At very low flow rates, to the left of the TPC, the pressure drop in the tubing is mainly controlled by the hydrostatic pressure of the fluid column. The average density, which directly governs the hydrostatic pressure drop, is influenced predominantly by the relative amount of liquids in the pipe, due to the generally big density difference between gasses and liquids. Under these conditions the well is producing in the bubble flow regime. At the TPC minimum, slightly to the left liquids are lifted by slug flow. On the long way to the surface the

gas starts to bypass the slugs and a big part of the liquid falls back. Therefore, the overall liquid transport is very inefficient. [2, p. 45]

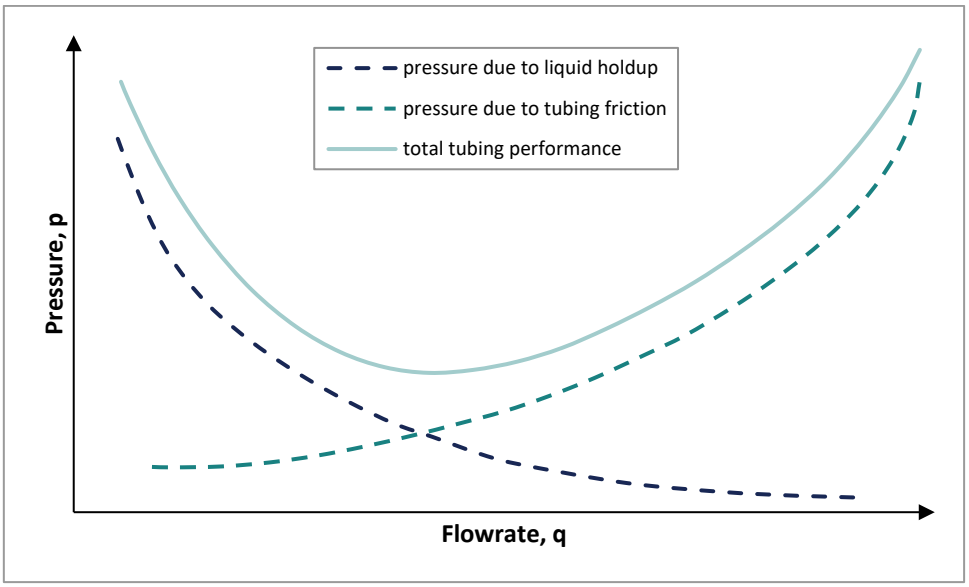

Figure 21: Components the tubing pressure drop [2, p. 46]

To the left of the minimum, flow is generally considered to be instable and prone to liquid loading. The mist flow to the right of the minimum on the other hand is rather stable and liquid loading is unlikely to occur. Therefore, in absence of up-to-date and reliable IPR data liquid loading can be predicted from the TPC alone as a first approach. The measured gas flow rate is marked in the TPC and as long as it is to the right of its minimum, liquids are unlikely to accumulate in the wellbore. [2, pp. 45-46] Two vertical gas flow correlations that model the influence of liquids are the one from Gray [48] and the one proposed by Duns and Ros [49].

For modelling two phase flow, often single-phase pressure drop models are adapted for two-phase flow by simply exchanging the fluid parameters by mixture parameters. Defining or modeling these mixture parameters in a way that the flow model models the two-phase flow properly is by no means straightforward and several approaches were developed. In the following, a few important terms that are often mentioned in the context of two-phase flow are explained. [44, p. 64]

3.1.1 Liquid holdup

Liquid holdup (H_l) is the fraction of the volume that is filled with liquid for a specific pipe section, see **eq. 28**. Letting the length of the pipe approach zero, the liquid holdup becomes the fraction of cross-sectional area that is occupied by liquid. [2, pp. 64, 65]

$$H_l = \frac{Volume\ of\ liquid\ in\ pipe\ section}{Volume\ of\ the\ pipe\ section} \qquad (28)$$

H_l liquid holdup [-]

The value of liquid holdup varies between zero and one. In analog, the gas holdup is defined. The sum of liquid- and gas holdup always equals one, see **eq. 29**. This expresses the fact that there are no void spaces in the pipe. [2, p. 65]

$$H_g = 1 - H_l \qquad (29)$$

H_g gas holdup [-]

3.1.2 No-slip liquid holdup

The no-slip liquid holdup is a theoretical, imaginary value for the liquid holdup, that is calculated as if the liquid and gas phase were flowing at the same velocity, which means without slippage. It is defined because it can be calculated easily and straight forward from the in-situ volumetric rates by **eq. 30** and **eq. 31** respectively. [2, p. 65]

$$\lambda_l = \frac{q_l}{q_l + q_g} \qquad (30)$$

$$\lambda_g = 1 - \lambda_l = \frac{q_l}{q_l + q_g} \qquad (31)$$

λ_l no-slip liquid holdup [-]
λ_g no-slip gas holdup [-]
q_l volumetric liquid flow rate [m³/s]
q_g volumetric gas flow rate [m³/s]

3.1.3 Superficial velocity

The superficial velocity is the velocity with which a fluid would flow at the same volumetric rate if it could occupy the whole pipe cross-section. Thus the superficial gas velocity is defined with **eq. 32**. [2, p. 65]

$$v_{sg} = \frac{q_g}{A} \qquad (32)$$

v_{sg} superficial gas velocity [m/s]
A pipe inside cross-sectional area [m²]

Since the gas holdup resembles the average fraction of the cross-section that is occupied by gas, the real gas velocity is defined by **eq. 33**. [2, p. 65]

$$v_g = \frac{q_g}{A H_g} \qquad (33)$$

v_g actual gas velocity [m/s]

Analogue, superficial- and actual real liquid velocities are calculated in **eq. 34** to **eq. 35**. [2, p. 66]

$$v_{sl} = \frac{q_l}{A} \qquad (34)$$

$$v_l = \frac{q_l}{AH_l} \qquad (35)$$

v_{sl} superficial liquid velocity [m/s]
v_l actual liquid velocity [m/s]

A mixture velocity was defined as the sum of the volumetric phase flow rates divided by the pipe cross-section, see **eq. 36**. The actual velocity of a fluid is always higher than its superficial one because there is less space available for the fluid to flow in parallel. Thus it has to flow in series but at a higher velocity. [2, p. 66]

$$v_{sm} = \frac{q_l + q_g}{A} = v_{sl} + v_{sg} \qquad (36)$$

v_{sm} (superficial) mixture velocity [m/s]

The slippage is the difference in actual velocity, defined in **eq. 37**. [2, p. 66]

$$v_s = v_g - v_l = \frac{v_{sg}}{H_g} - \frac{v_{sl}}{H_l} \qquad (37)$$

v_s slippage or slip velocity [m/s]

Rearranging stated equations yields different expressions for actual- and no-slip liquid holdup given with **eq. 38** and **eq. 39**. [2, p. 66]

$$H_l = \frac{v_s - v_m + \left[(v_m - v_s)^2 + 4v_s v_{sl}\right]^{1/2}}{2v_s} \qquad (38)$$

$$\lambda_l = \frac{v_{sl}}{v_m} \qquad (39)$$

3.1.4 Mixture density

In pipe pressure drop calculations the fluid density has an effect on the potential energy (elevation pressure drop), kinetic energy changes (acceleration pressure drop) as well as friction losses. For single phase fluids, the density estimation is done with equations of state (EOS), which are already developed in a great variety, with simplifications and specializations for different fields of application. [2, p. 65]

To calculate the mixture density of oil and water assuming there is no slip between the two phases **eq. 40** to **eq. 42** use an arithmetic average-type approach. [2, p. 65]

$$\rho_l = \rho_o f_o + \rho_w f_w \qquad (40)$$

$$f_o = \frac{q_o}{q_o + q_w} \quad (41)$$

$$f_w = 1 - f_o \quad (42)$$

ρ_l liquid density [kg/m³]
ρ_w water density [kg/m³]
ρ_o oil density [kg/m³]
q_o volumetric oil flow rate [m³/s]
q_w volumetric water flow rate [m³/s]
f_o producing oil fraction [-]
f_w producing water fraction [-]

The calculation of the overall gas-liquid mixture density makes use of the liquid holdup concept. To calculate the pressure drop due to elevation change conventionally **eq. 43** is utilized. **Eq. 44** is applicable for correlations or models where slippage is not considered anyway. Finally for computing the Reynolds number or friction losses the mixture density defined in **eq. 45**s should be used. [2, p. 65]

$$\rho_s = \rho_l H_l + \rho_g H_g \quad (43)$$

$$\rho_n = \rho_l \lambda_l + \rho_g \lambda_g \quad (44)$$

$$\rho_k = \frac{\rho_l {\lambda_l}^2}{H_l} + \frac{\rho_g {\lambda_g}^2}{H_g} \quad (45)$$

ρ_s fluid density considering slip [kg/m³]
ρ_n fluid density neglecting slip [kg/m³]
ρ_k fluid density for Re and friction calculations [kg/m³]
ρ_g gas density [kg/m³]

3.1.5 Mixture viscosity

The two-phase mixture velocity of two liquid phases like oil and water is usually calculated as an arithmetic average shown in **eq. 46**. This relation is not valid in case an emulsion forms. [2, p. 66]

$$\mu_l = \mu_o f_o + \mu_w f_w \quad (46)$$

μ_l liquid viscosity [Pa s]
μ_o oil viscosity [Pa s]
μ_w water viscosity [Pa s]

For the gas-liquid mixture viscosity, there is no consensus among scientists. **Eq. 47** to **eq. 49** state three of the more popular models. [2, p. 66]

$$\mu_n = \mu_l \lambda_l + \mu_g \lambda_g \quad (47)$$

$$\mu_s = \mu_l H_l + \mu_g H_g \qquad (48)$$

$$\mu_s = {\mu_l}^{H_l} * {\mu_g}^{H_g} \qquad (49)$$

μ_n mixture viscosity neglecting slip [Pa s]
μ_s mixture viscosity considering slip [Pa s]

The individual phase viscosities are usually either measured or estimated with empirical correlations. [2, p. 66]

3.1.6 Mixture surface tension

The mixture surface tension for a liquid-liquid, two-phase system like water and oil is given by **eq. 50**. To estimate gas-liquid mixture density empirical correlations should be used because of the complex dependencies on oil gravity, gas gravity, pressure, temperature, and dissolved gas. [2, p. 66]

$$\sigma_l = \sigma_o f_o + \sigma_w f_w \qquad (50)$$

σ_l liquid surface tension [N/m]
σ_o oil surface tension [N/m]
σ_w water surface tension [N/m]

3.1.7 Gray's vertical flow correlation for gas wells

The starting point for the development of the Gray correlation was the pressure balance of vertically flowing, single phase, compressible fluids and is denoted in **eq. 51** converted to metric/SI units. The first term on the right-hand side is usually referred to as hydrostatic pressure loss and the second one as friction pressure loss. The third term or loss is caused by acceleration or inertia forces, depending on the perspective. [48, p. 38]

$$dp = \rho\ g\ dh + \frac{f\rho v^2}{2d} dh - (v\rho)^2 d\left(\frac{1}{\rho}\right) \qquad (51)$$

dp pressure drop differential [Pa]
dh height differential [m]
f Darcy friction factor [-]
ρ fluid density [kg/m³]
v fluid velocity [m/s]
d tubing ID [m]
g gravitational acceleration [m/s²]

Eq. 51 can be applied to multiphase flow provided that adequate mixture properties are found. For the hydrostatic pressure drop, Gray proposed to use the mixture density considering slip defined in **eq. 35**. For friction and acceleration pressure drop calculations, he used the no-slip mixture density given in **eq. 36**. This results in **eq. 52** or with the definitions for the mixture densities inserted in **eq. 53**.

$$dp = \rho_s \, g \, dh + \frac{f \rho_n v^2}{2d} dh - (v\rho_n)^2 d\left(\frac{1}{\rho_n}\right) \quad (52)$$

$$dp = (\rho_g H_g + \rho_l(1 - H_g)) \, g \, dh + \frac{f\left(\rho_g \lambda_g + \rho_l(1-\lambda_g)\right)v^2}{2dg} dh - \left(v\left(\rho_g \lambda_g + \rho_l(1-\lambda_g)\right)\right)^2 d\left(\frac{1}{\left(\rho_g \lambda_g + \rho_l(1-\lambda_g)\right)}\right) \quad (53)$$

ρ_s fluid density considering slip [kg/m³]
ρ_n fluid density neglecting slip [kg/m³]
λ_g no-slip gas holdup [-]
H_g gas holdup [-]
ρ_l liquid density [kg/m³]
ρ_g gas density [kg/m³]

Furthermore, Gray suggested that the gas holdup (H_g) relies on the following three dimensionless numbers defined in **eq. 54**, **eq. 55** and **eq. 56**.

$$N_V = \frac{{\rho_n}^2 {v_{sm}}^4}{g\sigma_l(\rho_l - \rho_g)} \quad (54)$$

$$N_D = \frac{g(\rho_l - \rho_g)d^2}{\sigma_l} \quad (55)$$

$$R = \frac{v_{so} + v_{sw}}{v_{sg}} \quad (56)$$

N_V velocity number [-]
N_D nominal diameter [-]
R superficial liquid to gas ratio [-]
v_{sm} superficial mixture velocity [m/s]
v_{so} superficial oil velocity [m/s]
v_{sw} superficial water velocity [m/s]
σ_l liquid surface tension [N/m]

The superficial mixture velocity used in **eq. 54** has been previously defined in **eq. 42**. Finally, he proposed **eq. 57** and **eq. 58** as a correlation to estimate the gas holdup (H_g).

$$H_g = \frac{1 - e^{-2.314\left(N_V\left(1 + \frac{205.0}{N_D}\right)\right)^B}}{R+1} \quad (57)$$

$$B = 0.0814\left(1 - 0.0554 \ln\left(1 + \frac{730R}{R+1}\right)\right) \quad (58)$$

The liquid surface tension (σ_l) is considered to be some kind of mixture of gas-oil surface tension and gas-water surface tension. For the development of this flow correlation, Gray did not use the approach stated in **eq. 50** but developed his own correlation. This correlation was found by regression analysis done during the development of **eq. 57** and **58** and is stated in **eq. 59**.

$$\sigma_l = \frac{q_o\sigma_o + 0.617 q_w \sigma_w}{q_o + 0.617 q_w} \quad (59)$$

q_o in situ volumetric oil flow rate [m³/s]
q_w in situ volumetric water flow rate [m³/s]

The interfacial tension of the respective liquid phases is estimated via **eq. 60** and **61** which are correlations based on the data from Katz [50] and converted to SI units. [48, p. 39]

$$\sigma_o = 0.4536\left(0.0474 - 1.3 * 10^{-4}\left(\left(T\frac{9}{5}\right) - 460\right)\left(\frac{0.02089(p_d - p)}{0.02089 p_d - 2120}\right)^{2.5}\right) \quad (60)$$

$$\sigma_w = 0.4536(2.115 - 0.1119\ln(0.02089p))\left(0.174 - 2.09 * 10^{-4}\left(\left(T\frac{9}{5}\right) - 460\right)\right) \quad (61)$$

p pressure [Pa]
p_d dew point pressure [Pa]
T temperature [K]

Eq. 62 to **66** estimate the dew point pressure [51, p. 6] and are adapted to the SI unit system.

$$p_d = \frac{144}{0.02089}\left(1000 + \sqrt{\alpha}\right) \quad (62)$$

$$\alpha = A_1 S_o - A_2 - 100\left(T\frac{9}{5} - 585 + \acute{B}(S_o - 0.69)^{2.05}\right)^2 \quad (63)$$

$$\acute{B} = \begin{cases} 1.965 * 10^4 \; if \; S_o > 0.69 \\ 0 \; if \; S_o \leq 0.69 \end{cases} \quad (64)$$

$$A_1 = \begin{cases} 6.380 * 10^8 \; if \; S_o > 0.765 \\ 8.780 * 10^7 \; if \; S_o \leq 0.765 \end{cases} \quad (65)$$

$$A_2 = \begin{cases} 4.794 * 10^8 \; if \; S_o > 0.765 \\ 5.814 * 10^7 \; if \; S_o \leq 0.765 \end{cases} \quad (66)$$

S_o specific gravity of the oil [-]

For calculating the friction pressure loss Gray took the basic Darcy-Weisbach [52] approach and assumed the flow to be turbulent. To account for the additional irreversible losses due to multiphase phenomena he developed correlations for a pseudo wall roughness which is then used with a Colebrook-White equation [53] to obtain a friction factor.

$$\varepsilon = \begin{cases} \acute{\varepsilon} = 28.5\frac{\sigma_l}{\rho_n {v_{sm}}^2} \; if \; R \geq 0.007 \\ \varepsilon_g + R\frac{\acute{\varepsilon} - \varepsilon_g}{0.007} \; if \; R < 0.007 \end{cases} \quad (67)$$

$$\varepsilon \geq 0.3048(2.77 * 10^{-5}) \quad (68)$$

ε pseudo wall roughness [m]

ε_g pipe wall roughness to gas [m]

The original version of **eq. 67** published in [48, p. 39] contained the misprint 0.0007 in the denominator of the second part of the equation. Oudeman [54] states the correct version which is also presented here, in **eq. 67**. The pseudo wall roughness (ε) is limited by **eq. 68**. The default pipe wall roughness to gas is suggested to be $2.3876*10^{-5}$ ($9.4*10^{-4}$ in) by Gray. [48, p. 39] The Reynolds number used in the Colebrook-White equation is either set to 10^7 [55], [56] or calculated with **eq. 69** [57] which utilizes the mixing rule presented in **eq. 49**.

$$Re = \frac{v_{sm}\rho_n d}{\mu_l^{(1-H_g)}\mu_g^{(H_g)}} \qquad (69)$$

3.1.8 Modification to Gray's flow correlation

For low flow rates, the gas holdup of the original Gray correlation approaches zero and the slip mixture density (ρ_s) subsequently reduces to liquid density (ρ_l). According to Nymoen this severely over estimates the hydrostatic pressure drop for lower rates. He therefore suggests to calculate the hydrostatic component based on the no-slip mixture density (ρ_n) instead. Consequently **eq. 52** and **53** are modified resulting in **eq. 70** and **71**. Figure 22 illustrates the consequences of this modification. [55]

$$dp = \rho_n\, g\, dh + \frac{f\rho_n v^2}{2d} dh - (v\rho_n)^2 d\left(\frac{1}{\rho_n}\right) \qquad (70)$$

$$dp = \left(\rho_g\lambda_g + \rho_l(1-\lambda_g)\right)\, g\, dh + \frac{f\left(\rho_g\lambda_g+\rho_l(1-\lambda_g)\right)v^2}{2dg} dh - \left(v\left(\rho_g\lambda_g + \rho_l(1-\lambda_g)\right)\right)^2 d\left(\frac{1}{\left(\rho_g\lambda_g+\rho_l(1-\lambda_g)\right)}\right) \qquad (71)$$

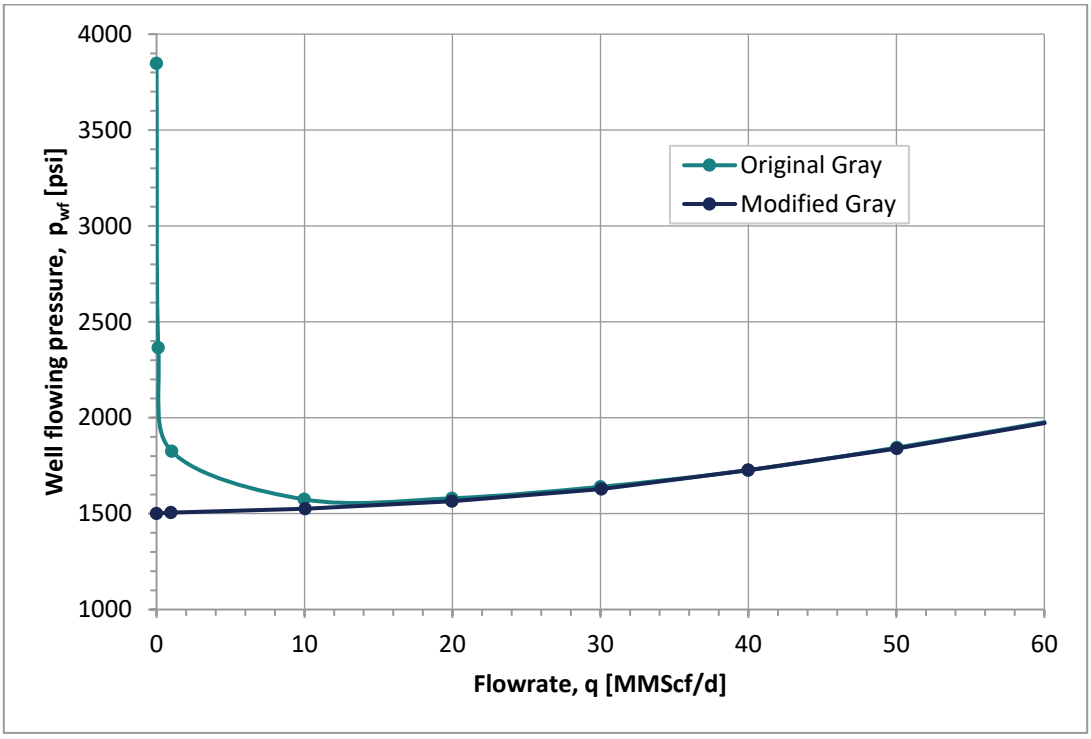

Figure 22: Comparison between original and modified Gray VLP correlation [55, p. 26]

Basically, it depends on the starting conditions which correlation to use. Is the well completely liquid free and produces at low rates with a given LGR the modified Gray will be more realistic. However, in case, the well has been operated for a long time period at such low flow rates liquid loading has caused a liquid column and a different flow regime in the wellbore. Under such conditions the flow regime changes to slug or even bubble flow. The high-pressure losses of these flow regimes are better captured by the original Gray correlation.

3.1.9 Flow in an annulus

The modeling technique described in the following is about the pressure losses that occur when gas and small volumes of liquids flow concurrently through an annulus between two pipes. It is deliberately called “flow in an annulus” to draw a clear distinction from the “annular flow” -regime.

The simplest approach is to take the cross-section area of the annulus and use any pressure loss correlation with the diameter of a pipe that would have the same cross-section area. For well-modeling programs, this is very convenient since the main algorithm of the pressure loss calculation can stay untouched. This is especially important in case it is a proprietary third-party correlation to which the source code is unknown and thus cannot be changed. However, comparing it to field tests shows that the predicted pressure is significantly too low. The underprediction is more severe for high flow rate field tests, suggesting that the error is related to the friction pressure loss calculation. Although velocities are correctly calculated with the equivalent area approach, the pipe surface area that is in contact with the flowing fluid, which is indicated by the so-called wetted perimeter, is severely underestimated. [54, p. 5]

By arbitrarily raising the hydraulic wall roughness by a factor of ten the error goes down only for some test cases but the overall average error stays too large. Raising the roughness has an especially low impact on scenarios with a high liquid-gas ratio (LGR). [54, p. 5]

For single phase flow through channels or pipes with arbitrarily shaped cross sections, the friction is calculated with the hydraulic diameter (D_H) defined by **eq. 72**. [54, p. 5]

$$D_H = \frac{A}{P} \qquad (72)$$

D_H hydraulic diameter [m]
A cross section area [m²]
P wetted perimeter [m]

It can be easily shown that the hydraulic diameter of the annulus between two concentric circular pipes can be calculated with **eq. 73**.

$$D_H = D_2 - D_1 \qquad (73)$$

D_2 inside diameter of the outer tube [m]
D_1 outside diameter of the inner tube [m]

With regards to the Gray correlation, the hydraulic diameter should be used instead of the pipe inside diameter in the second term (friction) on the right-hand side of **eq. 51** and in the calculation of the Bond number, **eq. 55**. However wherever the diameter is used to calculate cross-section areas and subsequently velocities from flow rates the true cross section area must be used. This approach can even be adapted for eccentric annuli also shown by Oudeman. [54, p. 5]

3.1.10 Vertical foam flow correlations

As discussed later, one possibility for deliquification is to use surfactants to aggregate gas and liquids into foam. In order to perform nodal analysis or other well modeling techniques, it is necessary to accurately predict the flow behavior of foam and particularly the pressure losses in the tubing of the wellbore. Compared to conventional multiphase flow, foam flow modeling is not as advanced yet. Some generally popular approaches were nicely summarized by [58] and are presented in the following.

3.1.10.1 Homogenous model

The simplest approach is to assume that by inducing foam formation the slippage between gas and liquids reduces to zero. Thus the gas hold up is directly calculated by the no-slip hold up (λ_g) defined in **eq. 31**. However, comparing it to field test data shows that this assumption does not hold. Although the slippage is low for foam flow it is not zero. [58, p. 5]

3.1.10.2 Slippage model

This model accounts for the bubble rise velocity relative to the mixture velocity. The slip velocity is defined with **eq. 74**. The constant C varies with different velocity distributions. For foam lifting applications the gas fraction is rather high and the constant C is close to one.

$$v_s = v_g - C(v_{sm}) \qquad (74)$$

v_s slippage or slip velocity [m/s]
v_g in situ gas velocity [m/s]
v_{sm} (superficial) mixture velocity [m/s]
C velocity profile factor [-]

The slippage velocity can be estimated by **eq. 75**. [59, p. 283]

$$v_s = 1.53\left(\frac{g\sigma_l(\rho_l-\rho_g)}{{\rho_l}^2}\right)^{1/4} \qquad (75)$$

σ_l liquid surface tension [N/m]
ρ_l liquid density [kg/m³]
ρ_g gas density [kg/m³]

Eq. **75** was improved by [60] to account for bubble swarm resulting in **eq. 76**.

$$v_s = 1.53\left(\frac{g\sigma_l(\rho_l-\rho_g)}{{\rho_l}^2}\right)^{1/4}\left(1-H_g\right)^n \qquad (76)$$

n tweaking exponent [-]
H_g gas holdup [-]

The actual in situ gas velocity (v_g) in **eq. 74** can be expressed in terms of gas hold up (H_g) and superficial velocity (v_{sg}). Furthermore, the slippage velocity (v_s) can be eliminated by equating **eq. 74** and **eq. 76**, which results in **eq. 77**. [58, p. 5]

$$1.53\left(\frac{g\sigma_l(\rho_l-\rho_g)}{{\rho_l}^2}\right)^{1/4}\left(1-H_g\right)^n = \frac{v_{sg}}{H_g} - C(v_{sm}) \qquad (77)$$

Using numerical, iterative methods **eq. 77** can be solved for the gas hold up (H_g). Values of 1.2 for factor C and 0.5 for the exponent n yield the best least squares fit to field test data. [58, p. 6]

When the true gas hold up is calculated considering slip, the slip density (ρ_s) can be calculated with **eq. 35**.

$$\Gamma = \frac{v_g}{v_g+v_l} \qquad (78)$$

$$\mu_f = \frac{\mu_l}{1-\Gamma^m} \qquad (79)$$

Γ foam quality [-]
μ_f foam viscosity [Pa s]
μ_l liquid viscosity [Pa s]
m exponent [-]

Foam viscosity, on the other hand, is much more complicated. It can be estimated with **eq. 78** and **79**. The relationship between foam quality and foam viscosity is illustrated in Figure 23. According to Hatschek [61], the exponent m should be 0.33 but Mitchell [62] showed later experimentally that a value of 0.49 is more appropriate.

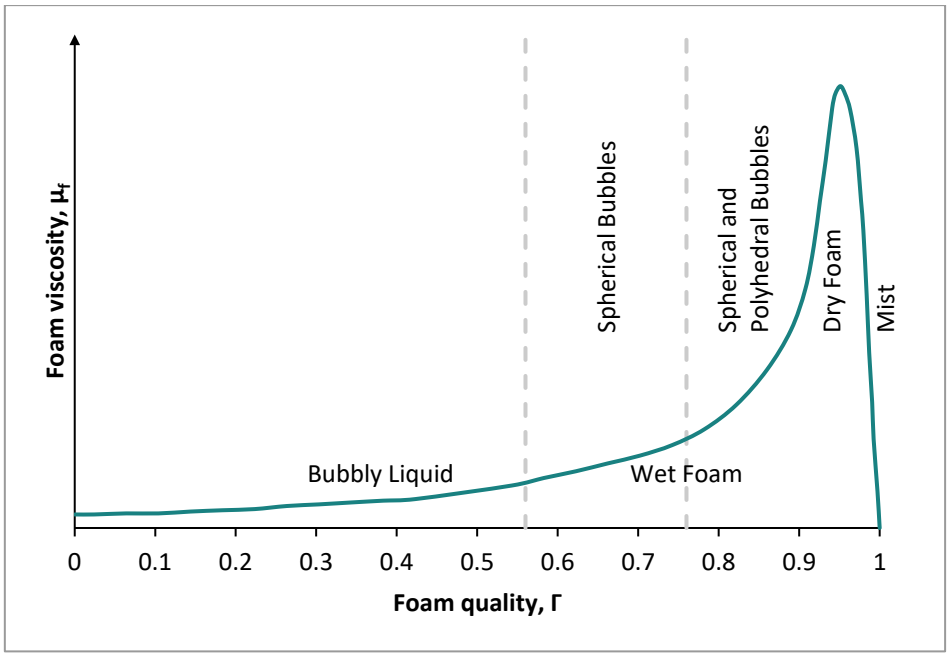

Figure 23: Hypothetical foam viscosity vs. foam quality relationship [62]

For the calculation of the friction losses, some kind of multiphase Reynolds number for foam flow is needed and defined with **eq. 80**.

$$Re_f = \frac{\rho_m v_{sm} d}{\mu_f} \qquad (80)$$

Re_f Reynolds number for foam [-]

As long as the Reynolds number ($\mathrm{Re_f}$) stays below 2300 the Darcy friction factor conventionally can be calculated with **eq. 81**. However, Deshpande [63] modified it based on 300 test points to **eq. 82**. It must be noted that Deshpande [63] stated the Fanning friction factor in the original publication while Soni [58] used the same definition in the friction pressure drop calculation as Darcy friction factor. The Fanning friction factor is one-fourth of the Darcy friction factor which is given in **eq. 81** and **82**.

$$f_f = 4\frac{16}{Re_f} \qquad (81)$$

$$f_f = 4\frac{18.36}{Re_f^{0.97}} \qquad (82)$$

f_f Darcy friction factor for foam [-]

In case the Reynolds number is higher the Colebrook-White equation [53] or the explicit version developed by Zigrang and Sylvester [64] given in **eq. 83** should be used.

$$\frac{1}{\sqrt{f_f}} = -2\,log\left(\frac{\varepsilon/d}{3.7} - \frac{5.02}{Re_f} log\left(\varepsilon/d - \frac{5.02}{Re_f} log\left(\frac{\varepsilon/d}{3.7} + \frac{13}{Re_f}\right)\right)\right) \qquad (83)$$

ε pipe wall roughness [m]

d pipe diameter [m]

Finally, the pressure losses in the vertical pipe can be calculated with **eq. 84** in which the acceleration pressure drop is neglected. According to Soni [58], it tends to overpredict the pressure drop.

$$dp = \rho_s \, g \, dh + \frac{f_f \rho_s {v_{sm}}^2}{2d} dh \qquad (84)$$

3.1.10.3 Basic drift flux model

Since the factor C in **eq. 74** depends on the velocity distribution it becomes one for fully developed plug foam flow and **eq. 74** reduces to **eq. 85**. The gas hold up (H_g) should be calculated with **eq. 86**. However, when compared to field test data the pressure is over predicted at low pressure drops and under predicted at higher ones. [58]

$$v_s = v_g - v_{sm} \qquad (85)$$

$$1.53 \left(\frac{g \sigma_l (\rho_l - \rho_g)}{{\rho_l}^2} \right)^{1/4} = \frac{v_{sg}}{H_g} - v_{sm} \qquad (86)$$

3.1.10.4 Modified drift flux model

To overcome the shortcomings of the basic drift flux model it was modified by Soni [58] by setting the constant C to 1.03. This yields **eq. 87**. Although the prediction was much better a good match was only achieved by modifying the liquid surface tension for each well individually. It has to be noted that these values for the surface tensions do not represent the true surface tension, instead, they are a way to factor in the different bubble rise velocities, which is also a strong function of surfactant type, surfactant concentration, brine composition, salinity, and temperature. Since this data was not available their effects were lumped together into what could be called pseudo surface tension. [58]

$$1.53 \left(\frac{g \sigma_l (\rho_l - \rho_g)}{{\rho_l}^2} \right)^{1/4} = \frac{v_{sg}}{H_g} - 1.03 v_{sm} \qquad (87)$$

3.2 Inflow performance relationship

The inflow performance relationship describes the pressure drop of the produced fluid from reservoir pressure to wellbore pressure for different flowing conditions. At zero flow rate, the IPR pressure is the reservoir pressure since there are no friction losses without flow. At zero well flowing pressure, the flow rate is at its maximum which is called absolute open flow potential (AOF). The pressure drop from the reservoir to the wellbore is often also referred to as (pressure-) drawdown. The flow rate that can be achieved with a particular drawdown is governed by so many different reservoir, wellbore and completion parameters and their complex interaction that an IPR can be considered unique for a particular well. Figure 24 shows a typical inflow performance curve with reservoir pressure and AOF marked. Additionally,

arbitrarily selected operating points (OP_1 to OP_4) are highlighted and illustrate that by lowering the well flowing pressure the flow rate will be increased. [2, pp. 46-47]

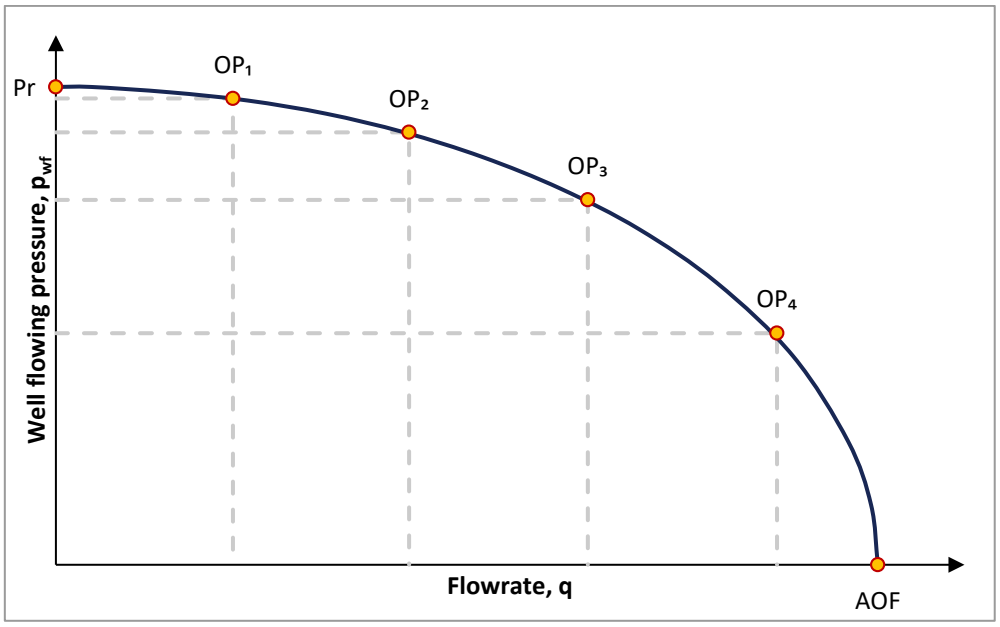

Figure 24: Typical inflow performance relationship [2, p. 47]

To accurately capture imperfect radial flow patterns and general reduction of permeability in the near wellbore zone damage, the skin factor was introduced. In particular, skin accounts for partial completion of the whole reservoir layer, insufficient slot- or perforation density, reduction in relative permeability by near wellbore phase changes, turbulent flow regime and reduction of the natural permeability by drilling and completion procedures. It is defined in a way that the well productivity decreases with positive skin and increases with negative skin. [65, p. 83] Skin is a very practical concept because the information needed to model the mentioned phenomena is often not available to the engineer. With the skin factor, all these effects are lumped together and it is determined by well testing or used as a setscrew to match the theoretical IPR to measurements.

Russell and Goodrich [66] introduced compressibility into the pseudo steady-state solution of the radial diffusivity equation which results in **eq. 88** which can be rearranged into **eq. 89**. This is a commonly used relation to generate IPR curves for gas wells.

$$\bar{p}^2 - {p_{wf}}^2 = \frac{q_g \mu_g z T p_{sc}}{\pi k_g h T_{sc}} \left(\ln \frac{r_e}{r_w} - \frac{3}{4} + S \right) \qquad (88)$$

$$q_g = \frac{\pi k_g h T_{sc} \left(\bar{p}^2 - {p_{wf}}^2 \right)}{z T p_{sc} \left(\ln \frac{r_e}{r_w} - \frac{3}{4} + S \right)} \qquad (89)$$

q_g volumetric gas flow rate [Sm³/s]
μ_g dynamic gas viscosity [Pa s]
p_{wf} well flowing pressure [Pa]
$\bar{p}$ average reservoir pressure [Pa]

r_e reservoir drainage radius [m]
r_w wellbore radius [m]
k_g effective gas permeability [m²]
s skin factor [-]
h reservoir height [m]

It is rare that all input data needed for **eq. 88** is available in the needed accuracy. Often only the empirical relationship between drawdown and flow rate is needed. Thus all reservoir and fluid properties can be lumped together into a constant C. Additionally, an exponent n was introduced to capture the effect of energy losses due to turbulent flow. n can vary from 0.5 for turbulent flow and 1.0 for purely laminar flow. **Eq. 90** is commonly known as backpressure equation. [67] Usually the two parameters are determined by well tests. A minimum of two well test points (two rates) are necessary because there are two unknown parameters, but four test points are recommend for error reduction. An easy, practical way to calculate these two values, if more than two test points are available, is to generate a log-log-plot with the test data and perform a least squares linear fit. On a log-log-plot the, backpressure equation becomes a linear equation, with n being the slope and $\log C$ being the Y-intercept.

$$q_g = C\left(\bar{p}^2 - {p_{wf}}^2\right)^n \qquad (90)$$

C performance coefficient [Sm³/(s Pa² ⁿ)]
n exponent accounting for turbulence [-]

For two test points, the exponent n can be calculated with **eq. 91** and the coefficient C with **eq. 92**.

$$n = \frac{\log(q_2) - \log(q_1)}{\log\left(\bar{p}^2 - {p_{wf}}^2\right)_2 - \log\left(\bar{p}^2 - {p_{wf}}^2\right)_1} \qquad (91)$$

$$C = \frac{q_1}{\left(\bar{p}^2 - {p_{wf}}^2\right)_1^{\,n}} \qquad (92)$$

The backpressure equation can be used to predict future productivity at different, usually reduced reservoir pressures, see **eq. 93** and **eq. 94**. [2, p. 49]

$$q_{g,f} = C_f\left(\bar{p}_f{}^2 - {p_{wf}}^2\right)^n \qquad (93)$$

$$C_f = C_p \frac{\mu_{g,p} z_p}{\mu_{g,f} z_f} \qquad (94)$$

$q_{g,f}$ future gas flow rate
$\bar{p}_f$ future average reservoir pressure [Pa]
C_p present performance coefficient [Sm³/(s Pa² ⁿ)]
C_f future performance coefficient [Sm³/(s Pa² ⁿ)]
$\mu_{g,p}$ present gas viscosity [Pa s]
$\mu_{g,f}$ future gas viscosity [Pa s]

z_p present compressibility factor [-]

z_f future compressibility factor [-]

3.3 Operating point

The VLP- and IPR-curve can have two intersection points, which are illustrated in Figure 25. Both intersections satisfy the two conditions for a nodal solution point (same rate, same pressure). However the one between C and D is stable, the one between A and B is instable and will not be reached in reality.

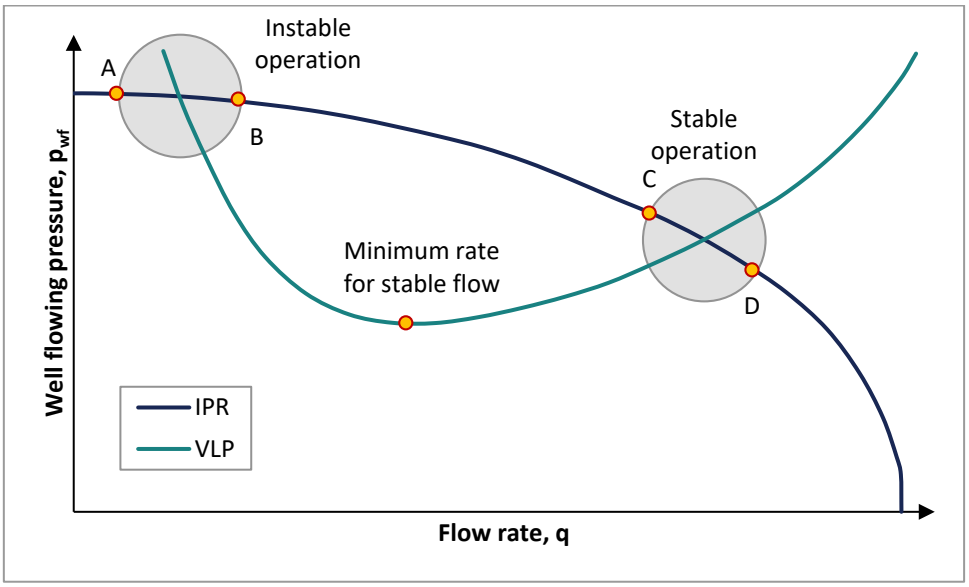

Figure 25: Potential operating points [2, p. 50]

Figure 26 illustrates the effect of a flow rate fluctuation at the stable operating point. [2, p. 51]

1. The gas rate fluctuates and increases from the operating point to point D.
2. At the higher rate, the VLP-pressure is higher, because of increased friction losses thus the well flowing pressure is increased as well.
3. However, an increased well flowing pressure is synonymous with a reduced drawdown and according to the IPR-curve, a reduction in drawdown means a lower flow rate.

Similar conclusions can be drawn for a flowrate fluctuation towards point C. Consequently, the flow rate always corrects itself and this operating point is stable. [2, p. 51]

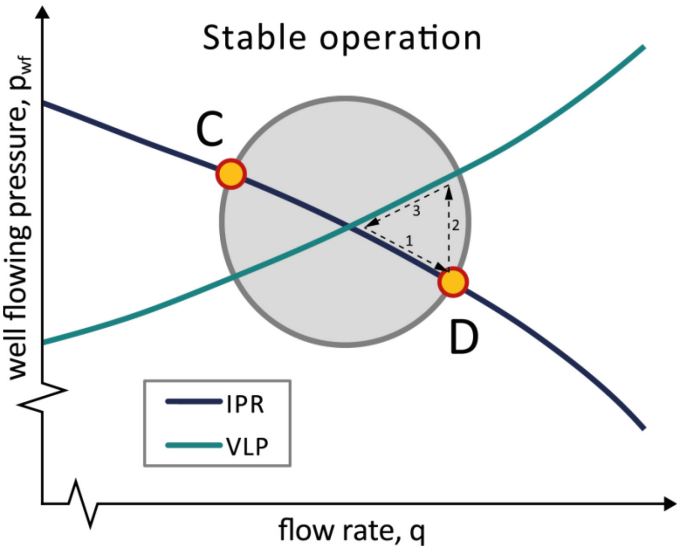

Figure 26: Stable operating point [2, p. 51]

Figure 27 shows the effect of a flowrate disturbance at the instable operating point. [2, p. 51]

1. The gas flow rate is reduced towards point A.
2. At point A the VLP-pressure is higher because of increased liquid holdup and the well flowing pressure therefore rises.
3. At the higher well flowing pressure or reduced drawdown, the flow rate decreases even further.

Thus a fluctuation towards lower flow rates will steadily increase the liquid holdup until the well loads up and is killed. On the other hand, a deflection to increased rates will cause the flow rate to increase continuously further ending up at the operating point to the right, shown above in Figure 26. Therefore, the left operating point is not stable and a real well will not flow at this rate although it is a valid solution for mathematical equations of the nodal analysis. [2, pp. 50-51]

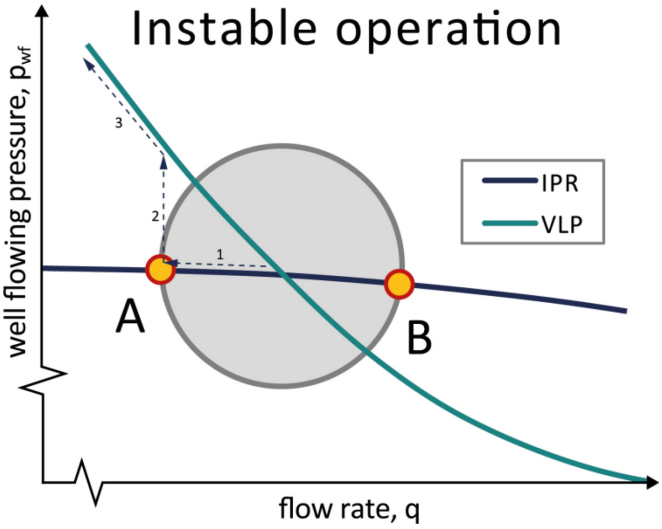

Figure 27: Instable operating point [2, p. 51]

So the stability of the operating points depends on the gradients of IPR and VLP. They must have opposite signs to reach a dynamic balance or a stable operating point. Since the IPR usually has a negative gradient over the whole range a stable operation is only possible to the right of the VLP minimum, where it has a positive gradient. However, it is important to note that although to the right of the minimum the operation is stable from a nodal analysis point of view, the gas velocity might be still below the critical velocity and liquids will accumulate. [2, pp. 51, 52]

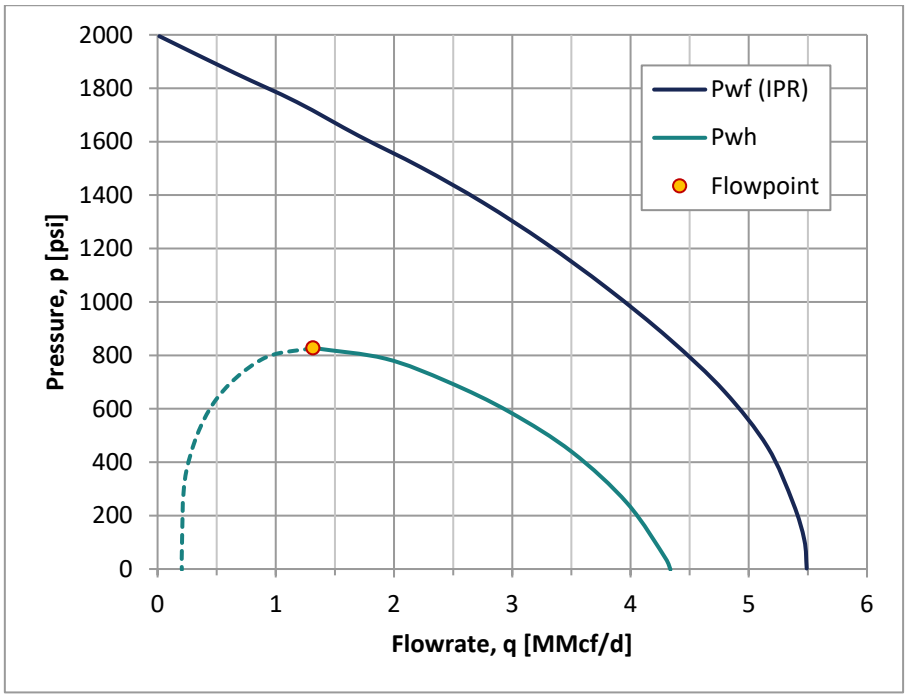

Figure 28: Downhole-, wellhead flowing pressures and flow point [68, p. 1380]

A different approach is to look at the wellhead pressure for different rates. Figure 28 plots the downhole- and the wellhead flowing pressure over the flow rate. The wellhead flowing pressure curve is sometimes called outflow performance which means flow out of the well. From a nodal analysis point of view, it is another inflow performance but with the nodal point at the wellhead. The maximum of the wellhead pressure curve is termed flow point. Above the flow point, the well is stable below it is instable. [68]

It is important to differentiate between this stability and whether a well flows above or below the critical velocity. There the model investigates whether the gas velocity is high enough to lift the biggest expected liquid droplets. Here the interaction of the pressure loss characteristic of reservoir radial flow and vertical pipe flow in the tubing is studied. Nonetheless, when a well is instable and loads up, it has in both cases the same root cause. The VLP-models capture the same phenomenon from a “macro”- and the critical velocity models from a “micro-” point of view. It is suggested to perform nodal analysis and aim for a stable flow condition. In addition, the critical flow rate should be checked at key points like top and bottom of the well. [2, p. 53]

4 Methods for resolving liquid loading problems

Numerous artificial lifting methods are suited for gas well deliquification. Nonetheless this thesis focuses on tubing size optimization, wellhead compression, foam lift, and plunger lift, which are the ones that have been implemented at least once in OMV Austria. All the other popular deliquification methods have distinct disadvantages and are therefore not the first choice. Sucker rod pumps and electrical submersible pumps (ESPs) are very susceptible to gas and would need special highly effective downhole separators and an open completion. Additionally, the cost of ESPs is hardly justifiable. Progressive cavity pumps (PCPs) although fairly tolerant to gas comprise of an elastomer stator which can swell and deteriorate in contact with the light hydrocarbons found in the gas condensate. Gas lift and jet pump installations need expensive surface equipment and additional surface lines.

4.1 Production tubing size reduction - “velocity string”

As discussed in Section *2.4 Modeling liquid loading* the gas velocity is inverse proportional to the cross-section area of the pipe and subsequently to the squared tubing ID. For a given flow rate a reduction in tubing size, therefore, implies an increase in flow velocity. The tubing should be as large as possible to minimize friction but small enough to prevent liquid loading. Both of these conditions must be obeyed over the whole length of the tubing string and as long into the future as possible. [2, p. 61]

4.1.1 Drawbacks of smaller tubing sizes

High gas rates through small tubing can cause extremely high friction losses which cause an unnecessarily high BHFP and consequently low production rate.

An operational issue is that pressure- and other testing equipment, as well as coiled tubing, does not fit through the tubing anymore. Therefore, 1.05 in, 1.315 in, 1.66 in and often even 1.9 in OD tubing is rather unpopular with field personnel.

As already mentioned a balance between exceeding the critical velocity and avoiding excessive friction must be found. However, this optimum changes as the productivity of the well declines. From a nodal analysis point of view that would mean that over time the IPR curve shifts and or changes its shape. Alternative deliquification methods that might be inferior at current conditions could be more effective at future conditions and therefore be the overall superior and more sustainable solution.

The same volume of liquid in small tubing generates a higher liquid column than in a bigger one. The consequently larger hydrostatic pressure can make unloading very difficult or even impossible. Especially the 1 in tubing is well known to be hard to unload. [2, p. 62]

4.1.2 Finding the right size

Usually, there are two concepts available for predicting whether a tubing size is prone to liquid loading. The first on is nodal analysis itself, the VLP-curve reveals the optimal flow rate for the

lowest BHFP. The second one is one of the presented critical velocity models. However, to get an actual velocity to which the critical velocity can be compared, nodal analysis should be applied as well.

For illustration, the IPR and VLPs for different tubing sizes (IDs) for the example well, described in Table 2, were generated and are shown in Figure 29. For the IPR the backpressure equation (**eq. 90**) was utilized and the VLPs were calculated with the Gray [48] correlation.

Table 2: Descriptive parameters of an example well [2, p. 63]

Well depth	10 000 ft
Bottom hole temperature	180°F
Surface flowing temperature	80°F
Surface flowing pressure	100 psi
Gas gravity	0.65
Water gravity	1.02
Condensate gravity	57 API
Water rate	2 bbl/MMscf
Condensate rate	10 bbl/MMscf
Reservoir pressure	1000 psi
Backpressure exponent n	1.04
Performance coefficient C	0.002 Mscf/(d psi$^{2\,n}$)

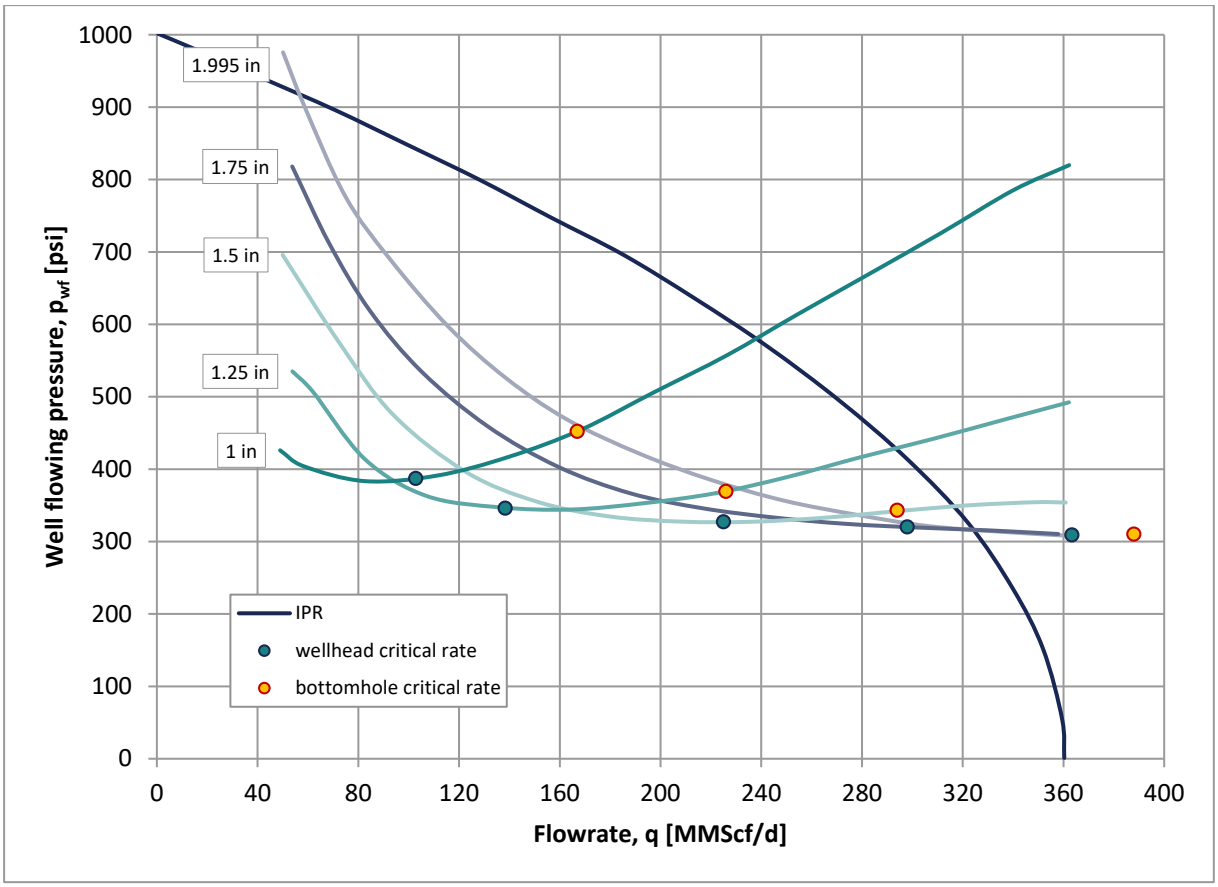

Figure 29: Tubing performance and critical rates for different sizes [2, p. 64]

The ***1.995 in ID tubing*** has a VLP with its minimum clearly to the right of the intersection with the IPR curve. The critical rate at the wellhead is larger than the AOF of this well and the critical rate at bottom hole conditions is off the charts. So this tubing size is clearly too large for this well conditions.

The ***1.75 in ID tubing*** features a VLP-curve that is very flat in the region around its minimum where it intersects the IPR. Therefore, it is not clear where the actual minimum and with this tubing the well will most likely be instable. The critical rate at wellhead conditions is to the left of the nodal solution point, however, the downhole critical rate is to the right. Therefore, this tubing size is still too large.

For the ***1.5 in ID tubing*** the VLP minimum and the critical rate are clearly too the left of the intersection point. Although also the critical rate at bottom hole conditions is lower than the expected actual rate it is fairly close to the intersection point. Thus a future reservoir pressure decline will shift the IPR and consequently also the intersection point to the left. Then the well would produce shortly below the critical rate, load up and then the rate will drop even lower. So the 1.5 in ID tubing is fine and actually the optimal choice as long as the IPR/VLP models are accurate and parameters, like reservoir pressure or skin, don't change.

The ***1.25 in ID tubing*** has the VLP minimum and all critical rates clearly left of the intersection point. It yields an expected production of over 76% of the AOF. Therefore, this size would be

a good balance between high production rate, avoiding liquid loading and safety against future changes.

The ***1 in ID tubing*** will also produce clearly above all critical rates and the inflection point of the VLP-curve. However, the 1 in ID tubing causes high friction losses and will yield only 61% of the AOF. Therefore, this size is acceptable in terms of preventing liquid loading but is far from optimal because of the low gas production rate.

These calculations assume a constant tubing ID and only check for liquid loading in the tubing. If the completion includes a tapered string or the tubing ends in a great distance from the perforations the critical velocity calculations should be performed at different selected depths. One of the reasons why VLP correlations are inaccurate is that on assumes average fluid properties. To overcome this, nodal analysis computer programs divide the borehole into small sections for which it is reasonable to assume constant (average) boundary conditions. As a side effect, the critical velocity can be calculated for all sections separately. If the actual gas velocity is below the critical one, which is also called Turner velocity, the section is flagged.

Even if there is no reliable IPR data available a comparison of the actual rate with the VLP-curve and the critical rates can be indicative of the problem source. [2, pp. 62-68]

4.1.3 Velocity string implementation

Instead of changing out the whole production tubing a coiled-tubing with the desired ID is inserted into the tubing and the tubing-coiled-tubing annulus is sealed with a packer. This installation is often referred to as velocity string. Theoretically, the smaller flow conduit is only necessary for the section where the gas velocity is below the critical velocity. So there also is the possibility to install a velocity only for a particular interval.

Furthermore, the landing depth of the tubing is important. Ideally, the tubing should end as close as possible to the top perforations but not below the upper one-third of the perforated interval. When setting the tubing too low, liquids will fill up the tubing-casing annulus during shut-in which have to be displaced through the tubing at start-up. The resulting high fluid level in the tubing will cause significant problems during unloading.

In the section below the end of the tubing, the flow path has a where large cross-sectional area (casing ID) and consequently gas velocities are comparably low, commonly below the critical velocity. Therefore, this section usually has a high liquid hold up which adds to the backpressure on the reservoir. The longer this section is the higher this backpressure will be and the lower the production. Therefore, it is also crucial not to set the tubing too high. In case of an existing installation where this problem is identified, there is the possibility of hanging off a smaller tubing from the end of the existing tubing. [2, pp. 69-75]

4.1.4 Summary

Changing the tubing size to a smaller one is an effective method of deliquification, especially for high production rates of several hundred Mscf/d. The ID should be considerably above 1 in

to avoid clearance problems with downhole tools and limitations in unloading methods. The criterions for size determination are the stability of flow in a nodal analysis sense and critical velocities at different points, like wellhead and bottom hole. To be conservative the highest of these rates should be taken to decide on the correct size. The optimal tubing landing depth is right at the top of the perforated interval, deviation either up or down are both detrimental to the performance. A well can be liquid loaded although there is no sudden fall off in the production history visible. The well might just have liquid loading problems since the beginning and could actually achieve way higher rates. To evaluate the success of a smaller tubing the gas production rate immediately after the change out is not significant. The slope of the production decline, on the other hand, is a good indicator of the performance of a new completion. [2, p. 76]

4.2 Wellhead compression

From Figure 16 it is easy to see that a reduction in wellhead pressure will result in an increased drawdown and therefore higher rate. The flowline pressure is the lower limit to the wellhead pressure reduction. To achieve wellhead pressures below the flowline pressure, a compressor near the wellhead is necessary. Besides the increased production, the well's lifetime will be extended significantly. In a gas well, a lower wellhead pressure has the following two effects which reduce the chance of liquid loading.

1. The increased drawdown causes a higher volumetric production rate which means a higher gas flow velocity throughout the well, given that the completion is continuous. If the increased velocity exceeds the critical velocity all liquids are lifted from the wellbore.
2. The overall lower pressure in the wellbore allows for more gas expansion. Therefore, even for an identical surface flowrate at standard conditions, the in situ, downhole volumetric gas flow rate will be higher. Consequently, also the actual gas velocity will be higher and compare more favorably to the critical velocity.

So surface or wellhead compression will increase gas production directly and as a consequence, if the rate increase is high enough, liquid loading problems will be avoided. Additionally, the absence of the backpressure resulting from liquid loading will increase the production even more. [2, pp. 79-80]

4.2.1 Wellhead compression in nodal analysis

To evaluate the impact of a changing wellhead pressure on the overall gas well performance, nodal analysis is a powerful tool. Figure 30 illustrates that a wellhead flowing pressure reduction from 500 psi to 100 psi causes the gas rate to increase from 1700 Mscf/d to around 2500 Mscf/d for an illustrative example gas well. Furthermore, it shows that for decreased reservoir pressure (p_{r3}) a WHFP of 500 psi will most likely cause already liquid loading problems since the VLP-IPR-intersection is in the instable region. However, for lower wellhead flowing pressures, the production will still be stable. The possible improvements are dependent on the shape of the IPR in general and the IPR gradient in the solution region in particular. A

flat IPR curve will result in significant improvements, a steep IPR curve, which is characteristic for tight gas reservoirs will yield poor results or none at all. [2, pp. 80-81]

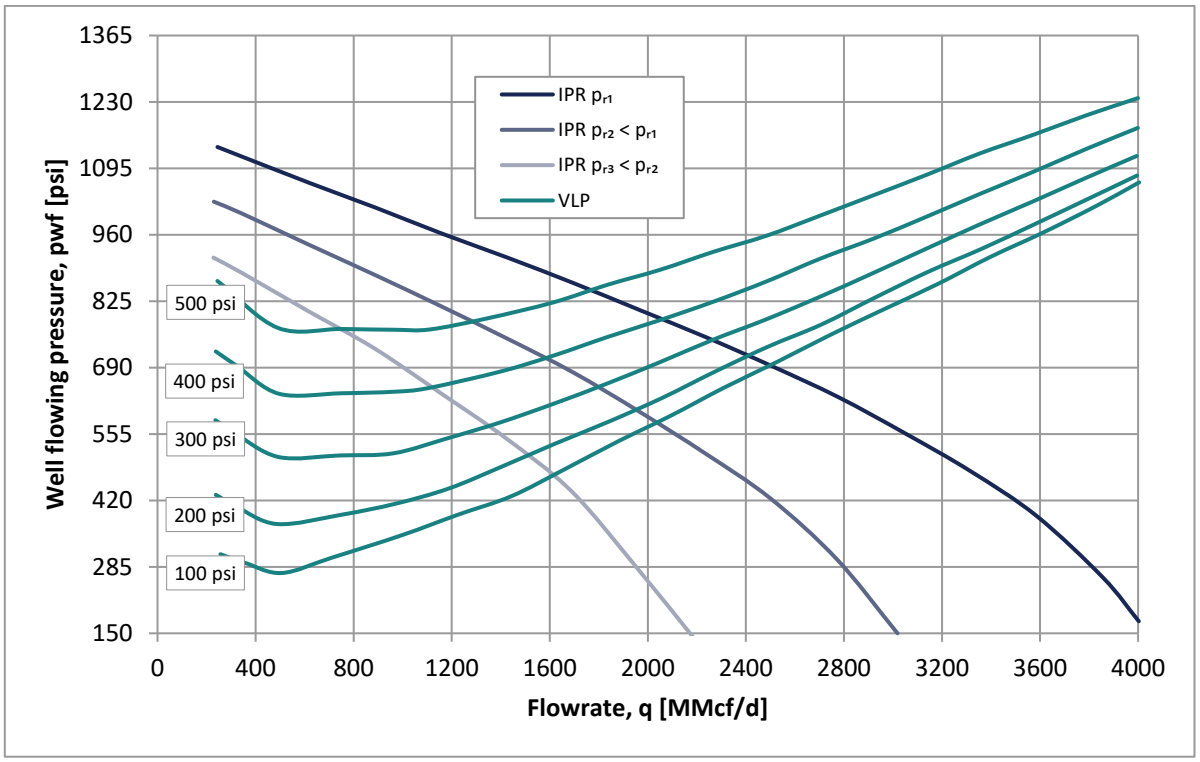

Figure 30: Wellhead compression in nodal analysis [2, p. 80]

4.2.2 Implementation

Pressure reduction at the wellhead can be realized by a central compressor station lowering the pressure of the gathering pipeline network or on a per wellhead basis. The lowest wellhead pressures are possible with compressors right at the wellhead. The most common compressor types and their characteristic properties are summarized in Table 3.

Table 3: Gas compressor types and characteristics [69]

Compressor type	**Characteristic properties**
Rotary lobe	• Low cost per cfm • Air cooled • ~2.0 compression ratio • Small amounts of liquids acceptable • High range of flow rates possible (50-12000 cfm) • Power frame supporting bearings, gears, and shafts
Re-injected rotary lobe	• Low cost per cfm • Air cooled • ~4.0 compression ratio, high vacuum • Small amounts of liquids acceptable • High range of displacements possible (50-12000 cfm) • Power frame supporting bearings, gears, and shafts • Needs Intercooler

Rotary valve	• Medium cost per cfm • Liquid cooled, jacket • ~4.5 compression ratio • Medium flowrate/displacement • Power frame is required • External oil lubrication system • Lost lubrication to the gas • No liquids can be ingested
Liquid ring	• Medium cost per cfm • Liquid is injected • ~4.5 compression ratio • High displacement • Power frame is required • Cooling system for the seal liquid required • Gas-liquid separator required • Liquids are acceptable but will mix with and contaminate the sealing liquid • ~25 psi delta pressure
Liquid injected rotary screw	• Higher cost per cfm • Liquid injected • ~6.0 compression ratio • Medium displacement • Power frame is required • Cooling system for the seal liquid required • Gas-liquid separator required • Liquids are acceptable but will mix with and contaminate the sealing liquid • High compression ratios possible • Few wearing parts • High mechanical and adiabatic efficiency • Should be operated according to specifications • 250 psi is max. discharge pressure • Liquid/oil selection and testing is critical
Reciprocating	• High cost per cfm • Air or liquid cooled • ~4.0 compression ratio • Power frame is required • Low displacement • No liquid ingestion allowed • Valve losses influence compression ratio and volumetric efficiency • Very flexible in terms of suction and discharge pressures • Discharge pressure only limited by discharge temperature and the rod load rating of the frame • Simple to maintain • Valve maintenance causes cost and downtime and is governed by the gas quality • Poor efficiency for low suction pressures
Sliding vane	• Medium cost per cfm • Liquid cooled jacket • ~3-4.5 compression ratio

	• Power frame is required • Medium displacement • External lubrication system required • Lost lubrication to the gas • No liquid ingestion acceptable • Simple operation • Simple design, easy to manufacture • Isolated bearing with separate lube system for sour service • Blade performance and wear are determined by gas quality; can get stuck because of solids • Lower discharge pressure and lower volume applications

Alternatively to mechanical compressors, wellhead compression can be implemented with gas jet compressors, also called eductors which are similar to jet pumps. With gas as power fluid, they achieve compression ratios up to 2 and with liquid power fluids even higher ones. The operating principle of an eductor is based on Bernoulli's law. The power fluid is forced through a small nozzle by high pressure. Due to the small nozzle, the velocity increases according to the continuity equation. Based on Bernoulli's law the high velocity results in a low pressure right after the nozzle. The suction ports connect to the wellhead and gas is sucked in by the low pressure. Gas mixes with the power fluid and momentum is transferred. The velocity reduction in the diffuser causes a pressure increase resulting in the discharge pressure. Eductors don't have moving parts and are therefore highly reliable and need little maintenance. Generally, they are also easy to install and operate and handle liquid slugs nicely. The nozzle sizes can be changed to adapt the eductor to different conditions. However, an eductor is only a viable option if the power fluid is available at the well site, from e. g. a nearby high-pressure gas well. [2, pp. 85-93]

4.3 Foam lift

In foam, the liquid is trapped in the thin film between the bubbles. These shapes have a very large surface compared to their volume. Therefore, the gas slippage in multiphase flow and the chance of liquid loading is significantly reduced. Figure 31 shows that especially for lower superficial gas velocities the difference in pressure losses between pure water and foam is remarkable. The lab test for Figure 31 was done in a 2 in pipe, with water at a rate of 6 bbl/d and air was used as the gas phase.

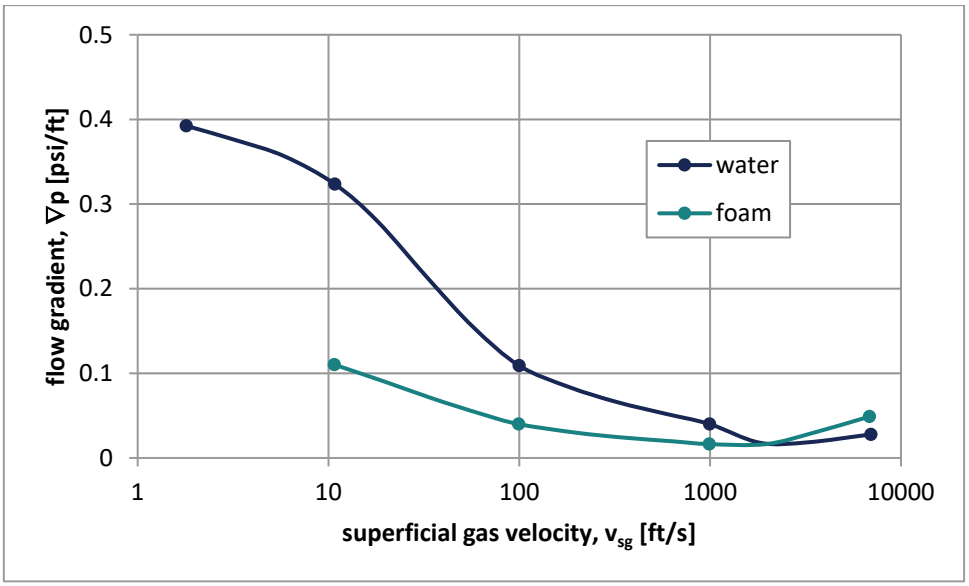

Figure 31: Pressure gradient from laboratory flow tests at atmospheric pressure [2, p. 148]

4.3.1 Foam structure and stability

In the two-phase liquid foam, liquid is the continuous and gas the dispersed phase. Typically the gas bubbles develop a polyhedral form. The surfaces of these polyhedra are liquid films and called lamellae. These lamellae meet in lines which are called plateau borders, while these, in turn, meet in vertices. The general geometric terminology of foam is illustrated in Figure 32. [70, p. 83]

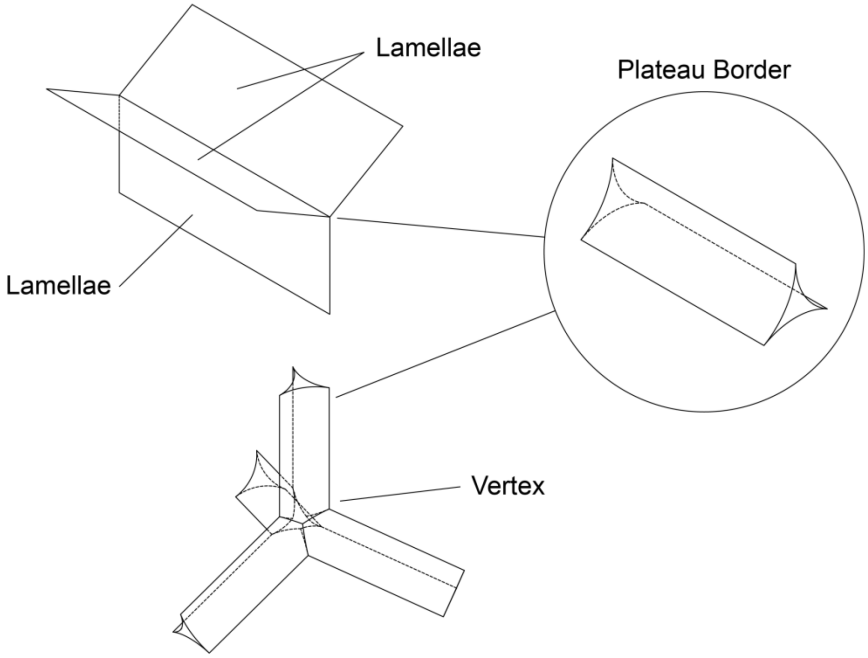

Figure 32: Liquid foam - basic geometries [70, p. 83]

To understand the stability of foam a closer look at the liquid film between the gas bubbles is necessary which is illustrated in Figure 33. The surfactants have a polar head which is oriented towards the liquid film inside and a nonpolar tail which is oriented towards the gas phase.

However, in reality, depending on the properties of the gas phase, the tails do not or protrude less from the liquid film than drawn in Figure 33.

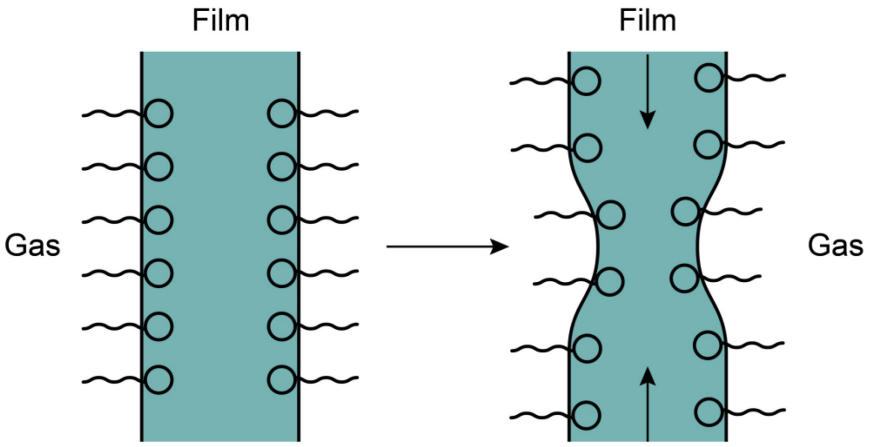

Figure 33: Gibbs-Marangoni effect [71, p. 8.7]

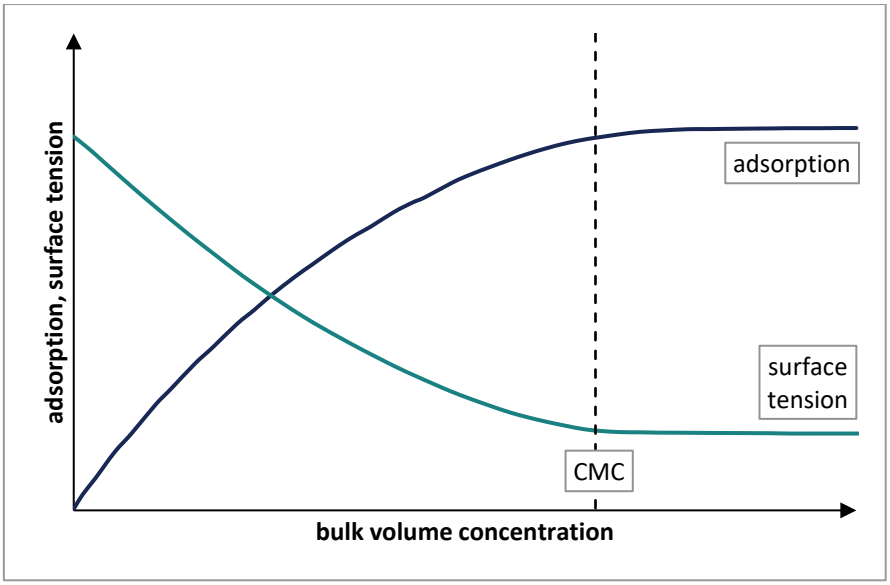

Figure 34: Surface tension and adsorption versus concentration [71, p. 8.7]

Figure 34 shows the effect of changing surfactant concentration in the bulk volume of the liquid film on the surface tension and adsorption. CMC stands for critical micelle concentration. It denotes a surfactant concentration above which surfactants aggregate into spherical groups throughout the bulk of the liquid. Above the CMC the liquid acts like a surfactant buffer which keeps the adsorption as well as surface tension almost constant. The adsorption indicates the relative amount of surfactants (adsorbate) at the liquid-gas interface. Hence it increases with increasing surfactant concentration in the bulk volume. The surface tension is reduced with increasing surfactant concentration. When combining these two relationships one can see that the surface tension or interfacial tension (IFT) increases with decreasing adsorption. In other words the higher the surface density of surfactants the lower the IFT, see Figure 35. [72, pp. 425, 426]

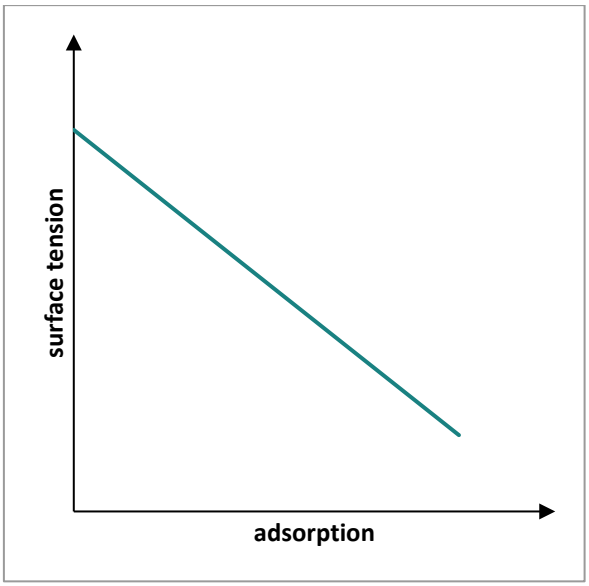

Figure 35: Surface tension versus adsorption cross plot

If the film thins due to external forces as indicated in Figure 33 on the right, the surfactant surface density or adsorption decreases an subsequently surface tension increases locally. The induced surface tension gradient counteracts further thinning causes the film to contract and become thicker. This restoring process is often referred to as healing while the antagonism between IFT and adsorption is widely known as Gibbs [73] – Marangoni [74] effect. [71, p. 8.6] A too low surface tension would, therefore, be unfavorable in terms of foam stability. However generally gas-liquid IFTs are even with very effective surfactants still above 20 mN/m. [72, p. 426]

For the following the pressure of the gas phase is assumed constant which is reasonable because of the rather low density and viscosity. The self-healing phenomenon of the liquid film can also be interpreted in terms of capillary pressure. Generally, the capillary pressure is the pressure difference across the interface between two immiscible phases. According to the Young [75] – Laplace [76] equation (**eq. 95**), the capillary pressure is inverse proportional to the principal radii of interfacial curvature. Therefore, the pressure in the thinned section is lower than in the surrounding parts of the liquid film. The resulting pressure gradient causes the liquid to flow into the thinned section until it is healed. [72, p. 426]

$$p_c = \sigma \left(\frac{1}{R_1} + \frac{1}{R_2} \right) \qquad (95)$$

p_c	capillary pressure [Pa]
σ	surface tension, IFT [N/m]
R_1, R_2	principle radii of the surface curvature [m]

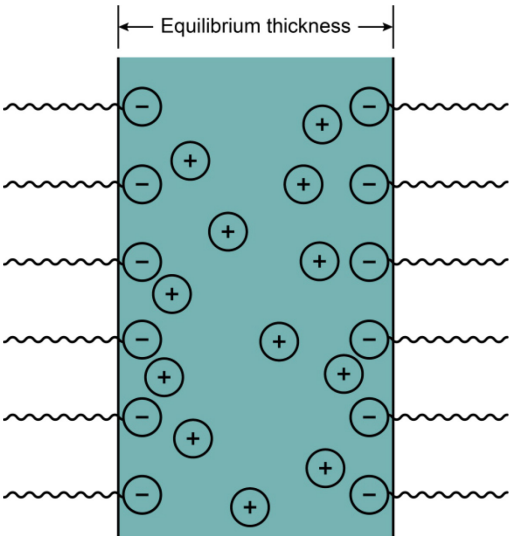

Figure 36: Electrical double layer in the liquid film [71, p. 8.10]

Without any external forces or disturbances, the liquid film develops equilibrium between repulsive electrostatic forces induced by the surfactant layers and attractive Van der Waals forces between all molecules in the liquid. The resulting film thickness is thus termed equilibrium thickness. If for any reason, the liquid film gets significantly thinner than that, it will rupture. [71, pp. 8.9-10] Spontaneous film thinning and the eventual collapse of the foam happen for one of the following reasons:

Real foam is not homogenous and there are bubbles of different sizes. Resulting from **eq. 95** the pressure in smaller gas bubbles is higher than in bigger ones or the atmosphere. The resulting difference in chemical potential causes the gas to diffuse through the liquid film towards the bigger bubbles. Therefore, small bubbles vanish and bigger bubbles become so big that the liquid film gets too thin and ruptures. This process is often called Ostwald Ripening [77] and is controlled by the bubble size distribution and the diffusivity of the gas in the liquid. [72, pp. 426, 427]

On a macroscopic view gas and liquid tend to separate due to the interaction of density difference and gravity. The liquid is drained from the films between the gas bubbles until a foam with very high GLR is left. The lamellae are very thin and meet at angles of 120°, see Figure 37. The plateau- or Gibbs border remain thicker because of their curvature the capillary pressure is locally lower and liquid is sucked in from the lamellae. [72, p. 427]

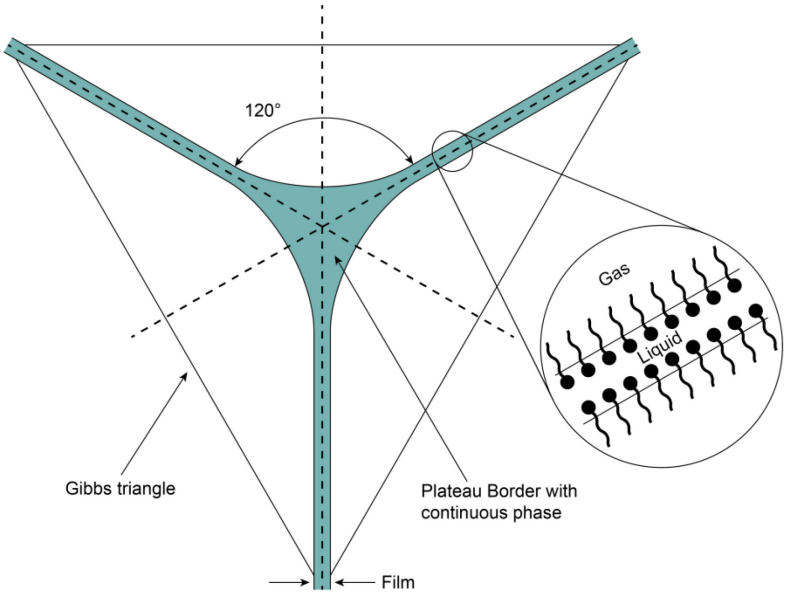

Figure 37: Geometry of plateau borders [78]

4.3.2 Critical velocity models for foam

There were several slightly different attempts made to adapt Turner's critical velocity equation (**eq. 7**) in order to be valid for foam lift application by [79], [80], [81], [82], [83], [84]. Figure 38 illustrates the idea that the liquid droplet reversal model(s) could still hold by assuming that the droplets are no longer liquid but consist of foam. Thus the two modeled phases are now gas and foam, although the foam itself is a two-phase dispersion of gas and liquid. This means that the following input parameters to **eq. 7** change by the use of surfactants. First, the interfacial tension (σ) between gas and liquid is lowered directly by the surfactants. Secondly, the droplet density is reduced from the liquid density to the foam bulk density. Furthermore, some of this modifications account for a changed droplet size. Inserting these modified parameters into **eq. 7** will result in a lower critical velocity, which is expected for foam.

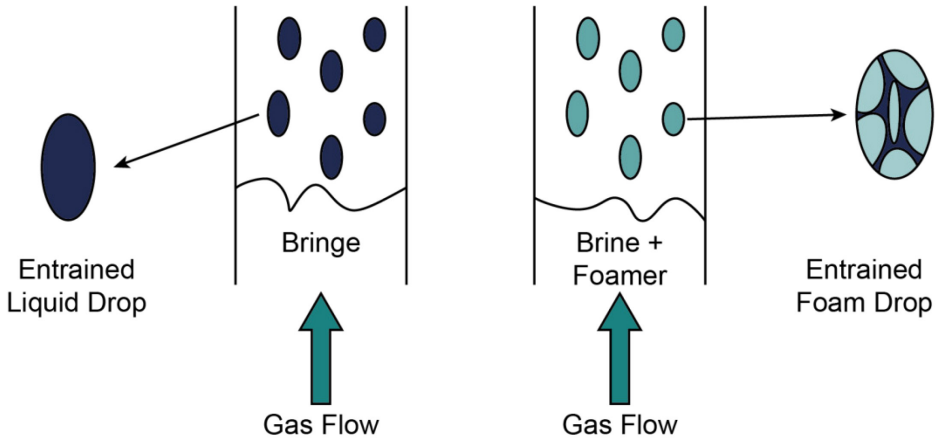

Figure 38: Turner's droplet model modified for foam [79, p. 180]

Figure 39 shows the measured influence of surfactant concentration in the liquid phase on surface tension and foam density for a commercially available surfactant product.

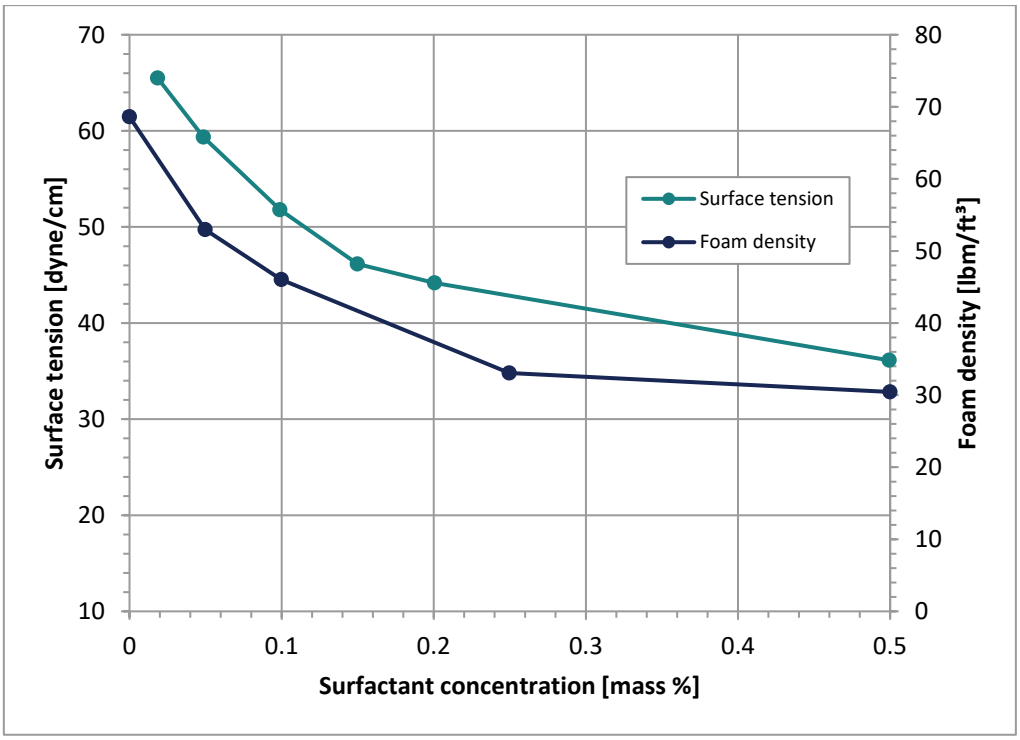

Figure 39: Effect of surfactant concentration on surface tension and foam density [82]

However since the interfacial tension appears in **eq. 7** to the power of 0.25 a decrease in surface tension by 50% leads to a critical velocity decrease of 16%. This does not match the reduction in critical velocity observed from field data. [85, p. 368] Recently attempts were made to derive a new model for predicting the critical velocity and pressure drop for vertical gas-foam flow. [86] The model is based on the liquid film flow reversal transition criterion from [87] and is modified using data collected from benchtop and large-scale flow experiments done by [88].

4.3.3 Surfactant types

As already mentioned the surfactant molecules comprise of a water-soluble (hydrophilic, lipophobic) and an oil-soluble (hydrophobic, lipophilic) part. This causes the molecules to aggregate at the water-nonwater phase interface. If the non-water phase is a gas this interface can be referred to as liquid surface, hence the name ***surf***ace ***act***ive ***a***gen***ts***. Surfactants are usually classified into the following categories according to their ionic character: [2, p. 155]

Nonionic surfactants are often made up of polyoxyethylated alcohol- and phenol-compounds. Opposite to many other substances, nonionic surfactants are more soluble in colder water. If the water is heated, the solubility is reduced and eventually, at the cloud point of approximately 66°C, the surfactant precipitates out of the solution in significant amounts and the solution becomes cloudy. High salt concentrations lower the overall solubility and thus the cloud point. Polyoxyethylated surfactants can range from water- to oil-soluble. Since they are nonionic they are very little affected by the activity or chemical composition of the produced water. Hence they are recommended in case the brine composition is unknown. Furthermore, compared to ionic surfactants they cause fewer emulsion problems. [2, pp. 155, 156]

Anionic surfactants are typically created by sulfating nonionic surfactants. Adding the SO_4 makes the surfactant more anionic and thus polar, which increases the water solubility. They also exist in different homologs. The ones with 10 to 12 carbon atoms are in the mid-range of water-oil solubility and recommend for deliquification. Several anionic surfactants are negatively affected by high salt concentrations. [2, p. 156]

Cationic surfactants are often more effective in brines compared to freshwater. Examples are different quaternary ammonium compounds. The low molecular weight cationic surfactants have high ability to foam hydrocarbon-brine mixtures. Higher molecular weight ones are better for high hydrocarbon percentages but they are less effective in brine. Cationic surfactants can cause severe emulsion problems, especially at high concentrations. [2, p. 156]

Amphoteric surfactants are cationic in acids, anionic in alkaline solutions and nonionic in neutral solutions. They were found to be more effective at higher temperatures (around 93°C) compared to other surfactant types while being less effective at ambient temperatures. [2, p. 156]

Generally, foaming hydrocarbons, here condensates, is less effective than foaming water because they cannot develop polar bonds with the surfactants. Liquids containing more than 70% to 80% of hydrocarbons are rather difficult to foam and more expensive foaming agents have to be used. However, many gas wells, relevant for deliquification, produce either just water or water with a low fraction of condensate. [2, p. 158]

4.3.4 Implementation

There are several options on how to get the surfactants down to the liquids to be lifted. They can be grouped into batch treatments which are performed on demand and continuous injection.

For a ***batch treatment,*** the well is often shut in and the severity of liquid loading is estimated from the casing-tubing pressure difference. From this estimated liquid volume the needed surfactant quantity is inferred. This is then mixed into 20 gallons (76 l) of previously produced fluid or compatible water. This mixture is then lubricated or pumped into the tubing. Alternative to liquid surfactants, so-called ***soap sticks*** can be used. Batch treatments are applicable on wells that require unloading not very often. [2, p. 166]

Continuous foam injection is realized by injecting liquid down the casing-tubing annulus or through the tubing, in the rare case that the annulus is used for production. If the gas well is completed with packer an additional capillary string/chemical injection line has to be installed. This line is either run inside the tubing or is banded to the outside of the tubing. At the surface there usually is the surfactant tank and a precise metering pump. The pump can be either electrically driven or pneumatically with gas from the annulus. The surfactants coat the inside of the capillary string. To avoid that, the solution should be either diluted or washed down with a compatible fluid. It is recommended to dilute 1 part of surfactant concentrate in 10 parts of water. In low-temperature environments or in winter the diluting liquid should contain 50%

ethylene glycol. **Eq. 96** states the necessary surfactant concentration in the surface tank for a fixed injection rate. The minimum effective foam concentration is often assumed from 0.1% to 0.5%. After some time when a big part of the liquids is lifted, the production will increase and the surfactant can be reduced. The goal is a maximum gas production at the lowest amount of injected foamer. [2, pp. 166-170]

$$C_s = C_E \frac{L_p + L_i}{L_i} \qquad (96)$$

C_s surface concentration [%]
C_E minimum effective concentration [%]
L_p liquid production rate [m³/d]
L_l chemical injection rate [m³/d]

4.3.5 Surface de-foaming

At the surface the produced foam has to be broken in order for gas, oil and water separation to work effectively. If the amount of surfactants used is not too high the foam deteriorates on its own due to the previously mentioned reasons after sitting still for some time. The speed of deterioration can be enhanced by lowering the surfactant concentration by adding water. If water containing nonionic surfactants are heated up above the cloud point, the concentration of dissolved, effective surfactants is reduced and hence also foam stability. There are also chemicals, often called de-emulsifier, which counteract the effect of the foaming surfactants. For the reason of surface de-foaming, the foam should be optimized towards being just stable enough to lift liquids but still easy to break. [2, p. 150]

4.3.6 Summary

Foaming is a suitable deliquification method for a liquid that consists of more than 80% water otherwise it is difficult and expensive. However, most gas wells produce liquids with high water content. Before field application, different surfactants should be tested with a liquid sample from the wellbore under consideration. Foaming can be combined with certain other lift methods and can also be used to stabilize erratic gas production rates. In the rather rare cases of packerless completions, the surfactants can be poured into the annulus either batch-wise or continuously. Alternatively, solid soap sticks can be, manually or automatically, thrown down the tubing. In case a packer is installed, a capillary injection line is usually banded to the outside of the tubing and injects below the packer. [2, pp. 174-175]

4.4 Intermittent production

In order to control the oscillating pressure phenomenon, described in *2.5.6 Annulus heading* and reduce its negative impacts a so-called intermitter valve can be installed in the tubing at the wellhead. This is a motor valve which is controlled by the casing pressure. The controlled heading cycle stages are described below and illustrated in Figure 40.

1. The gas percolates into the annulus and raises the casing pressure. The increased casing pressure opens the motor valve. Gas has accumulated in the top of the tubing which now starts to flow and expand. The reducing pressure also makes the liquid-gas mixture below the gas column flow upwards.
2. The pressure reduction propagates downwards and into the annulus. Thus the gas in the annulus expands and displaces the liquids into the tubing. Consequently the weight of the fluid mixture in the tubing increases which is recognizable by a reduction in tubing head pressure.
3. When the expanding annulus gas breaks through into the tubing the tubing pressure at the wellhead rises again.
4. The gas expansion in the annulus goes along with a pressure reduction at the casing head. When the casing pressure falls below a predefined minimum the motor valve is actuated to close. The flow into the well still continues while liquid and gas start flowing into the annulus again. Thus the existing gas in the annulus is compressed and the casing pressure rises until the predetermined maximum is reached. Then the motor valve opens once more and the cycle repeats.

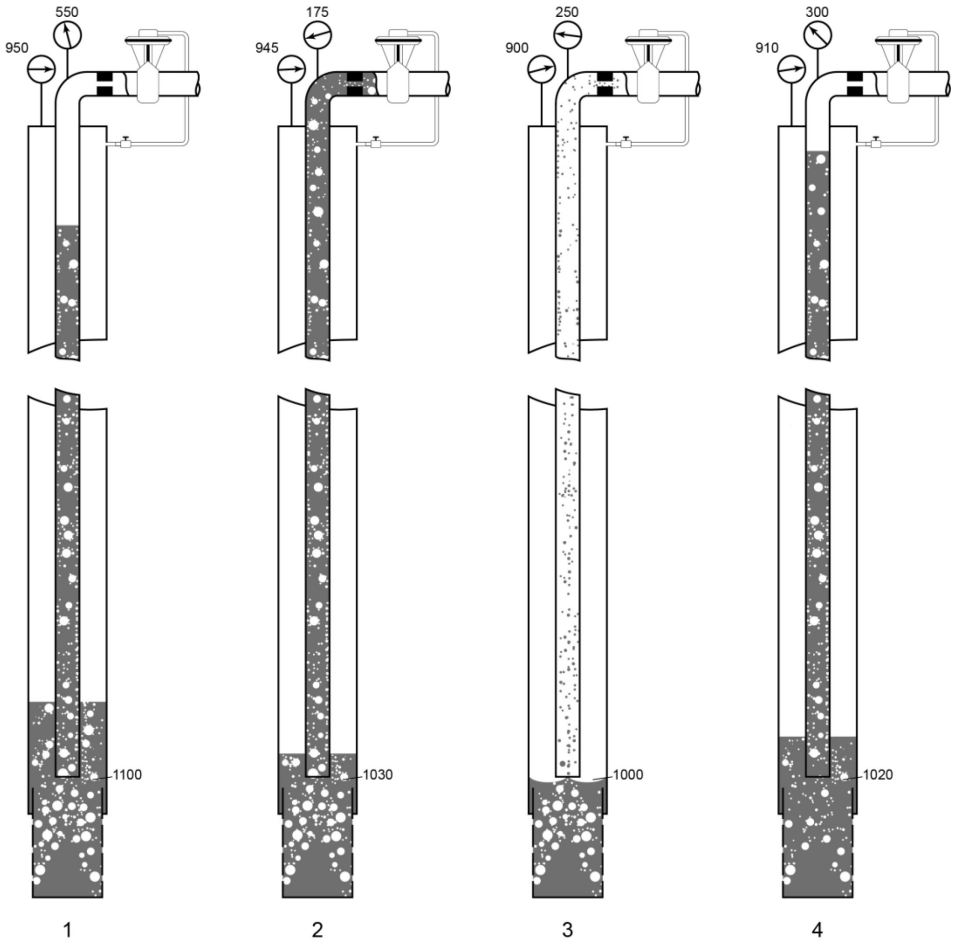

Figure 40: Casing controlled intermittent flow [42, p. 137]

When wells suffer under annulus heading installing a casing-pressure-controlled intermitter valve will increase the gas production rate and lengthen the overall lifetime of the well. An intermitter is recommended as a better alternative to choking down a heading gas well and to

regulate, stabilize and increase the flow of new but low GLR wells until they reach steady flow at the desired rate. However, it should not be installed in case a pump would yield better results. For operating parameters, the choke bean size should be just large enough to ensure a continuous casing pressure drop during the flow period but not any larger. The opening and closing casing pressures should be chosen in a way that gas flows around the end of the tubing, and tubing pressure can build up. Leaving the valve open longer is not necessary and not desirable. [42, p. 137]

4.5 Plunger lift

The previously proposed intermittent production still has a lot of slippage between gas- and liquid phase. Therefore, the lifting of the liquids, or deliquification, is rather inefficient. Plunger lift is an enhancement to intermittent production by minimizing or eliminating slippage and liquid fallback. The plunger is a piston that travels up and down the wellbore and acts as a barrier or seal to separate gas and liquids. It is considered an artificial lift method but uses only the energy from the reservoir for lifting. Thereby it does not matter, whether it is a high liquid content gas well or a high GLR oil well it can be used for both and works the same.

4.5.1 Plunger lift cycle and operation

Figure 41 illustrates a plunger lift cycle distinguishing between five different stages:

1. The well is shut in and the pressure in the wellbore rises slowly towards the reservoir pressure.
2. When the pressure in the casing has reached a certain value the tubing valve at the surface is opened. The accumulated gas in the tubing is produced thus the pressure in the tubing lowered. Therefore, the gas in the annulus starts to expand and push the plunger together with the liquid slug on top of it to surface.
3. The liquid slug reaches the wellhead and is discharged through the tubing. Afterwards, the pressure of the flowing gas holds up the plunger.
4. Since the storage capacity of the casing-tubing annulus and the near wellbore region is limited the pressure and the production rate starts to decline after some time. Also the gas velocity decreases and naturally liquid starts to accumulate downhole.
5. After a certain time, the valve at the surface is shut and the plunger starts traveling downwards. In the liquid-filled tubing section, the plunger velocity becomes rather slow. Then the cycle starts over. [2, pp. 99, 100]

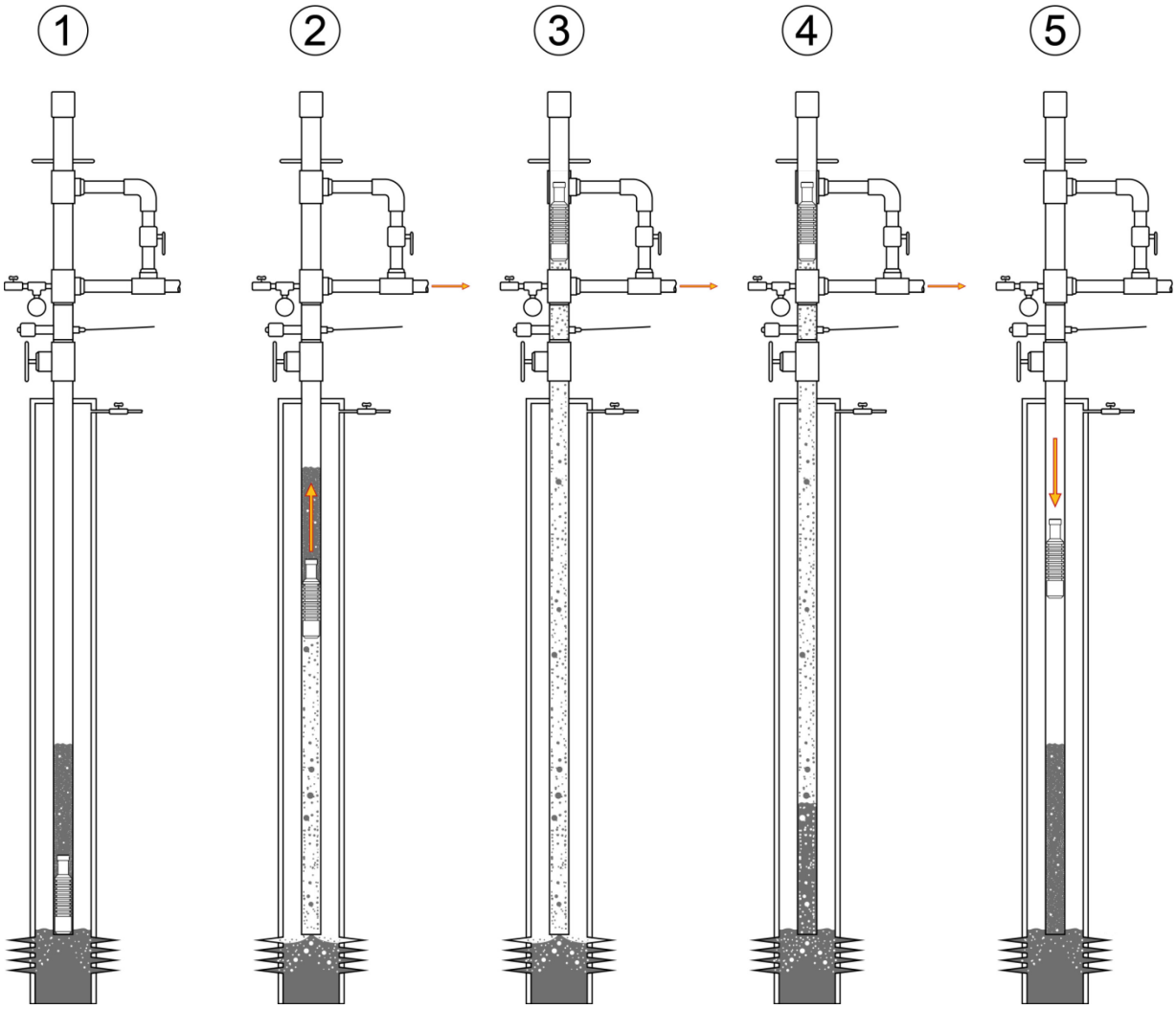

Figure 41: Plunger lift cycle [2, p. 99]

Figure 42 shows a typical pressure and flowrate response during a plunger lift cycle in a well without packer. The difference between casing pressure and tubing pressure at the end of the shut-in period indicates the height of the liquid slug in the tubing. After the valve is opened the tubing pressure quickly equalizes with the flow line pressure and the casing pressure starts to slowly decrease. The spikes in tubing- and flowline pressure as well as the flow rate signal the arrival of the plunger. The casing pressure is at its minimum when the plunger arrives or shortly thereafter. At this point, the gas in the casing is completely expanded or blown down. As liquids start to accumulate in the tubing the casing pressure will go up. After shut in the pressure in the casing builds faster and the tubing pressure has a sharp increase due to the elimination of friction pressure losses. After a short time period, the tubing pressure usually follows the casing pressure with an offset due to the hydrostatic pressure of the liquid slug. When the casing pressure has reached the predetermined value or after a certain time period the cycle starts over again. [89, pp. 844, 845]

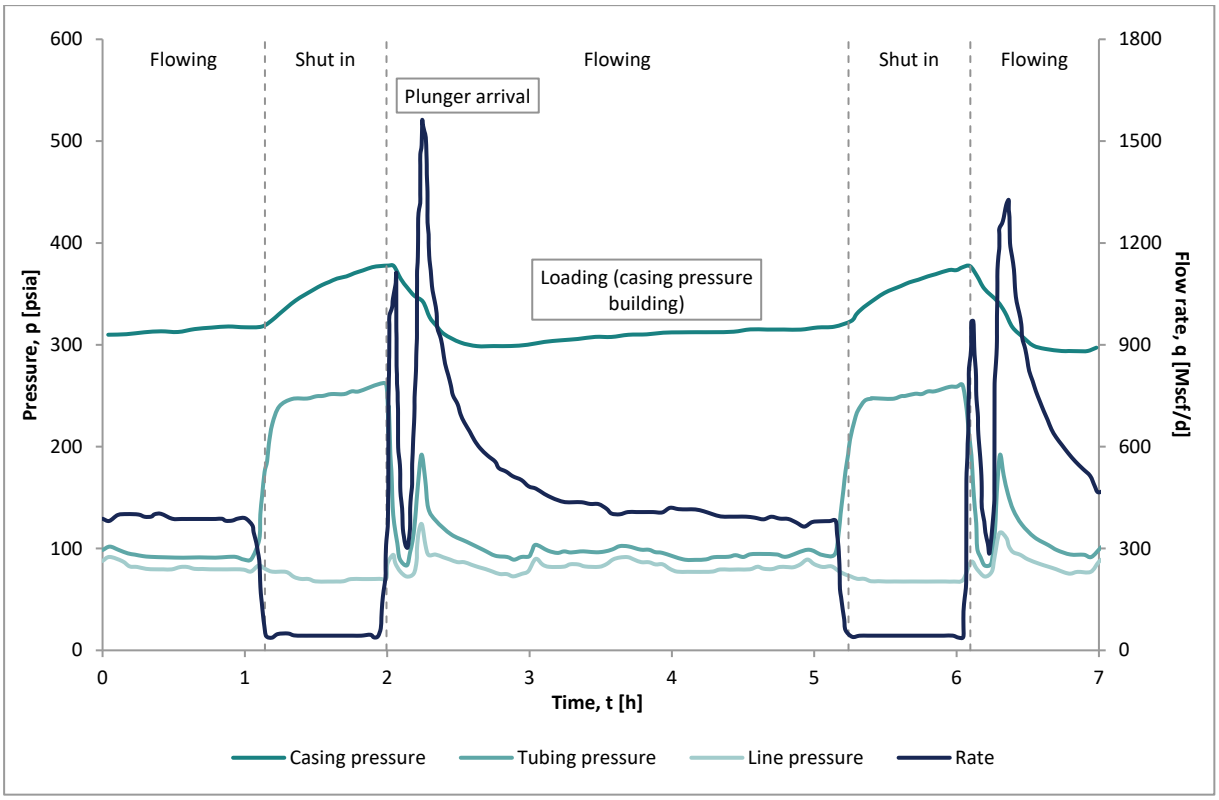

Figure 42: Typical pressure response of a plunger lift cycle [89, p. 844]

4.5.2 Plunger lift feasibility

Although the plunger lift system itself is rather cheap, the installation, additional equipment, downtime and lost production in case of a failure can be significant. Therefore, it is important to evaluate beforehand whether plunger lift is applicable for a specific well. There are a few rules-of-thumb that have proved useful over the years.

First of all the well should have a high GLR, at least around 233 Sm^3/m^3 for every 1000 m true vertical depth (TVD). This is equivalent to 400 scf/bbl for every 1000 ft of TVD. However, this rule does not consider the reservoir pressure and it is assumed that no packer is installed. It can give falls predictions for wells that are right at the border.

Figure 43 presents a more accurate way to judge on the feasibility of plunger lift for a 2 in and a 2 ½ in plunger. The net operating pressure is the difference between maximum casing pressure, that is reached at the end of a reasonable shut-in period, and the flowline pressure. Reasonable shut-in period means in the range of hours, not days or weeks. The line pressure has to be the flowing wellhead pressure, not the static one. The difference lies in the friction in the flow lines of the gathering system. One would select the net operating pressure on the horizontal axis, move up to the according well depth and see whether the resulting GLR is lower than the actual one.

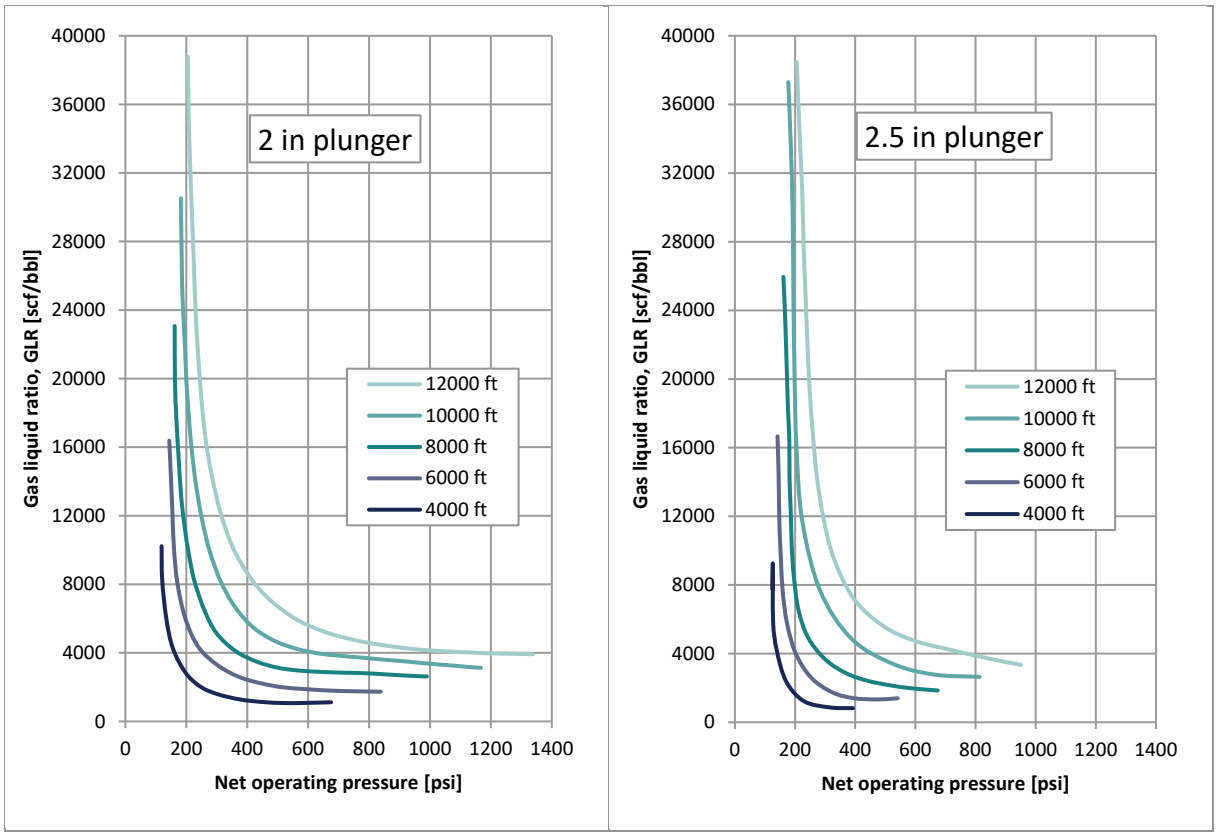

Figure 43: Plunger lift feasibility for a 2 in and a 2 1/2 in plunger [90]

The technique using the nomographs presented in Figure 43 has the shortcoming that it ignores the casing volume which is important. The bigger the casing size the more energy is stored at the same pressure. [2, pp. 102-105]

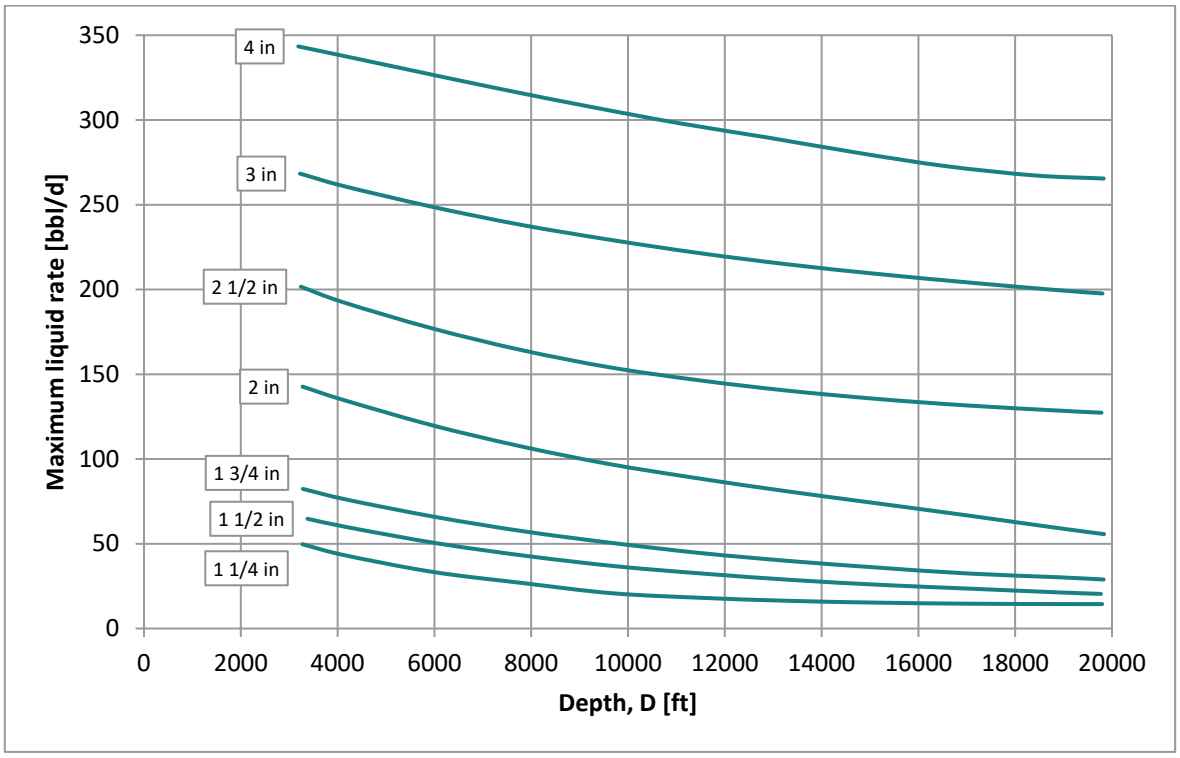

Figure 44: Maximum liquid production for a plunger lift system [91]

Figure 44 gives a suggestion about the maximum acceptable liquid production rate versus depth for different tubing/plunger sizes. This graph is used by selecting the well depth at the horizontal axis, moving up to the used tubing size and the maximum allowable daily liquid production can be read from the vertical axis.

As already stated the casing volume has a big influence on the plunger lift performance, therefore packerless completions are preferred. Nonetheless, there were successful plunger lift installations with a packer, which had sufficient reservoir pressure, good productivity, and a high GLR. With Figure 45 the necessary GLR for wells with and without packer can be estimated.

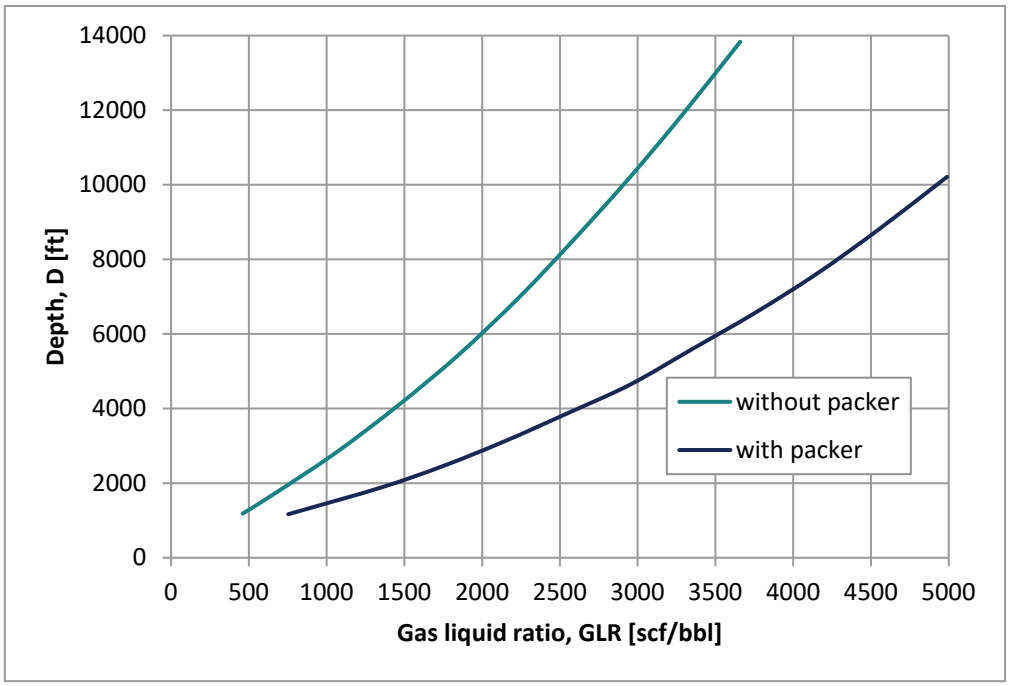

Figure 45: Minimum GLR for plunger lift with and without packer [91]

It is not only important to decide whether a plunger lift system would work at all but it is also interesting how it will perform compared to other deliquification methods. Nodal analysis would be a great tool to evaluate the expected performance. However, since plunger lift is a cyclic process there is no constant flowrate or node pressure. A model was developed by [92] to get an average bottom hole pressure for the plunger lift cycle. The averaging is done in a way that the flow rate resulting from the pressure will match the actual average flow rate. This is calculated for different flow rates resulting in what could be considered an “equivalent VLP”. Figure 46 shows how an example comparison between velocity strings and plunger lift could look like in nodal analysis. [2, pp. 107, 108]

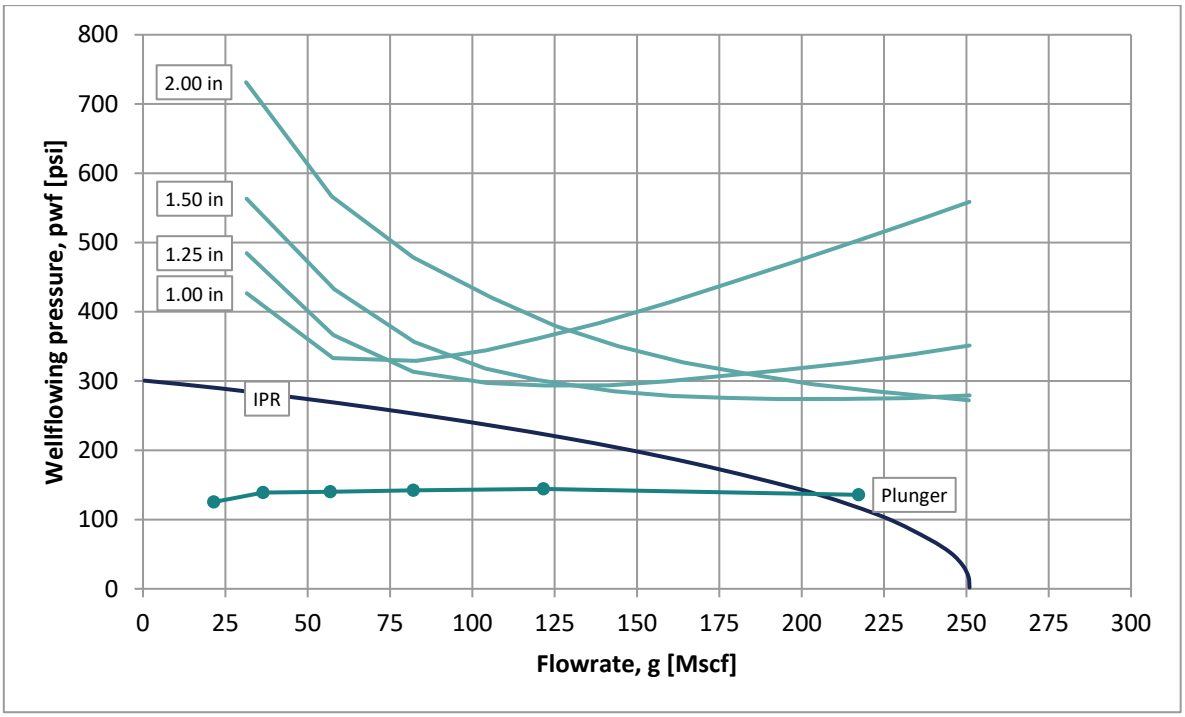

Figure 46: Plunger lift performance in nodal analysis [92]

4.5.3 Components of a plunger lift system

Figure 47 shows an overview of a typical plunger lift installation. It consists at least of the plunger itself, a plunger stop, usually including a bumper spring, a lubricator, a catcher and a motor valve. Additionally, there can be a standing valve in the plunger stop, an arrival sensor, several pressure sensors (tubing, casing, flowline), secondary flow port, bleed and bypass valves as well as control equipment.

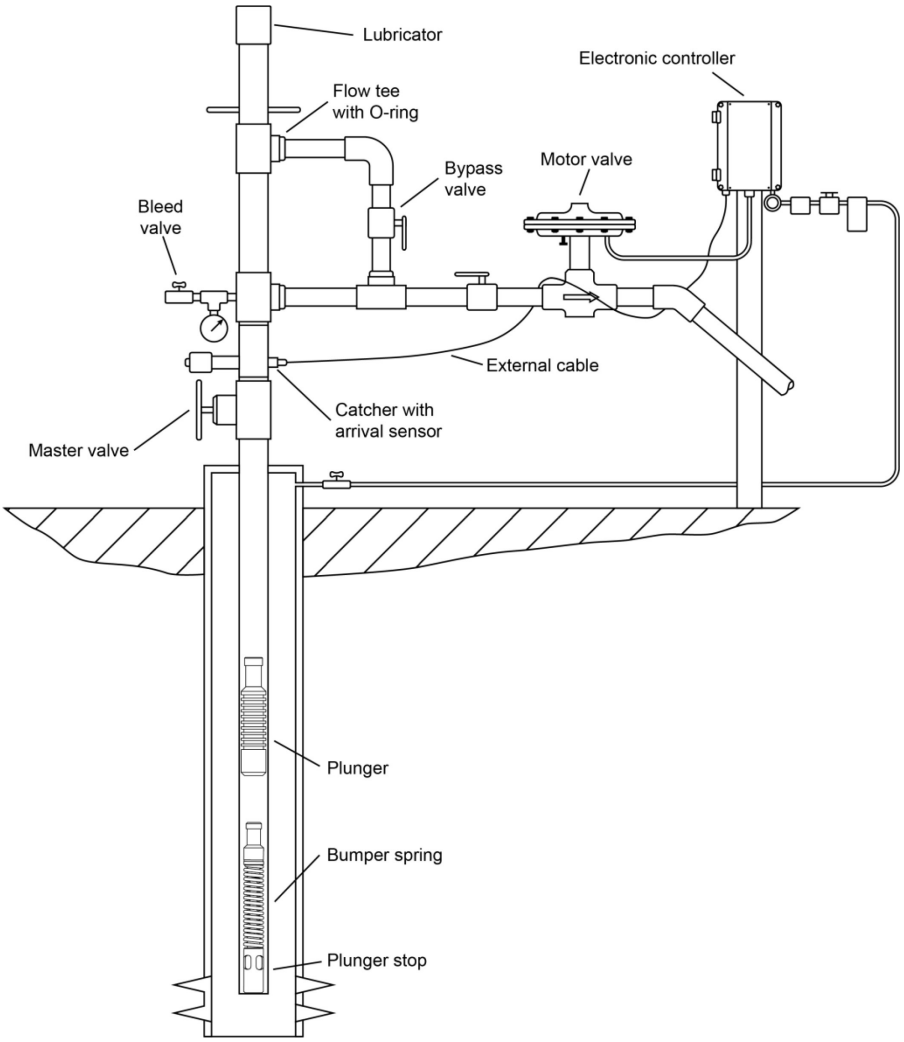

Figure 47: Typical plunger lift setup [92, p. 235]

4.5.3.1 Plunger stop

The plunger stop is usually placed somewhere near the end of the tubing and it marks the endpoint of the plunger travel.

The ***seat-cup stop*** assembly has cups and seats in a profile nipple similar to an insert sucker rod pump. They are the most common type of plunger stops since they can be seated and retrieved easily by slickline. Although it can even be seated simply by dropping it down the tubing, it is recommended to run it on slickline to ensure proper seating.

The ***tubing stop*** can be placed anywhere inside the tubing. It has slips, which, when activated open up and bite into the inside wall of the tubing. The tubing stop is convenient when the tubing was run without a seating nipple or the stop has to be placed some distance above the end of the tubing.

The ***collar stop*** has special slips that are designed to be set in the collar recesses. It is very similar to the tubing stop but can only be seated at whole tubing lengths. Seating and retrieving is very easy so much so that they can come unseated by high gas flow.

The ***pin-collar stop*** is a regular tubing collar with a pin welded into the inside of it, which is screwed to the lower end of the tubing. It is very low cost, has a low-pressure drop and is very simple. However, it eliminates the possibility to run in tools past the end of the tubing and replacing it without pulling the tubing is not possible. [89, pp. 864, 865]

4.5.3.2 Bumper spring

The bumper spring is not mandatory for a plunger lift installation. It is installed to prevent damage to the plunger, plunger stop or tubing by the severe impact of the plunger in case the tubing is completely dry without any liquid accumulation. It is especially useful for more advanced but also complicated and fragile plunger types. [89, pp. 865-866]

4.5.3.3 Standing valve

To maximize the liquid lifting performance it is important that a maximum of liquid stays in the tubing. The plunger itself has no static sealing capabilities otherwise it would not travel down through the liquid slug but float on top of it. To overcome this, a check valve can be integrated into the plunger stop. This is more critical when the reservoir pressure is very low and the liquids would quickly flow back into the near wellbore zone of the formation. However when the well loads up due to any reason the tubing and casing cannot equalize anymore. Therefore, there are types of standing valves that have small grooves in the seat to allow for a very small amount of leakage. This allows for albeit slow equalization. Of course, there is an additional pressure drop across the valve, and sand or scale can plug or damage it. [89, p. 866]

4.5.3.4 Strainer nipple

A strainer nipple is a kind of filter that is screwed to the end of the tubing to prevent sand and debris from entering the tubing. However, there is an increased risk of plugging. [89, p. 866]

4.5.3.5 Lubricator and Catcher assembly

The ***lubricator*** marks the upper end of the plunger travel. It is built in a way that it can be easily opened but still seals when screwed together hand-tight. In combination with the catcher mechanism, it is used to retrieve and deploy the plunger. To dampen the impact of the plunger a shock spring is installed. The flow ports tie the tubing into the flow line. During the flow period, the plunger is held up just by the fluid pressure so it tends to float right at the flow port which means it acts like a choke. To mitigate that, many lubricators have two flow ports. It is important that the lubricator is of matching ID and is installed exactly plumb. Otherwise, the arriving plunger will bend it straight and this back and forth will cause the lubricator assembly to fatigue and fail.

A ***lubricator extension*** is an optional, additional pipe that is placed between the upper flow port and the end of the lubricator. When the plunger passes the upper flow port it loses the driving force because the gas discharges to the flow line and the liquid in front of it acts as a cushion. The additional length provides for a gentler deceleration. Lubricator extensions are also necessary in case a long plunger type is used. [89, pp. 866-868]

4.5.3.6 Plunger sensor

Plunger (arrival) sensors were formerly used to simply count the number of plunger arrivals. Nowadays they are used in combination with advanced controllers to infer the travel speed of the plunger and subsequently optimize the flow and shut-in periods. However, in case, this sensor fails the controller could permanently shut in or even worse, the well could load up. Usually, they are implemented either as magnetic or acoustic sensors. The current from cathodic protection can interfere with the measurement of the sensor. [89, p. 868]

4.5.3.7 Motor valve

Very often pneumatically actuated valves are used but also hydraulic and electric actuation is possible. It is very important to keep these valves in good shape because already a small leak could cause the well to load up. Also, the sizing is important a too small valve acts as a choke and causes an additional parasitic pressure loss. [89, p. 868]

4.5.3.8 Plunger

There is a variety of different plunger types available on the market. They range from very simple but robust to very sophisticated but therefore more fragile. They are even often customizable and built to order. In the following, a few of the more common ones are listed.

The ***bar stock*** plunger is a very simple, sometimes hollow metal cylinder. The outside has grooves, spirals or other turbulence creating shapes. The gas which is blowing by creates turbulence and thus seals the plunger. It has the least effective sealing capabilities but is very durable.

The ***wobble washer plunger*** has many loose fitting washers stacked on top of each other. Its advantage over the bar stock plunger is that the lateral freedom to movement allows the plunger to pass by some tubing imperfections or small obstructions. However, its seal is still very bad. There is a high risk associated with the washers breaking and falling down into the bumper spring. To fish these metal fragments can be a rather tedious job.

The ***pad plunger*** is very popular because they offer a good balance between robustness and sealing capabilities. It has several metal pads, which are spring loaded so that they stay in good contact with the tubing wall even in case of slight shape changes. However, due to the spring loading, it also has higher mechanical friction with the tubing and falls more slowly. If sand or debris gets behind the pads of the plunger, they cannot retract and the plunger will most likely get stuck.

The ***sealed pad plunger*** is a modified version of the regular pad plunger. The back side of the pads has a tongue which fits into a groove that is machined into the plunger main body. This reduces the gas blow-by behind the pads and thus increases the overall seal. Alternatively, also other types of seals can be implemented behind the pad.

The ***retractable pad plunger*** incorporates a shift rod. This rod is mechanically linked to the pad and extends as well as retracts them. When the plunger arrives at the wellhead it hits the

lubricator and the shift bar is actuated. This causes the pads to retract to allow for a fast down travel. The impact on the shift bar by the plunger hitting the bumper spring causes the pads to extend again to provide a good seal during the up travel. The mechanical interaction of several moving parts makes this plunger a lot less durable and reliable.

The ***brush plunger*** offers a very good seal and is still able to travel down fast. However, the synthetic fibers of the brush bristles are prone to wear quickly. If a stiff bristle is chosen the wear is less severe but the OD of the brush cannot be much larger than the tubing ID otherwise the plunger will get stuck. Softer bristles, on the other hand, wear quicker but the brush can have an overall larger OD allowing for more wear. Since some polymer materials are susceptible to heat this is also a concern.

The ***internal bypass*** can basically be built into any plunger type. Similar to the one with retractable pads it has a shift rod that opens and closes a bypass passage through the plunger. There is also a version of this without any shift rod which consists of the plunger itself and a separate ball beneath it. They fall separately but rise as one unit. A bypass passage generally allows for a faster down travel.

The ***side-pocket-mandrel plunger*** is a special plunger designed to work in gas lifted wells, where conventional plungers would get stuck at the side pocket mandrels. To cope with the significant ID increases and provide a continuous seal, also at the side pocket mandrels these plungers are longer, usually from 5 ft to 20 ft (~1.5 m to 6 m). This type is also useful when the completion string contains any other short segments with increased ID. [89, pp. 870-873]

4.5.4 Plunger lift design considerations

A more efficient seal reduces the slippage and allows therefore for a slower plunger travel. The necessary energy and pressure are thus lowered. [93] Also the plunger travel speed is an important parameter. A slow plunger causes more gas to slip by the plunger, whereas high plunger velocities cause the plunger to be pushed through the liquid slug. The velocity is optimal when the gas blow-by is just large enough to create the turbulence necessary for sealing. This is illustrated in Figure 48. [89, p. 869] Poorly sealing plungers need velocities from 4 m/s to 6 m/s while good plungers get along with 2 m/s to 4 m/s. [93]

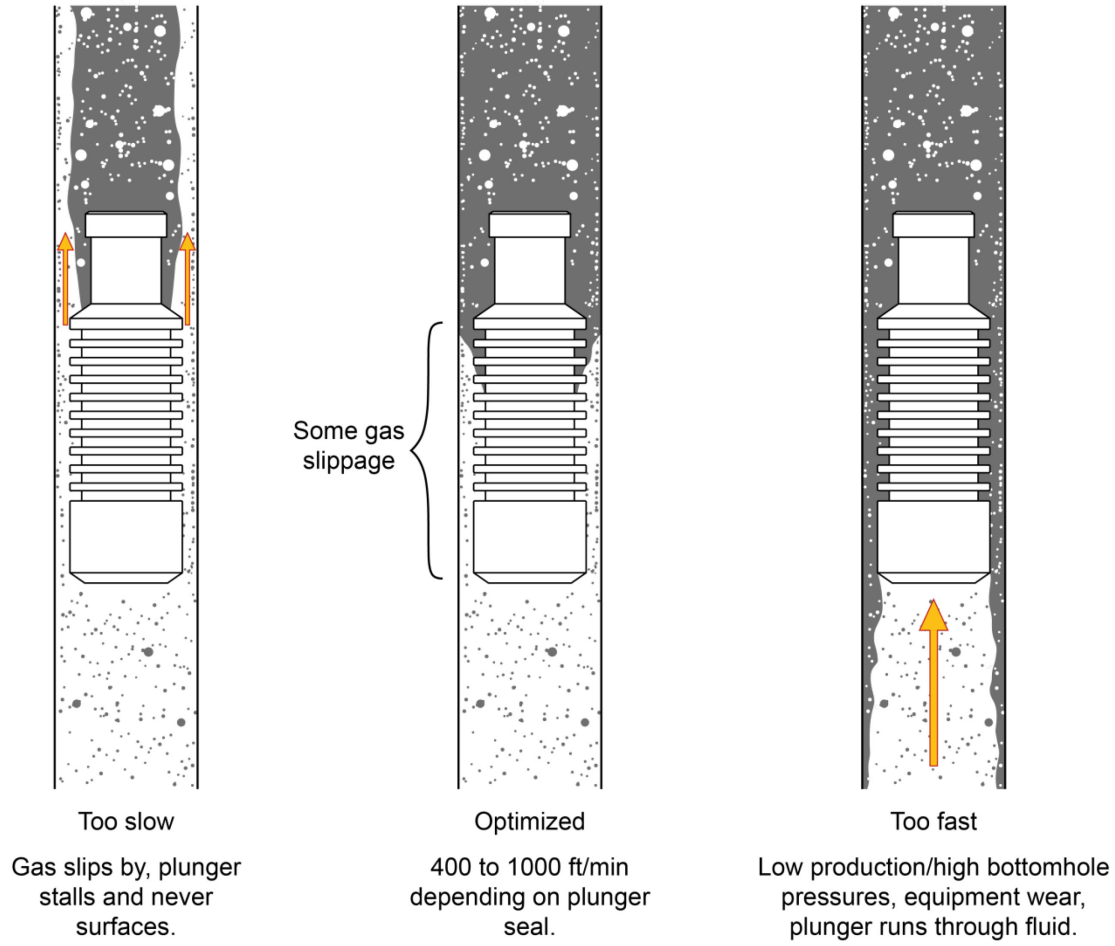

Figure 48: Plunger travel speed optimization [94]

For wells with strong IPR and thus fast pressure build up a faster plunger descent would reduce shut in duration as well as bottom hole pressures. However, if the pressure has not reached the desired value when the plunger reaches the bottom a fast plunger descent will not yield any benefits. The plunger-descend velocity depends on the plunger type, tubing inside wall condition, and inclination of the well. Common plunger descent speeds in gas-filled tubing lie between 2.5 m/s and 5 m/s but also extreme cases of 1 m/s and 10 m/s were documented. In liquid filled tubing the plunger travels downwards with usually 0.8 m/s to 1.3 m/s but also extremely low values from 0.13 m/s to 0.25 m/s were reported. [94] [93] [95] [96]

Of course, the plunger size is determined directly by the tubing ID. However, when comparing the nomographs for the 2 in and the 2 ½ in plunger in Figure 43 there is an advantage for the bigger plunger. This is because a certain volume of liquid causes a higher column in the smaller tubing and thus causes a higher hydrostatic pressure, which is illustrated in Figure 49. Hence it takes a lower casing pressure for lifting the same amount of liquid with a bigger plunger. This is contrary to the idea of velocity strings. So during tubing size selection, when liquid loading is expected it has to be decided whether to go for a small tubing to stay above the critical velocity as long as possible or expect to use a plunger in the future which would benefit from a bigger tubing. [89, p. 862]

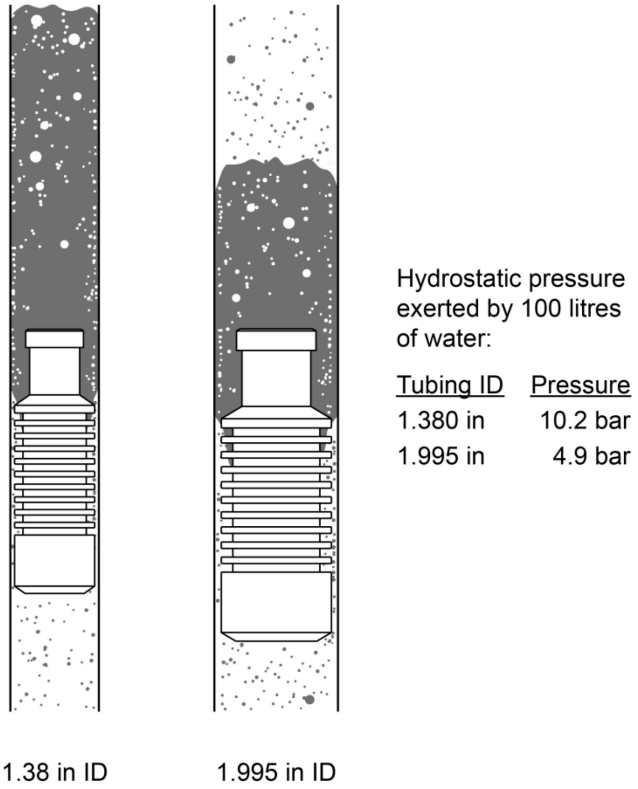

Figure 49: Effect of tubing/plunger size on the performance [94]

Besides the tubing size also the setting depth of the production tubing is critical. Also with plunger lift, the end of the tubing should be as close to the top perforations or in the upper third of the perforated interval. Setting the tubing too high can cause the interval from the perforations up to the tubing to be permanently filled with liquid which adds to the hydrostatic pressure drop. Setting the tubing too low is even worse because the liquid that accumulates during the shut-in period in the annulus has to flow down below the perforations before entering the tubing. And during the flow period, the liquid from the casing enters the tubing behind the plunger. On the one hand, this means additional pressure is needed to lift the plunger. On the other hand, the whole idea of plunger lift is undermined when part of the liquid is behind the plunger, there will again be a lot of liquid fall-back and the well might load up. [89, p. 863]

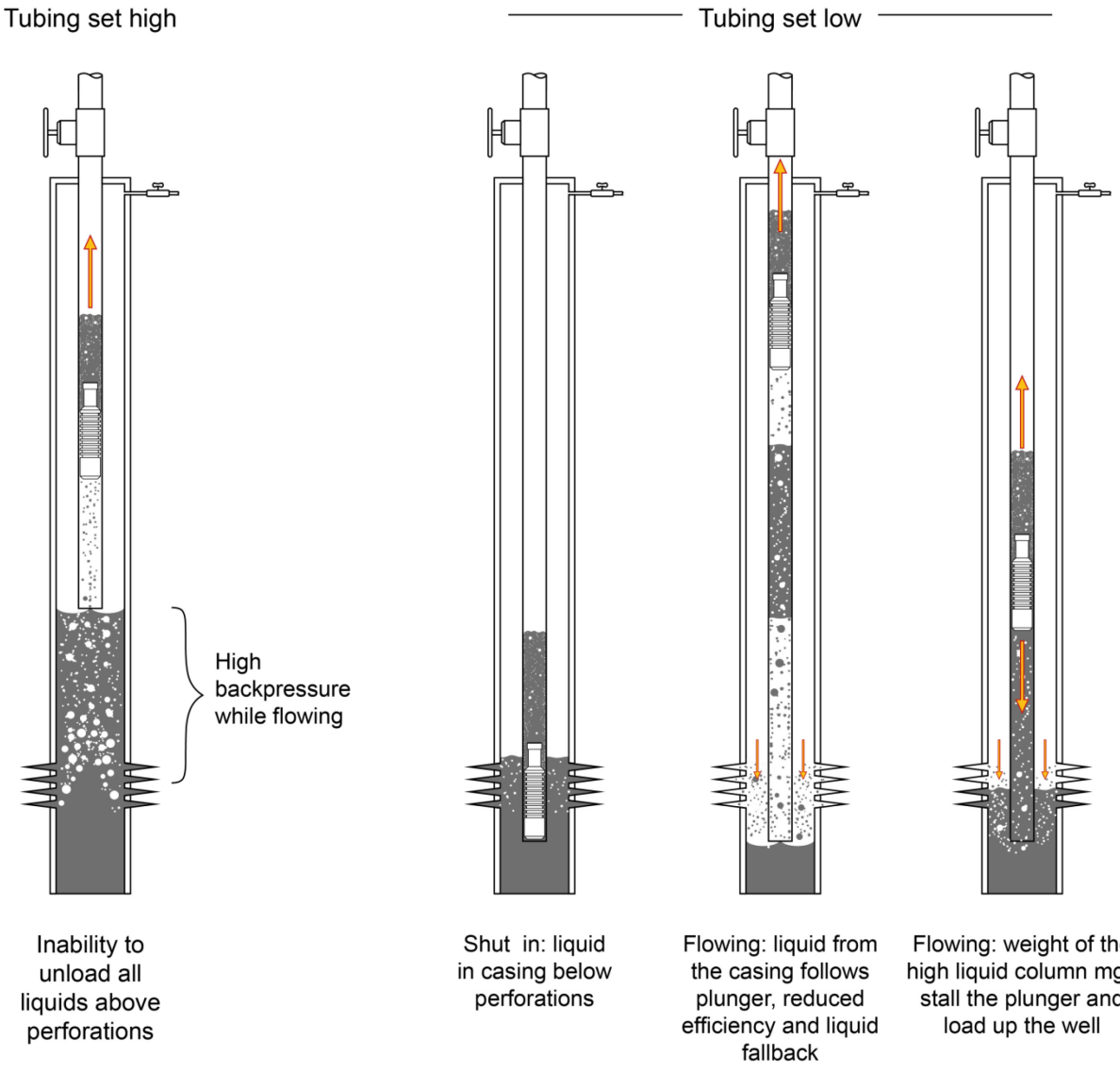

Figure 50: The effect of tubing setting depth on the plunger lift system [94]

4.5.5 Plunger lift models

Generally, the shut-in period controls the available lifting force with the reservoir pressure being the limit. The inflow performance and wellbore storage control how fast the pressure builds. The length of the flow period, on the other hand, controls the amount of liquid that is allowed to accumulate during one cycle. The longer the flow period the bigger the liquid slug eventually if the flow period is too long the slug will be too big and the well is loaded. [89, p. 845]

Naturally, the highest overall gas flow rate is reached when the average bottom hole pressure is the lowest. The lowest average BHP is reached with the shortest shut in time. So the recommended approach is to go for the lowest possible shut in time which is dictated by the time it takes the plunger to descend. The casing pressure that is built in this time limits, in turn, the volume of the liquid slug an thus the duration of the flow period. [97] [98] [94]

To estimate the required casing pressure and thus the duration of the shut-in period, there is a rule of thumb that the hydrostatic pressure caused by the liquid slug above to plunger can be 50% to 60% of the net operating pressure. The net operating pressure was previously defined as the difference between casing build pressure ($p_{csg,max}$) and maximum flow line pressure ($p_{l,max}$). This relationship is expressed with **eq. 97** and rearranging yields the unknown casing build pressure, **eq. 98**. This criterion is considered a rather conservative estimate of the pressure requirements. [89, pp. 850, 851]

$$p_{l,h} = a \cdot \left(p_{csg,max} - p_{l,max}\right) \tag{97}$$

$$p_{csg,max} = \frac{p_{l,h}}{a} + p_{l,max} \tag{98}$$

$p_{l,h}$ hydrostatic pressure of the slug [Pa]
$p_{csg,max}$ shut in casing/build pressure [Pa]
$p_{l,max}$ maximum flow line pressure [Pa]
a constant from 0.5 to 0.6 [-]

A slightly more sophisticated model was proposed by Foss and Gaul [99]. It is based on a force balance at the end of the tubing given in **eq. 99**.

$$\left(p_{csg} + p_{g,h,ann} - p_{g,f,ann}\right)A_{tbg} = F_{pl,g} + F_{pl,f} + \left(p_{g,f,tbg,1} + p_{g,h,tbg,1} + p_{l,h} + p_{l,f} + p_{g,f,tbg,2} + p_{g,h,tbg,2} + p_{tbg} + p_{l,prod}\right)A_{tbg} \tag{99}$$

p_{csg} casing pressure at the surface [Pa]
$p_{g,h,ann}$ hydrostatic pressure of the gas column in the annulus [Pa]
$p_{g,f,ann}$ friction pressure loss of the gas in the annulus [Pa]
A_{tbg} inside crossectional area of the tubing [m²]
$F_{pl,g}$ weight of the plunger [N]
$F_{pl,f}$ plunger sidewall friction [N]
$p_{g,f,tbg,1}$ friction pressure loss of the gas under the plunger [Pa]
$p_{g,h,tbg,1}$ hydrostatic pressure of the gas column in the tubing under the plunger [Pa]
$p_{l,f}$ friction pressure loss of the liquid slug [Pa]
$p_{g,f,tbg,2}$ friction pressure loss of the gas above the plunger [Pa]
$p_{g,h,tbg,2}$ hydrostatic pressure of the gas column in the tubing above the plunger [Pa]
p_{tbg} tubing pressure at the surface [Pa]
$p_{l,prod}$ pressure to account for produced liquids underneath the plunger [Pa]

They assumed that the critical point of the plunger upstroke was most likely just when the liquid slug reaches the wellhead. Because then the casing pressure is at its minimum ($p_{csg,min}$). With this assumption and by neglecting the plunger friction, the difference in hydrostatic pressure in tubing and annulus, the effect of the produced liquids under the plunger, as well as the friction pressure loss of the gas in the annulus, **eq. 100** is obtained. [99, p. 129]

$$p_{csg,min} = \frac{F_{pl,g}}{A_{tbg}} + p_{g,f,tbg,1} + p_{l,h} + p_{l,f} + p_{tbg} \quad (100)$$

$p_{csg,min}$ casing pressure at the surface when plunger arrices [Pa]

Inserting an approximation for the gas friction and merging the hydrostatic and friction pressure of the slug into one parameter yields **eq. 101**. They are presented for three tubing sizes in Table 4. [99, p. 129]

$$p_{csg,min} = \left[\frac{F_{pl,g}}{A_{tbg}} + p_{tbg} + \left(\frac{p_{l,h}+p_{l,f}}{s}\right)s\right]\left(1 + \frac{D}{K}\right) \quad (101)$$

$\left(\frac{p_{l,h}+p_{l,f}}{s}\right)$ hydrostatic and friction pressure of the slug per volume [Pa/m³]
s liquid slug volume [m³]
D depth of the plunger stop [m]
K constant [m]

Table 4: Parameters for Foss and Gaul model converted to metric units [99, p. 129]

Tubing ID [in]	K [m]	$\left(\frac{p_{l,h}+p_{l,f}}{s}\right)$ [Pa/m³]
1.995	10211	7155525
2.441	13716	4423415
2.992	17556	2732109

These factors should be calculated using **eq. 102-104** instead according to Lea. [100, p. 2621] Where **eq. 102** is a straightforward hydrostatic pressure calculation and **eq. 103** and **eq. 104** are Darcy Weisbach friction pressure loss calculations. [52]

$$p_{l,h} = \rho_l g \frac{s}{A_{tbg}} \quad (102)$$

$$p_{l,f} = \frac{\rho_l v^2 f_l \frac{s}{A_{tbg}}}{2d} \quad (103)$$

$$\frac{1}{K} = \frac{\frac{M_a}{1000} v^2 f_g}{2d\overline{T_g}Rz} \quad (104)$$

ρ_l liquid density [kg/m³]
M_a gas apparent molecular weight [g/mol]
d tubing ID [m]
f_l Darcy Weisbach friction factor for the liquid [-]
f_g Darcy Weisbach friction factor for the gas [-]
v veloctiy [m/s]
$\overline{T_g}$ absolute average gas Temperature [K]
z compressibility factor [-]

R specific gas constant [J kg^{-1} K^{-1}]

The maximum casing pressure is at the end of the shut-in period and it is estimated by accounting for gas expansion with **eq. 105**. [101, p. 4]

$$p_{csg,max} = p_{csg,min} \cdot \frac{A_{ann}+A_{tbg}}{A_{ann}} \qquad (105)$$

A_{ann} crossectional area of the casing-tubing annulus [m²]

If the inflow should be approximated by using a static IPR the average bottom hole pressure is needed. By neglecting the weight of the gas column in the annulus it is equal to the average casing pressure stated in **eq. 106**. [99, p. 129]

$$\overline{p_{csg}} = p_{csg,min}\left(1 + \frac{A_{tbg}}{2A_{ann}}\right) \qquad (106)$$

$\overline{p_{csg}}$ average casing pressure [Pa]

The required gas per cycle is calculated with **eq. 107** and **eq. 108**. The slippage factor F_{gs} accounts for gas that slips by the plunger. The literature states 2% slippage per 1000 ft of depth resulting in **eq. 109**. [89, p. 883] Foss and Gaul used a similar 1.15 slippage factor for 8000 ft deep wells. [99, p. 130]

$$V_g = F_{gs} V_t \frac{\overline{p_{csg}}}{p_{sc}} \frac{T_{sc}}{\overline{T_g}} \frac{1}{z} \qquad (107)$$

$$V_t = A_{tbg} D - s \qquad (108)$$

$$F_{gs} = 1 + \frac{D}{1000 \cdot 0{,}3048} 0.02 \qquad (109)$$

V_g require gas volume per cycle [m³]
F_{gs} Foss and Gaul slippage factor [-]
V_t tubing volume above the liquid slug [m³]
p_{sc} standard/surface pressure [Pa]
T_{sc} standard/surface temperature [K]

Eq. 110 estimates the maximum number of plunger lift cycles per day. [99, p. 130]

$$C_{max} = \frac{86400}{\frac{D - s/A_{tbg}}{\overline{v_{fg}}} + \frac{D}{\overline{v_r}} + \frac{s}{\overline{v_{fl}} A_{tbg}}} \qquad (110)$$

C_{max} maximum cycles per day [-]
$\overline{v_{fg}}$ average plunger falling velocity trough gas [m/s]
$\overline{v_r}$ average plunger rise velocity [m/s]
$\overline{v_{fl}}$ average plunger falling velocity trough liquid [m/s]

Foss and Gaul used a plunger rise velocity of 1000 ft/min, a plunger falling velocity through gas of 2000 ft/min and a plunger falling velocity through liquid of 172 ft/min. [99, p. 130]

Hacksma [97] is considered to be the first who integrated an IPR into the Foss and Gaul plunger model and elaborated some performance and optimization criteria. Abercrombie [102] developed performance charts based on the Foss and Gaul model but using a plunger falling velocity of 1000 ft/min instead.

The Foss and Gaul model calculates the force balance with the plunger at the wellhead but with average velocities. Instead of balancing the forces Lea inserted the forces into Newton's law and thus obtains the acceleration of the plunger. By integrating the acceleration he determined the plunger velocity at any point and integrating once more yielded the plunger's position. Further, he corrected for the hydrostatic pressure of the gas in tubing and annulus as well as the gas and liquid friction in the tubing. This dynamic model, however, doesn't take gas slippage into consideration and basically only models the upstroke dynamically. [100]

Over the years different dynamic models with varying complexity were developed by Rosina [103], Marcano and Chacin [104], Baruzzi and Alahanati [105], Gasbarri and Wiggins [106].

Hashmi, Hasan, and Kabir came up with a totally new approach based on the conservation of energy. Basically, they distinguish two states, one where the plunger is sitting still at the bottom and the other one where the plunger just has arrived at the top. In the first state all considered energy is stored in the compressed gas in the annulus. In the second state, there is still some energy in the now expanded gas in annulus and tubing. The rest of the energy is stored as potential energy in the lifted plunger and liquid slug and part of it is converted to heat due to friction. They validated their model with field data. [107]

4.5.6 Control methods and optimization

As mentioned earlier a plunger lift system is optimized when it yields the maximum possible flow rate. It is a generally respected assumption that this is the case when the average bottom hole pressure over one cycle is the lowest. Based on reservoir pressure, GLR, well depth, completion and other characteristic parameter wells can be classified into minimum on- and minimum off wells. [108]

In a ***minimum off well*** the time it takes the plunger to reach bottom hole is long enough to build the required pressure to bring it back to surface. So as soon as the plunger arrives at the lower bumper spring the valve is opened again. Usually, the accumulated pressure energy is higher than what's needed to surface the plunger and there is some afterflow. So the parameter to be optimized is the afterflow time or the duration for which the valve stays open. [108]

A ***minimum on well*** cannot build enough pressure during the downstroke of the plunger. Thus the valve stays closed for some additional time until the pressure is just high enough that the plunger can reach the surface. Naturally, this type should have no afterflow and the optimization parameter it the shut-in time. [108]

The whole system is controlled by what is called a plunger controller, which basically just controls the opening and closing times of the valve. The different control methods are set apart by model and input data they use to calculate those times. [89, p. 873]

A ***manual on-off timer*** is basically just a timer switch that opens and closes the motor valve after predetermined, set time periods. It takes a lot of trial and error until the set points are reasonably optimal and they need to be readjusted in case any well conditions change. Since it is unavoidable that parameters like, flow line pressure change these controllers are usually programmed conservatively. This minimizes the risk of liquid loading but the well is operating far from the optimum at lower production. [89, p. 873]

The ***pressure-differential controller*** monitors tubing-, casing- and line pressures and based on them determines the build- and flow period. Old pressure controllers just opened the motor valve when the casing pressure exceeded a predetermined value and closed it again when the lower set point was reached. Modern controllers implement some version of ***eq. 98*** or calculate the optimal build pressure from one of the other models. The flow period is estimated from the differential pressure which signals the slug size. Some of these controllers can adapt to changing operating conditions otherwise again they have to be programmed for worst case conditions. [89, pp. 874, 875]

The ***plunger velocity controlled on-off timer*** uses a plunger arrival sensor at the lubricator in combination with microprocessors to continually optimize the well. Simple versions only optimize for a low average bottom hole pressure, just high enough that the plunger reaches the surface. More advanced ones optimize the plunger velocity to ensure an optimal slug lifting efficiency. There is a disadvantage that some timers could optimize towards big slugs and long shut in times which results in a lower production. [89, pp. 875, 876]

The ***automated on-off and pressure monitoring controller*** is what's considered state of the art today. It needs flow rates, pressures and plunger arrival as inputs. Therefore, it can react very quickly to changing operating conditions. The flow period is estimated by comparing the gas flow rate to a calculated critical flow rate. Then the well is allowed to flow for a specified time duration after the critical rate is reached. The critical rate is continuously reevaluated using the actual, measured pressures. The build period is usually estimated from different pressure values using plunger lift models. The plunger velocity, which is inferred from the relation of valve opening and plunger arrival time, is utilized in form of shut-in- and flow multipliers. The flow multiplier specifies how long the valve stays open after the critical flow rate is reached. It can be implemented as a factor to the critical rate itself. [89, pp. 876, 877]

5 Development of three engineering tools

The set of tools were developed for three distinct purposes. Firstly it should provide an accurate prediction of the critical flow rate for different scenarios. Secondly, it should offer means to evaluate the technical feasibility of deliquification methods, in particular, plunger lift. Thirdly it should feature possibilities to predict the productivity of wells using different deliquification methods and thus make them comparable. The third one is especially important because if the flow rate is below the critical flow rate it is generally low, which means expensive re-completions are economically not justified This is also the reason why this thesis focuses on a subset of deliquification measures. Furthermore, these tools should be implemented in a user-friendly way to increase the chances that they will be frequently used by engineering staff in the future.

5.1 Critical velocity factor conversion tool

Most commercial software packages for well modeling implement some form of critical velocity modeling. The widely used PROSPER by Petroleum Experts implements it in the form of **eq. 111**. [109, p. 1277]

$$v_t = \alpha \sqrt[4]{\frac{\sigma(\rho_l - \rho_g)}{{\rho_g}^2}} \qquad (111)$$

v_t terminal velocity [ft/s]
σ gas liquid surface tension [dynes/cm]
ρ_g gas density [lbm/ft³]
ρ_l liquid density [lbm/ft³]
α critical velocity factor [$ft^{0.25}\ lbm^{0.25}\ cm^{0.25}\ s\ dyne^{0.25}$]

Since the gravitational acceleration is lumped into the critical velocity constant it is no longer dimensionless. Although the PROSPER Manual [109] does not state so, it is possible to find out that the critical velocity factor which can be specified in the preferences must be in the units of [$ft^{0.25}\ lbm^{0.25}\ cm^{0.25}\ s\ dyne^{0.25}$]. The original paper from Turner [7] uses lbf/ft for the surface tension thus one cannot directly insert the original Turner factor of 20.4 $(ft/s^2)^{0.25}$ in the preferences of PROSPER. Furthermore, several derivations in this thesis have been converted to the SI unit system for consistency reasons. To make conversion between different unit systems and the use of alternative critical velocity factors easier, a very simple conversion tool shown in Figure 51 was developed as an Excel Spreadsheet. Instead of specifying the units of the factor itself, which are usually not directly available, the user chooses the units of all other components of the equation.

		From:	To:
Interfacial Tension	σ	lbf/ft	dynes/cm
Density	ρ	lbm/ft³	lbm/ft³
Velocity	v	ft/s	ft/s
Turner type prefactor	α	20.40	1.86

Figure 51: Critical velocity factor unit conversion tool

It would be favorable if modeling software and literature used the critical velocity model in the form of **eq. 112**. Then the critical velocity factor would be dimensionless and any arbitrary but consistent unit system could be used.

$$v_t = \beta \sqrt[4]{\frac{g\sigma(\rho_l - \rho_g)}{{\rho_g}^2}} \qquad (112)$$

β critical velocity factor [-]

Although this tool itself does not provide any improvement for critical velocity prediction, it makes evaluating different models from literature a lot easier. For example, Coleman [9] suggested that the original Turner factor of 20.4 $(ft/s^2)^{0.25}$ is too high for low-pressure wells, the default value in PROSPER, however, is equivalent to 22.42 $(ft/s^2)^{0.25}$. To increase usability and prevent false inputs, the units are selected via a drop-down menu depicted in Figure 52. Furthermore, the drop-down list and the actual unit conversion is implemented in a way that additional units can be specified in a separate "Units & Constants" worksheet later on without breaking any formulas. Additionally, a consistent coloring scheme is used throughout all developed tools. Cells colored mint green receive direct user input and the ones that are colored grey feature a selection drop down menu for different options.

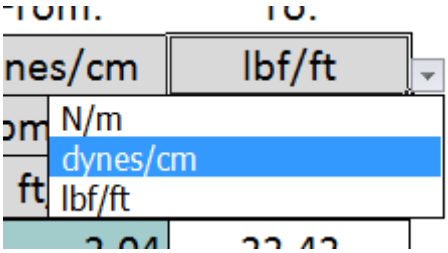

Figure 52: Unit selection drop down menu

5.2 Plunger lift feasibility evaluation tool

This tool features several automated "rule of thumb" correlations from *4.5.2 Plunger lift feasibility"*. Firstly it checks whether the GLR is above 400 bbl/scf/1000ft. Then it estimates the maximum possible liquid production from a digitized version of Figure 44. Finally, it estimates the required casing build pressure, the maximum liquid rate as well as the slug size at this maximum liquid rate according to an empirical model from Beeson et al. [90].

On a different worksheet, a full Gaul and Foss model is implemented as described in *"4.5.5 Plunger lift models"*. However all the rule of thumb models and also **eq. 105** are valid for packerless completions only. **Eq. 105** captures the effect of gas expansion during the plunger rise and is based on Boyle's law of isothermal expansion, **eq. 113**.

$$p_1 V_1 = p_2 V_2 \qquad (113)$$

p_1 initial pressure equivalent with [Pa]
p_2 final pressure [Pa]
V_1 initial volume [m³]
V_2 final volume [m³]

Rewriting it with terms commonly used in plunger lift modeling results in **eq. 114**.

$$p_{csg,max} V_{start} = p_{csg,min} V_{end} \qquad (114)$$

V_{start} volume beneath the plunger before it starts [m³]
V_{end} volume beneath the plunger when it has arrived at the surface [m³]

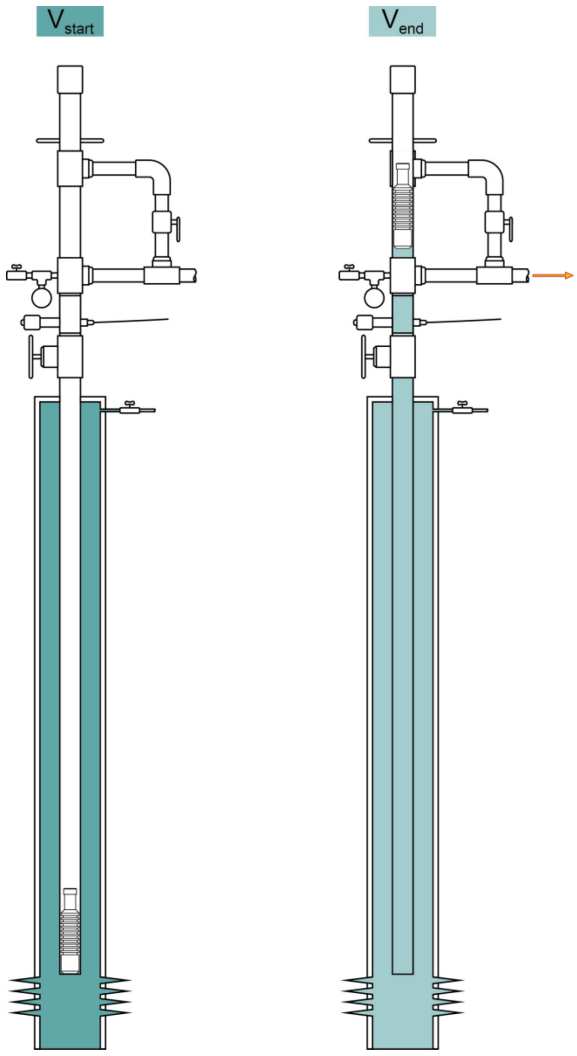

Figure 53: Plunger lift volume expansion without packer

Figure 53 illustrates V_{start} and V_{end} in case no packer is set and **eq. 115** and **116** define how they are calculated.

$$V_{start} = D_{perf}A_{csg,ID} - D_{tbg}\left(A_{tbg,OD} - A_{tbg,ID}\right) - DA_{tbg,ID} \quad (115)$$

$$V_{end} = D_{perf}A_{csg,ID} - D_{tbg}\left(A_{tbg,OD} - A_{tbg,ID}\right) \quad (116)$$

$A_{csg,ID}$ casing inside cross section area [m²]
$A_{tbg,ID}$ tubing inside cross section area [m²]
$A_{tbg,OD}$ tubing outside cross section area [m²]
D_{perf} mid perforation depth [m]
D_{tbg} depth of the end of the tubing [m]
D depth of the plunger stop [m]

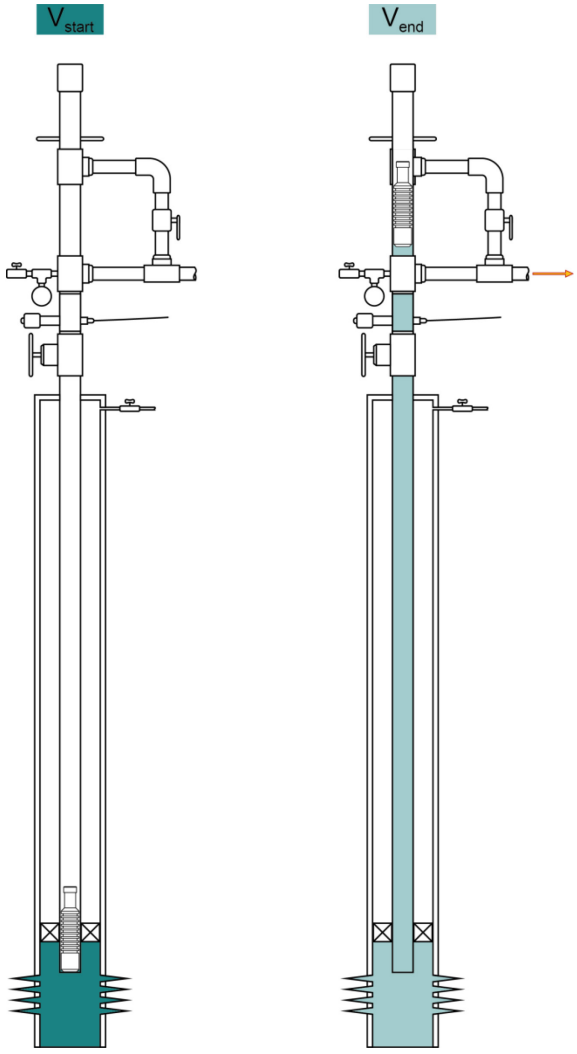

Figure 54: Plunger lift volume expansion with packer

Figure 54, on the other hand, shows them for the case of an installed packer also known as a closed completion with definitions given with **eq. 117** and **118**.

$$V_{start} = D_{perf}A_{csg,ID} - D_{tbg}\left(A_{tbg,OD} - A_{tbg,ID}\right) - DA_{tbg,ID} - D_{packer}\left(A_{csg,ID} - A_{tbg,OD}\right) \quad (117)$$

$$V_{end} = D_{perf}A_{csg,ID} - D_{tbg}\left(A_{tbg,OD} - A_{tbg,ID}\right) - D_{packer}\left(A_{csg,ID} - A_{tbg,OD}\right) \quad (118)$$

D_{packer} packer setting depth [m]

By including this modification the tool can estimate the build pressure in case a packer is installed, under the assumption that no gas is flowing into the wellbore during the plunger rise. This makes the build pressure estimation more conservative. Furthermore, gas slippage and liquid fallback past the plunger are neglected.

5.3 Well performance estimation tool

The well performance tool should serve multiple purposes. Firstly in terms of critical velocity prediction and tubing sizing it should provide a more flexible, adaptable and documented alternative to commercial software. Up to now, Petroleum Experts PROSPER has been used for these purposes inside OMV Austria, which has, despite its sophisticated modeling approaches, some limitations when it comes to niches like critical velocity prediction. Although it is possible to adjust the critical velocity factor as described in "*5.1 Critical velocity factor conversion tool*" it does not allow for different liquid loading models. Since it is commercial-, proprietary-, closed-source software not even the Nosseir model, which is just a slight modification or rather combination of Turner's and Coleman's models, can be implemented readily. Furthermore, the user has little control over where the critical velocity is evaluated. Thus a short section where flow occurs in the big ID of the casing causes the liquid loading warning to appear up to very high rates. Therefore, the actual critical rate, when the tubing starts to load can be overlooked easily. Finally, there is little documentation about which fluid properties are used to calculate the critical velocity not even mentioning if one would want to change the basis of calculation for some reason. Although PROSPER offers some foam models they are poorly documented making their implementation questionable. Lastly, it is entirely impossible to model a plunger lift system within PROSPER. Although the idea to model a time variant, cyclic process like the plunger lift with a steady state approach like nodal analysis seems unorthodox and might yield poor results compared to a fully dynamic model it should provide rough estimates for comparisons. This tool should further be developed in a somewhat object-oriented way to allow for easy modifications during the development and later on by others.

5.3.1 Why Excel, why VBA?

Microsoft Visual Basic for Applications (VBA) in combination with Microsoft Excel was chosen as the programming/scripting language for this project for the following reasons:

- The language itself and the syntax are simple, straight-forward and easy to learn for anyone with just very little programming experience.

- It offers very significant flexibility and performance advantages compared to just using Excel Worksheets. As soon as the project relies on iterative solution techniques it cannot be readily implemented exclusively using Excel Worksheets.
- However, Excel Worksheets make it easy to build a powerful user interface for input and output.
- Excel Charts provide everything that is needed in terms of data visualization without any additional workload.
- Excel features a very rich API so that almost all conventional Excel functions and features can be called and controlled from within the VBA code.
- Since this tool is developed with the intent to be an engineering tool, in other words, a user application, it cannot be programmed in something like Matlab, simply because it is economically not possible to get a Matlab license for every engineer's computer. Excel, on the other hand, is one of the applications that are installed on all computers in most companies by default.

5.3.2 General approach and structure

The overall setup is inspired by the conventional nodal analysis approach. Every instance of every model is represented by its own worksheet within Excel. This makes it possible to have multiple instances of the same model for comparison or tuning reasons, simply by copying worksheets. The worksheets can be one of several types which are described in more detail in the following. Additionally, the results from all VLPs and IPRs are summarized and plotted on top of each other on one "Main" worksheet for comparison reasons. Furthermore, this worksheet serves as a starting point from which new worksheets can be generated.

For the normal multiphase and foam flow model a more complex tubing setup, with multiple IDs can be modeled, which is crucial for liquid loading prediction purposes and therefore was a prerequisite. To be able to better analyze the effect of varying tubing IDs over the length of the wellbore, vertical gradient sheets are implemented for these two flow models. The plunger lift model provides besides the equivalent VLP calculation also a sheet which displays the modeled plunger lift cycle for a particular set of boundary conditions.

Besides the classes responsible for the actual physical modeling a significant amount of code is necessary for controlling input, output as well as interface and visualization. The unit conversion, to and from the SI unit system, is handled in the worksheets themselves as previously described. Every type of worksheet has its own type of controller in form of a VBA module. These controllers are called from a "Calculate" button on the worksheet. They read the input values, instantiate all relevant objects, set their properties accordingly and call the necessary functions to perform the calculation. After a particular calculation is finished the controller writes the results back to the worksheet and in some cases to the "Main" sheet. The updating of the charts' scaling and units is partially done within the controllers and partially in the VBA module that corresponds to the individual worksheets. Furthermore, two simple VBA forms were set up to handle the creation of new worksheets of a specified type and the data transfer between worksheets. Although this part of the program is responsible for the user-

friendly approach which was one of the prerequisites for an engineering tool, it is not described any further since it is not specific to the topic of deliquification.

5.3.3 Fluid property models

The model deals with three distinct fluids, oil, gas, and water. The project is set up in a way that these three fluids are implemented as separate classes, each of them containing several properties. However, water is characterized via its salinity, gas and oil via their specific gravity. Additionally, for oil, the specific gravity of the solution gas must be specified in order to predict the gas solubility and subsequently the density. When a fluid object gets instantiated during the setup routine of a particular model these characteristic properties have to be set. Then these objects have all necessary public functions/methods to compute the physical properties needed by any of the models. Surrounding conditions like pressure and temperature, which are needed for most property calculations, are received in form of parameters with the function call.

Oil, as well as water, contains two functions for estimating the surface tension. The ones presented in "*3.1.7 Gray's vertical flow correlation for gas wells"* are needed because Gray's flow correlation was developed and calibrated using these surface tension calculations. However, in the meantime, more accurate surface tension correlations have been developed which are shown in *"*Appendices - *Physical properties* of fluids*"*. These yield better results when used for things like critical velocity prediction. When used as part of Gray's correlation, it might perform poorly since it was not tuned with the new more accurate surface tension predictions. Therefore, both correlations are used each for their respective purpose. All PVT correlations used are described previously in *"*Appendices - *Physical properties* of fluids*"*.

5.3.4 The vertical multiphase flow model

This part of the tool implements the correlation presented in *3.1.7 Gray's vertical flow correlation for gas wells"*. When one considers the influence of changing pressure and temperature along the wellbore on the fluid properties and pressure loss calculations subsequently, it becomes obvious that this differential equation cannot be solved analytically. Therefore, the wellbore is discretized into small sections, the size of which can be specified by the user. The calculation starts at the wellhead because the wellhead pressure is a specified input value. Then all fluid properties and pressure losses of the next lower section are calculated using the conditions of the previous node. In the proper technical terminology, this is called the "forward Euler method".

Since the original publication [48, p. 41] only states dimensions, not units there is some controversy in different software programs and the literature. One point where discrepancies arise are the pressure units in the surface tension estimation of the original publication. Often it is assumed that [psi] were used but in fact, as Nymoen [55, p. 26] states in his thesis, the correct units are [lb_f/ft^2]. This is consistent with all the other units used when following the dimensions stated in the original publication and furthermore gives more reasonable results when compared to other surface tension correlations. The unit of the surface tension output is

not [dynes/cm], which is commonly assumed, but rather [lb_m/s^2] also correctly mentioned by Nymoen [55, p. 26]. Hereby it is important to distinguish between [lb_m] being a unit of mass and [lb_f] which is a unit of force. The output units of the pseudo wall roughness equation are even more difficult to guess. The dimensions stated in the original paper presume that a consistent unit system is used. Since for every other parameter of the type length, [ft] was used it follows that the pseudo wall roughness is also in [ft]. Another indication for this is hidden in the units of the input values of said equation. So unless the prefactor of 28.5 already contains the conversion from [ft] to [in] the output should be [ft] as well. The units of all other wall roughness parameters follow accordingly. The choice of [ft] as roughness unit is the most coherent and gives reasonable results, as shown during validation. By selecting these units the equations were, if necessary, adapted to the metric/SI system, yielding the ones presented under *3.1.7 Gray's vertical flow correlation for gas wells"*. Personal correspondence with Tore Nymoen (Shell) confirmed the ambiguity concerning the units. He kindly provided great ideas for validation and reasoning as well as part of the source code of his attempt at Gray's correlation.

For estimating the friction factor an explicit approximation of the Colebrook-White equation by Zigrang and Sylvester [64] was implemented. This equation like most other Colebrook-White approximations has a point of discontinuity at a relative roughness of 3.7, causing Gray's correlation to become instable at low rates. According to personal correspondence with Mikhail Tuzovskiy (Akadem Petroleum Technology Inc.) and their wiki [110] they limited the relative roughness to 0.05 for their implementation of Gray. In this tool, the limit was set to 1.5, which reduces the deviation from PROSPER results while still being stable. The multiphase Reynold's number for the friction factor equation is calculated with **eq. 69**. All mixture properties are calculated according to the rules presented in "*3.1 Tubing performance curve*".

In order to make the model handle dry gas nicely, in case of a liquid gas ratio (LGR) of zero all liquid mixture properties are set to water properties. This is necessary because otherwise, a division by zero would occur during the mixture property calculation. Furthermore, for a zero LGR **eq. 57** is overridden and gas holdup (H_g) is set to one. Gray's correlation itself with **eq. 57** would yield a gas holdup smaller than one which is not correct in case of single phase gas flow.

Since sometimes a velocity string is producing via the tubing-coiled tubing (CT) annulus it is necessary to adapt Gray's correlation for the different shape of the flow conduit. This is done using the approach stated in "*3.1.9 Flow in an annulus"*. The implementation of a hydraulic diameter and an equivalent cross-section area has the advantage that it simplifies to the original form for tubular flow when the OD is set to zero. This helps to streamline the program's code while keeping the functionality.

5.3.5 Validation of the vertical multiphase flow model

Since Gray's correlation is a central part of this tool and there are as already outlined many opportunities for misinterpretation of the original publication, it is necessary to find out whether it yields reasonable results. PROSPER is widely accepted in the industry, especially for their

pipe flow correlations. Gray's correlation is rather old and was implemented in PROSPER a long time ago, thus it is reasonable to consider their implementation for the generation of reference values. A hypothetical test well, with characteristics similar to many found in the Vienna basin, was set up to compare the two programs' performances. The basic data describing this hypothetical well is summarized in Table 5.

Table 5: Data of the hypothetical test well for mode validation

Tubing ID	50.7 mm
Tubing length	2000 m
Gas gravity (Air = 1)	0.6
Condensate density	735 kg/m³
Water salinity	20000 ppm
Wellhead pressure	7 bar
Wellhead temperature	15°C
Bottom hole temperature	70°C

Since the multiphase flow is much more complicated, due to the vast number of variables in terms of fluid properties, mixture properties, and slip estimation, first, dry gas modeling is compared. Figure 55 demonstrates that the results from PROSPER and the developed tool are pretty much identical. Considering how many different choices or assumptions had to be made during the implementation and that the model has not been tuned in any way, it is almost surprising how close the datasets match.

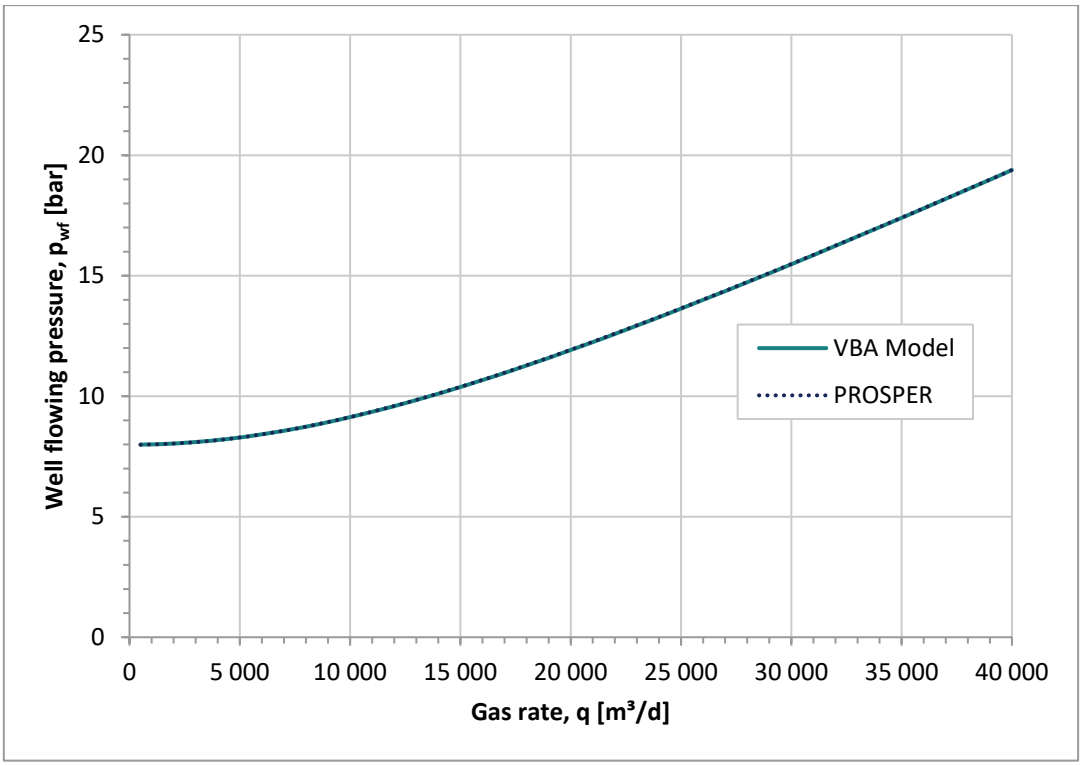

Figure 55: Dry gas VLP comparison

According to Oudeman [54, p. 5], Gray's correlation is known to yield good results for water gas ratios (WGRs) up to 20 bbl/MMScf (0.001123006 m³/Sm³). Therefore, the tool is tested for five different WGRs up to 20 bbl/MMScf. The results are presented and compared to the results from PROSPER in Figure 56. It shows that even for multiphase flow, with water being the liquid phase, the developed vertical flow model yields results which are basically identical to PROSPER.

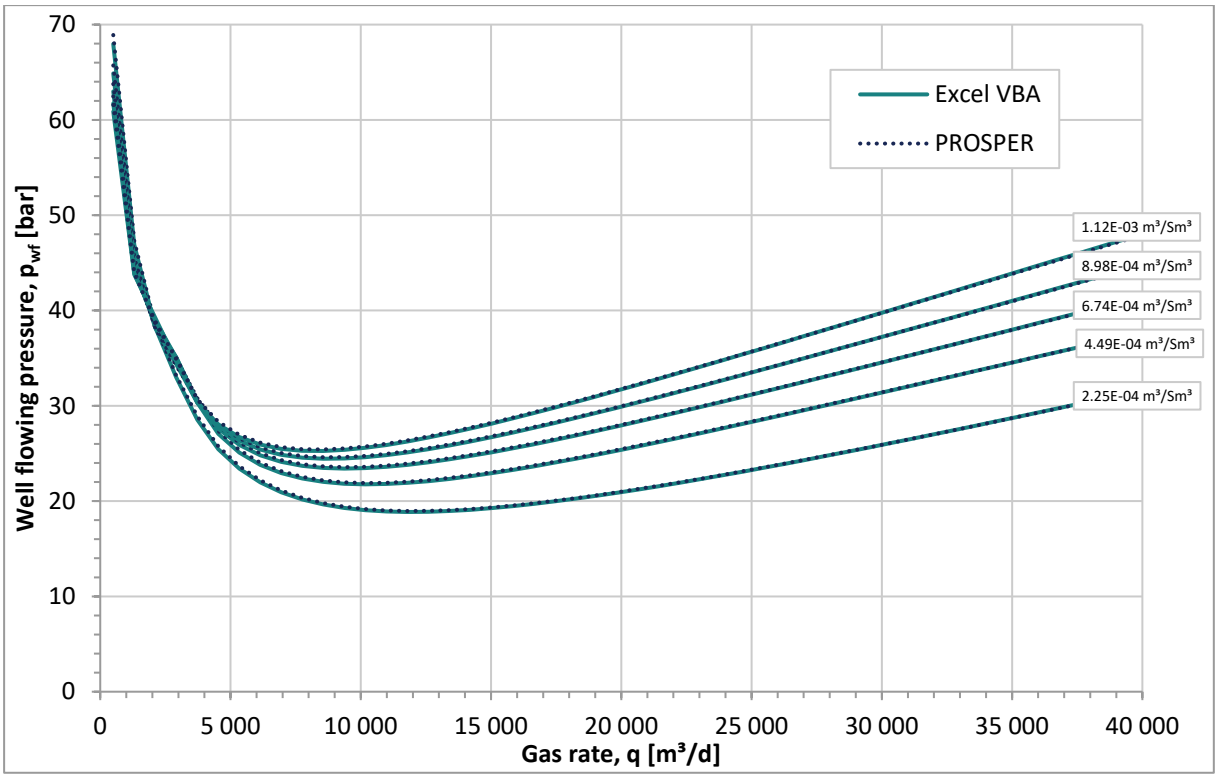

Figure 56: VLP comparison for different water-gas ratios

For the oil gas ratio (OGR), also referred to as condensate gas ratio, Gray stated that his correlation was tuned using OGRs up to 50 bbl/MMScf (0.0002808 m³/Sm³). Therefore, also the validation is done with five different OGRs up to that value. The results are shown in Figure 57. There is a significant difference between the results from PROSPER and VBA implementation of Gray's correlation. For low OGRs or low flowrates, PROSPER seems to model the wellbore as single phase dry gas which is confirmed by following statement from the PROSPER documentation.

> "The dry-wet gas model in PROSPER assumes that the condensate drops out at the separator and therefore treats the fluids as a single phase (gas) in the tubing. (Besides any possible water produced which will give two-phase flow)." [109, p. 1190]

It is not entirely clear why for higher flow rates and higher OGRs liquid condensate starts to appear in the wellbore and causes the points of discontinuity. Nonetheless, it could be argued that the discontinuous VLPs resulting from PROSPER are not capturing reality properly. Therefore, the discrepancies between the two datasets are attributed to different implementation philosophies and not caused by programming mistakes or unit interpretation errors. Furthermore, Kumar and Lea [51, p. 6] indicate that Gray used a particular empirical correlation to model the physical behavior of the condensate during the development of the vertical flow model which was only published in [111] and not included in [48].

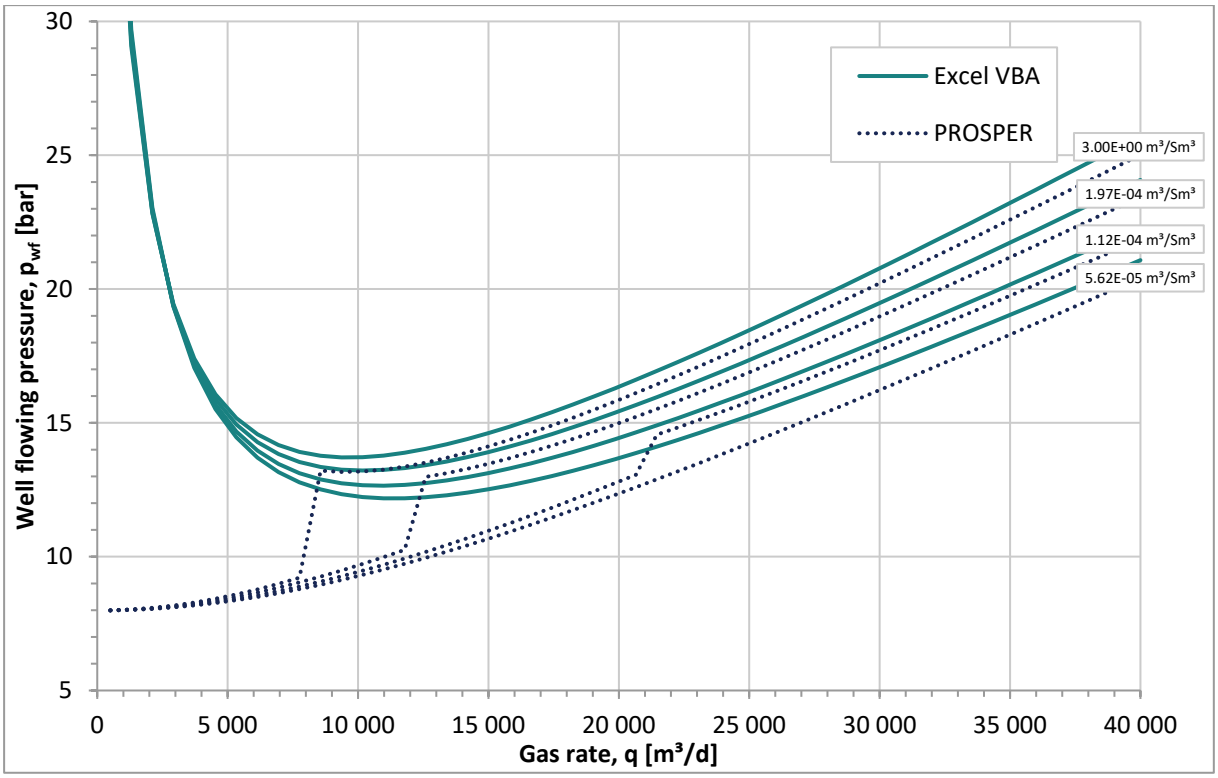

Figure 57: VLP comparison for different oil gas ratios

Figure 58 shows the comparison between pressure data retrieved from a production logging tool (PLT) and pressures predicted by the developed model. It is important to note that the 2 7/8" tubing reaches until 647,57 m, below that the gas flows in the 7" casing. The pressure gradient increase beneath 705 m is due to completion fluid that is slugged, lifted up by the gas from the last perforation interval a few meters but not any further. This, of course, is an entirely different flow regime to which Gray's correlation is not applicable. Therefore, the pressure was only predicted down to 700 m. When looking at the two datasets very closely it can be seen that the difference increases with depth. This is caused by the fact that in reality, when moving from the top down, naturally the gas flow rate in the well decreases with every perforation interval. The calculation, however, was done with the surface flow rate, which is the sum of the flow rates of the individual perforation intervals. Due to problems with the spinner (part of the PLT which indicates flowrate) during the PLT run, it is not possible to estimate the contribution of each perforation interval individually. So this comparison does not prove that the tool models real pressure gradients perfectly for all conditions but it shows that it yields reasonable, possibly realistic results without tuning, matching or tweaking of any fudge factors.

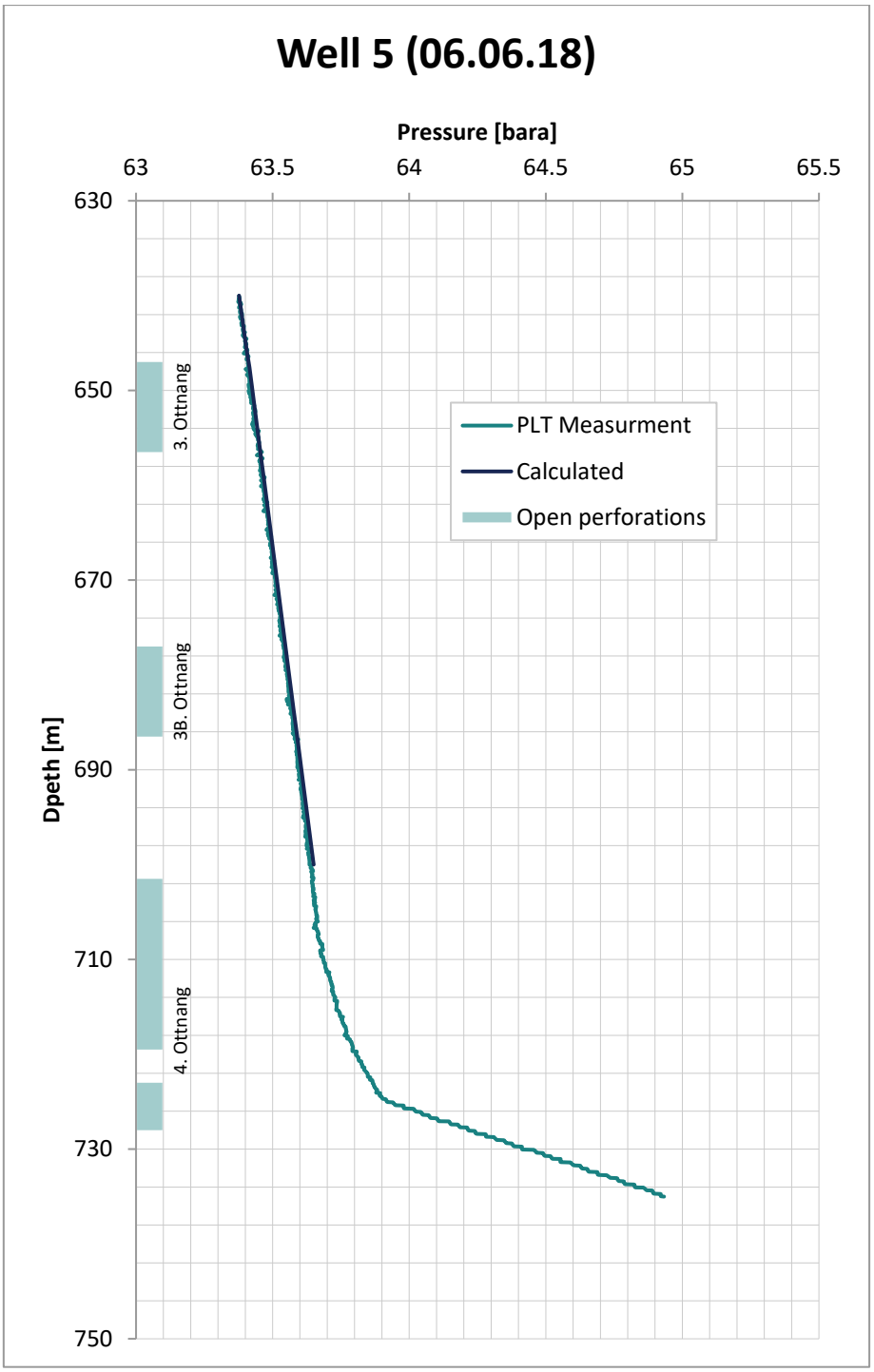

Figure 58: Comparison to PLT measurement

5.3.6 Foam flow models

All four foam flow models presented in "*3.1.10 Vertical foam flow correlations*" are included in the tool. The implementation is pretty straightforward and generally rather simple compared to Gray's correlation. The selection of the iteration procedure for **eq. 77** is important. The Newton Raphson method is very good for many engineering applications but turns out to be very instable for this problem and therefore not applicable. Thus fixed point iteration was chosen, which is generally converging slower than the equivalent Newton Raphson iteration, however, it is converging stably and reliably for this problem.

$$H_{g,i+1} = \frac{v_{sg}}{1.53\left(\frac{g\sigma_l(\rho_l-\rho_g)}{\rho_l{}^2}\right)^{1/4}\left(1-H_{g,i}\right)^n + C(v_{sm})} \quad (119)$$

$$\Delta H_g = \left|H_{g,i+1} - H_{g,i}\right| \quad (120)$$

$H_{g,i+1}$ gas holdup of the next iteration [-]
$H_{g,i}$ gas holdup of the previous iteration [-]
ΔH_g gas holdup change between iterations [-]

For the fixed point iteration **eq. 77** is rearranged into **eq. 119** and **eq. 120** is used to calculate the improvement per iteration. When the improvement falls below a preset precision the iteration is stopped and the current gas hold up used for further calculation.

As mentioned in "*3.1.10 Vertical foam flow correlations*" these flow correlations need a liquid surface tension estimation, which is as stated by Soni et al. [58] not an actual surface tension but rather a tuning parameter. In this tuning parameter, surface tension is lumped together with other effects for which the data is not available. Therefore, unlike PROSPER, this tool does not calculate or estimate this pseudo surface tension from correlations that link actual surface tension to surfactant concentration and leaves the pseudo surface tension as a user input. This value can be estimated for example by trying to match the correlations to measured field data.

5.3.7 Critical velocity models

For the normal multiphase flow, three models were implemented to calculate the critical velocity: Turner, Coleman and Nosseir, all described in detail in *2.4 Modeling liquid loading"*. While Turner and Coleman could be used in PROSPER by changing the "Turner constant" the automatic selection process, which is characteristic for the Nosseir model is not possible in PROSPER. The tool offers the choice between these three models from within the normal user interface. Additionally, the user can choose whether the critical velocity is calculated with oil/condensate properties, water properties or mixture properties. The mixture properties are calculated as described in *"3.1.4 Mixture density"* and *3.1.6 Mixture surface tension"* respectively. The surface tension estimation for water and oil is done with the correlations presented in "*0 Water-gas interfacial tension*" and "*0 Oil-gas interfacial tension*" respectively. Generally, the selection of PVT correlations and their implementation was done according to guidelines presented by Sutton. [112]

The critical velocity is calculated for every depth point in the gradient and compared to the superficial mixture velocity (v_{sm}), described in **eq. 36**. In order to determine the critical flowrate and mark it in the VLP curve, it has to be decided where to evaluate the critical velocity criterion. This means at which point in depth should the critical velocity be compared to the mixture velocity. The tool is set up in a way that the desired depth point can be specified from within the user interface. Alternatively, it offers the option to evaluate the critical velocity at the point in depth where the mixture velocity first falls below the critical velocity. In other words, the

critical rate is the highest rate at which mixture velocity is lower than the critical velocity at any point in the wellbore.

5.3.8 Plunger lift model

This plunger lift model is inspired by the one presented by Lea [92] and is based on the idea of calculating an equivalent VLP for a plunger lift system. Nodal analysis is a powerful technique but only works for steady-state flow. The plunger lift operation is not steady state, however, it is a cyclic process. Therefore, one might have the idea to average the effects of those cycles, resulting in pseudo-steady state downhole conditions. To do that the downhole pressure for one plunger cycle has to be calculated for one specific rate. Furthermore, for this calculation, this selected rate has to be assumed constant over the whole plunger cycle. This assumption is reasonable as long as the operating point lies in a rather steep-sloped part of the IPR, meaning that even a big change in pressure drawdown causes only a small change in flow rate. This is the case for tight reservoirs.

For this model the plunger cycle is split into four separate periods: pressure build-up, plunger rise, blow down and loading. For a real plunger system, these phases are triggered by distinct events. The pressure buildup starts when the motor valve at the surface is closed and ends when it is opened again. Then the plunger rise period lasts until the plunger reaches the surface. The transition between blow down and build up phase is less obvious and a rather fluid transition. Basically, blow-down lasts until the gas in the annulus is fully expanded and loading starts when the flow velocity drops below the critical velocity. The model is set up in a way that the slug size is predetermined by the user and the gas flow rate is calculated via GLR and the duration of one cycle. Since the calculation of the cycle is highly dependent on the gas flow rate, a starting value is assumed at the beginning. Then the calculation is iterated until the cycle time in combination with flowrate and GLR result in the predetermined slug size. The minimum possible cycle time is the sum of plunger rise time and plunger fall time, which is directly computable using the tubing length, rise and fall velocities as well as slug height. With this minimum cycle time, a flow rate is calculated which is used as a starting point for the iteration.

The ***buildup*** phase is modeled according to Gaul and Foss presented in “4.5.5 Plunger lift models”. However since the starting point pressure of the buildup is determined by the pressure at the end of the cycle, at the beginning, only the maximum build pressure is calculated. When starting- and end-pressure are known the build time is calculated using **eq. 121** which describes an isothermal change of state. Naturally, the lower limit of the build time is determined by the total plunger fall time.

$$t_{build} = \frac{(\bar{p}_{max} - p_{shutin}) M_a V_{ta}}{1000\, R \bar{T} q_g \bar{\rho}_{g,sc} \bar{z}} \qquad (121)$$

t_{build} build up time [s]
$\bar{p}_{max}$ average pressure in the wellbore at the end of the build [s]
p_{shutin} average pressure in the wellbore at the start of the build [s]

M_a	gas apparent molecular weight [g/mol]
R	universal gas constant, 8.3144598 [J/(mol K)]
V_{ta}	volume of open annulus and tubing [m³]
$\bar{T}$	average temperature in the wellbore [K]
$\rho_{g,sc}$	gas density at standard conditions [kg/m³]
z	compressibility factor [-]
q_g	gas flowrate (from the formation) [m³/s]

The ***plunger rise*** period is straightforward to calculate. Starting pressure is the end of the build pressure and the pressure at the end is the minimum pressure ($p_{csg,min}$) provided by the Gaul and Foss model. The duration of the plunger rise directly calculated from tubing length and the preset plunger rise velocity.

The ***blow-down*** phase is the more challenging part of the cycle to calculate. In reality, gas from the casing-tubing-annulus and gas from the formation flow up the tubing simultaneously. The flow rate from the annulus is governed by the difference between annulus pressure and backpressure. The pressure in the annulus, however, is determined by the cumulative flow rate from the annulus. Figuratively, the gas in the annulus acts during blow down very similarly to a big spring which is expanding. To replicate this in the model a continuity equation is formulated which relates the expanding gas to the flow in the tubing and the resulting backpressure. Because of the way the Gray correlation is set up, it is way faster to calculate the well flowing pressure (p_{wf}) for a given gas flow rate (q_g) than the other way round. So in order to improve performance as well as stability,2 the computation algorithm proposed by Lea [92] is modified slightly, while keeping all the physical assumptions. Generally, the material balance is done downhole at the entry of the tubing however the gas expansion in the annulus is modelled with average casing pressure and temperature. To convert between surface-, downhole- and average pressure **eq. 122-123** are used. The tool implements these equations also in other places.

$$p_{bh} = p_{csg}\, e^{\left(\frac{M_a g \bar{z}}{1000 R \bar{T}} D_{perf}\right)} \qquad (122)$$

$$\bar{p} = p_{csg}\, \frac{e^{\left(\frac{M_a g \bar{z}}{1000 R \bar{T}} D_{perf}\right)} - 1}{\frac{M_a g \bar{z}}{1000 R \bar{T}} D_{perf}} \qquad (123)$$

p_{csg}	casing pressure at the wellhead [Pa]
p_{bh}	(casing) pressure at bottom hole [Pa]
$\bar{p}$	average pressure in the casing [Pa]

The blow-down phase starts out by calculating the gas flow rate through the tubing ($q_{tbg,i}$) with modified Grays's correlation for the starting well flowing pressure. The modified Gray is chosen over the original one because the flowrate might be rather small however the tubing is free of liquids at this point. The well flowing pressure at the start, is the pressure at the end of the

plunger rise ($p_{csg,min} \rightarrow p_{wf,i}$)). Then a small change in tubing flow rate is assumed (Δq_{tbg}) and the new tubing flow rate calculated with **eq. 124**.

$$q_{tbg,i+1} = q_{tbg,i} - \Delta q_{tbg} \qquad (124)$$

$q_{tbg,i}$ gas flowrate through the tubing [m³/s]
Δq_{tbg} change in gas flowrate through the tubing [m³/s]
$q_{tbg,i+1}$ new gas flowrate through the tubing [m³/s]

For the new flow rate the new well flowing pressure ($p_{wf,i+1}$) is calculated using the modified Gray's correlation. Additionally, the inflow from the annulus is calculated using the new flow rate and flow rate from the reservoir as described by **eq. 125**.

$$q_{ann,i+1} = q_{tbg,i+1} - q_{g,i} \qquad (125)$$

$q_{g,i}$ gas flowrate from the formation [m³/s]
$q_{tbg,i+1}$ gas flowrate through the tubing [m³/s]
$q_{ann,i+1}$ gas flowrate from the annulus [m³/s]

Then the time duration, that is needed for the calculated flow from the annulus to cause the calculated pressure difference, is estimated using **eq. 126**. With this time step and the current well flowing pressure ($p_{wf,i+1}$) the next point in the pressure vs. time curve is generated. This process is repeated until the flow rate from the annulus falls below a predetermined threshold. This signals that the gas in the annulus has fully expanded and the well has blown down.

$$\Delta t_i = \frac{(\bar{p}_{i+1} - \bar{p}_i)}{\frac{1000 \bar{T} R \bar{p}_g}{M_a V_{ann}} - q_{ann,i+1}} \qquad (126)$$

Δt_i time step [s]
V_{ann} volume in the annulus (below packer) [m³]

The blowdown is generally calculated assuming a dry gas flow in the tubing. However, when the flow rate drops below the critical flow rate in any point of the tubing, it is assumed that the input LGR rises from the bottom with the mixture velocity as proposed by Lea [92].

The ***loading*** period starts when the gas in the annulus is fully expanded and it also models the tubing flow with rising LGR from the bottom. If the flow rate was already below the critical rate during the end of the blow-down, then this period starts out with the LGR already at a certain height in the tubing. The loading period proceeds until an arbitrarily chosen shut-in pressure is reached. This tool uses **eq. 127** to determine the shut-in pressure as suggested by Lea [92, p. 240]. In reality, this shut-in pressure depends mainly on the controlling an optimization method that is used. The plunger lift cycle is completed with the end of the loading phase.

$$p_{shutin} = \frac{1}{2}\left(p_{wf,0} - p_{bd,min}\right) \qquad (127)$$

$p_{wf,0}$ bottomhole pressure at the start of the blowdown [Pa]
$p_{bd,min}$ minimum bottomhole pressure during blowdown [Pa]

When the cycle has completed the duration of one cycle can be computed with **eq. 128** and subsequently the gas flow rate for the next iteration results from **eq. 129**.

$$t_{cycle} = \sum \Delta t_i \qquad (128)$$

$$q_{g,i+1} = GLR * \frac{s}{t_{cycle}} \qquad (129)$$

$q_{g,i+1}$ gas flowrate from the formation for the next iteration [m³/s]
s slug size [m³]
GLR gas liquid ratio [Sm³/m³]

$$\Delta q_g = \left| q_{g,i+1} - q_{g,i} \right| \qquad (130)$$

Δq_g difference of formation flowrates between iterations [m³/s]

When the difference between the new flow rate and the previous one, calculated with **eq. 130**, is below a preset threshold the iteration is stopped and the last calculated plunger cycle is considered as valid. Then the time-weighted pressure average is calculated and used as equivalent bottom hole flowing pressure for the last estimated gas rate ($q_{g,i}$).

This calculation is performed for different slug sizes resulting in many pairs of gas rate and corresponding well flowing pressure. Together they could be called an equivalent VLP of the plunger system. This equivalent VLP is the output of the plunger model and is used to compare the performance against other deliquification methods.

5.3.9 Inflow model

An inflow model (IPR) is also added to the model to put the different VLP curves into context on the “Main” worksheet. Although the IPR is integrated primarily for illustrative purposes, it enables the user to estimate the operating points of the different lifting types. Since reliable data for the Russel Goodrich IPR (**eq. 88**) is for many old gas wells not available the back pressure equation (**eq. 90**) is implemented for this tool. In order to make the IPR handling process similar to VLP handling, and thus simplify the program by reusing code, **eq. 90** was rearranged into **eq. 131**.

$$p_{wf} = \sqrt[2]{\bar{p}^2 - \left(\frac{q_g}{C}\right)^{1/n}} \qquad (131)$$

q_g volumetric gas flow rate [Sm³/s]
p_{wf} well flowing pressure [Pa]
$\bar{p}$ average reservoir pressure [Pa]

C performance coefficient [Sm³/(s Pa² ⁿ)]

n exponent accounting for turbulence [-]

6 Utilization, interpretation, and lessons learned

This chapter demonstrates, how the developed tools can be utilized, and presents the results and interpretations of said results. Additionally, different noteworthy possible pitfalls and lessons learned concerning the deliquification methods implemented in OMV Austria.

6.1 Evaluation location of the critical velocity criterion

For some wells with liquid loading problems, the point of loading is clearly visible in the production data log. For example, in Figure 59 the change in slope when the flow rate declines towards 410 m³/h is a good indication of the onset of liquid loading. It has to be noted that the vertical axis in Figure 59 has the unit [m³/h].

Figure 59: Production data of Well 3

At the same time, flowline pressure and temperature can be taken retrieved from similar logs. Using this data, some schematics of the downhole installation and the developed tool, one can try to calculate the critical flow rate. The resulting VLP curve is shown in Figure 60 and the predicted critical flow rate evaluated at the wellhead is 412 m³/h.

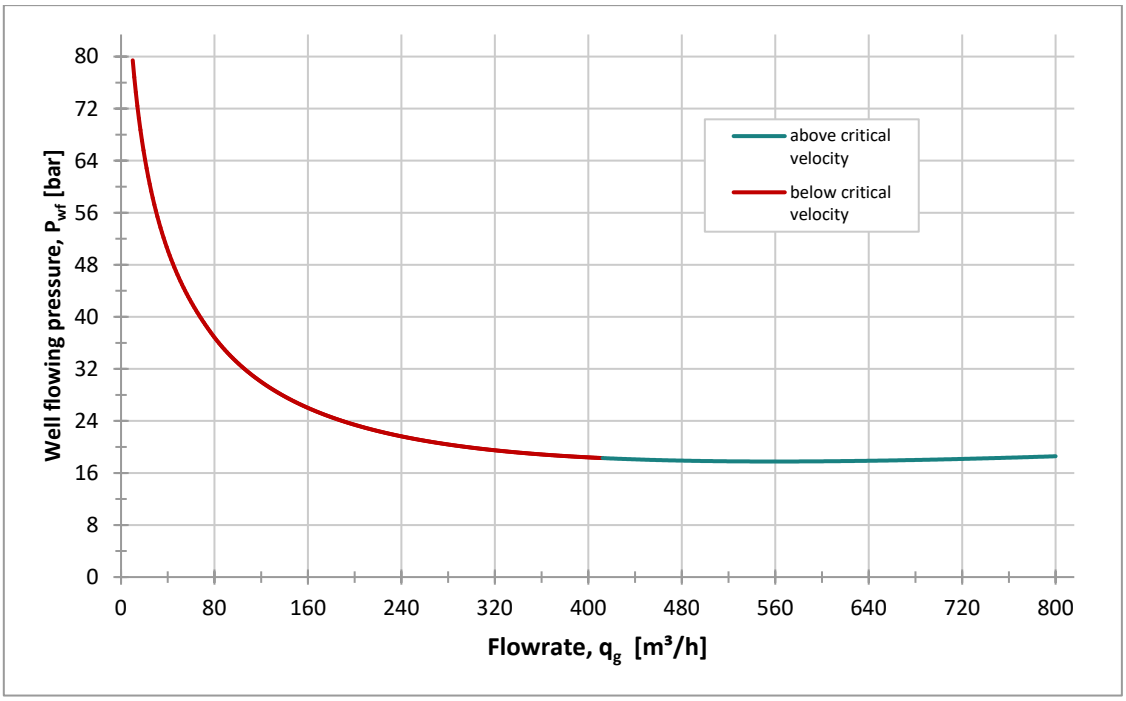

Figure 60: VLP of Well 3 on the 01.03.2017

This can be done for different wells and multiple loading events of loading in the history of considered wells. This results in a set of pairs of critical flow rates, one interpreted from production logs similar to Figure 59, and the other one is the corresponding, calculated critical flow rate. At first, the critical rate is calculated as the highest gas rate at which the gas velocity falls below the critical velocity. That is very similar to how it is evaluated in PROSPER. The liquid type for the calculation was chosen to be water since all of the considered wells produce at least some amount of water. Therefore, wells generally tend to load up with water already at higher gas rates and thus before the load up with condensate. As a critical velocity model, the Nosseir model is chosen, which equivalent to the Coleman model at the conditions of the considered wells. These critical rates are then plotted against the critical rates interpreted from field data in a cross plot style in Figure 61 in dark blue. Additionally, the 45° solid line in Figure 61 indicates where calculated and interpreted critical rates would ideally match. Comparing the calculated results to this line suggests that the calculation overpredicts the critical rate or in other words is too conservative. Next, the same critical velocity criterion is evaluated for the same loading events at the wellhead resulting with critical rates plotted in Figure 61 in turquoise.

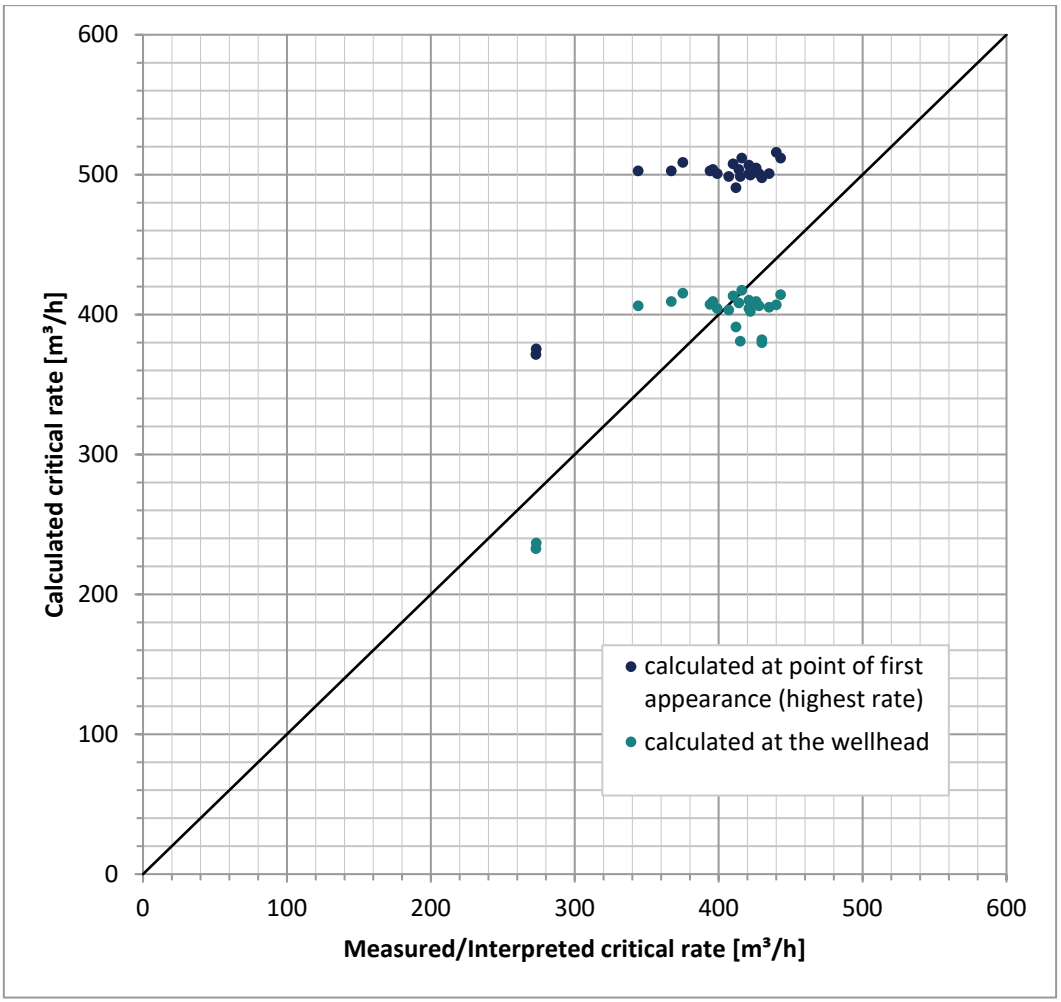

Figure 61: Comparison of two possible locations for critical velocity evaluation

In comparison, the values calculated at the wellhead predict the critical values much more accurately. Two possible explanations for this can be readily found.

Assuming that the tubing ID is constant over the whole depth for a particular well, usually the gas velocity and also the mixture velocity decreases with depth. This is due to gas expanding because of the reduction in pressure on the way to the wellhead. This effect of pressure reduction usually outweighs the opposite effect caused by temperature reduction. Also, the critical velocity decreases with depth but at a lower gradient. Therefore, the critical rate is first met in the lowest part of the tubing. However, in real wells, it could be argued that water is not yet condensing at these great depths but in fact much closer to the surface and the wellhead. This is plausible since the flowing gas at reservoir temperature heats up the whole downhole installation. Therefore, neither the temperature gradient of the tubing and casing, much less the actual gas temperature are linear with depth. The programmed model uses a linear gradient and assumes free water in the gas stream over the whole length of the tubing. In reality, gas velocity could be below critical velocity at some points in the wellbore but loading does not occur simply because there is no free water in the gas stream.

The second explanation is based on the assumption that the physics of the Turner model and all derivatives are wrong. This assumption is underpinned by recent studies presented in

2.4.7 Criticism on droplet flow reversal criteria". In that case, these models would have more the character of an empirical relationship. One property of empirical models is that they usually don't generalize as well as mechanistic models. Since the original Turner- and Coleman models were based and fitted to wellhead data it is self-evident that they show more accurate predictions for these conditions.

However, it is important to mention that the field data used for these deductions is rather limited and the conclusion thus not particularly sound. Nonetheless, the result is in line with literature recommendations which suggest evaluating critical velocity criteria at the wellhead unless the ID of the tubing is varying. In that case, the point with the largest diameter is determinative. [112, p. 184]

6.2 Plunger lift troubleshooting

Well 2 suffered from severe liquid loading and subsequently reduced production. In particular, a 500 m condensate column was measured which exerted significant backpressure on the formation. To remedy this problem a Weatherford plunger lift system was installed into the existing 2 7/8 production tubing. According to workover plans and report a "tubing stop" was installed downhole. However, it was installed into an existing landing nipple (Otis "X") and therefore it actually must have been a plunger stop of the seat-cup type. Further, the workover report mentions a standing valve in the plunger stop which is not referred to anywhere else. A collet was run and the bumper spring was dropped into the well. Also, the surface installations were changed which was actually done beforehand by setting a back pressure valve (BPV) into the tubing hanger. The most important data characterizing the well for plunger lift feasibility evaluation is presented in Table 6 and the installed plunger lift surface equipment is shown in Figure 62.

Table 6: Data relevant for plunger lift feasibility in Well 2

Tubing ID	62 mm
Tubing OD	73 mm
Casing ID	159 mm
Gas gravity (Air = 1)	0.6968
GLR	16000 Sm^3/m^3
Wellhead pressure	7 bar
Condensate density	735 kg/m^3
Bottom hole temperature	67.8°C
Mid perforation depth	2121.5 m
Depth of plunger stop	2100 m
End of tubing	2104 m
Packer setting depth	2103 m
Reservoir pressure	72.2 bar

Figure 62: Plunger lift surface equipment - Well 2

When taken under operation the plunger often did not surface, required a lot of attention by the field personnel and ultimately did just not yield the expected increase in stable gas production. In the following possible explanations why the plunger did not work are presented.

Firstly the motor valve of the surface installation was time controlled only, which per se requires a lot of adjustment by the field personnel compared to more advanced automated control mechanisms. However many of the more advanced control systems require a value of the instantaneous casing pressure. Since Well 2 originally was completed with a packer on the 2 7/8 tubing the annular volume is isolated from the production. Thus the casing pressure is totally unrelated to the plunger lift cycle and can therefore not be used for control.

Secondly, the installed packer might also be the reason why the plunger often did not arrive at surface. Using the data stated in Table 6 with the rules of thumb programmed into the plunger lift feasibility tool results in a casing build pressure of 9.2 - 18 bar depending on which correlation you use. Taking the conservative one of 18 bar which is a result of applying some interpolation to Figure 43 still suggests that a plunger lift would probably be feasible. The more advanced Gaul and Foss model predicts a casing build pressure of 15 bar. However all these estimation neglect the fact that Well 2 is completed with a packer near the end of the tubing reducing the volume of pressurized gas below the plunger significantly. When accounting for this with the method described in "*5.2 Plunger lift feasibility evaluation tool*" a casing build pressure of 174 bar. Although this probably overestimates the actual build pressure due to

several simplifications. One of them being that the Gaul and Foss model generally neglects the volume of gas entering the wellbore during plunger rise, which is however especially in this case reasonable because of the low permeability and high skin. None the less it clearly indicates the drastic effect a set packer in the completion has on plunger lift performance which was already suggested in Figure 45. Since 174 bar is clearly higher than the reservoir pressure of 72.2 bar the set packer is probably the main cause for the poor performance of the plunger lift system in Well 2.

6.3 Lessons learned in velocity string design

Roughly two years later the downhole and surface equipment of the plunger lift was removed from Well 2. Since a velocity string has been operated in Well 1 for more than ten years very successfully a 1 ¾ in coiled tubing was installed in Well 2 as well. Furthermore, additional perforations were shot to enhance production and overcome the high skin which is thought to be caused by the condensate banking phenomenon. However, this entailed a significant risk because the velocity string was designed for a gas flow rate based on the assumptions that the additional perforations were rather successful. Although it was known at that time that there was large uncertainty associated with the IPR estimations, it turned out that even the worst case scenario was hardly met. Therefore, Well 2 is still not flowing continuously and is loading up from time to time.

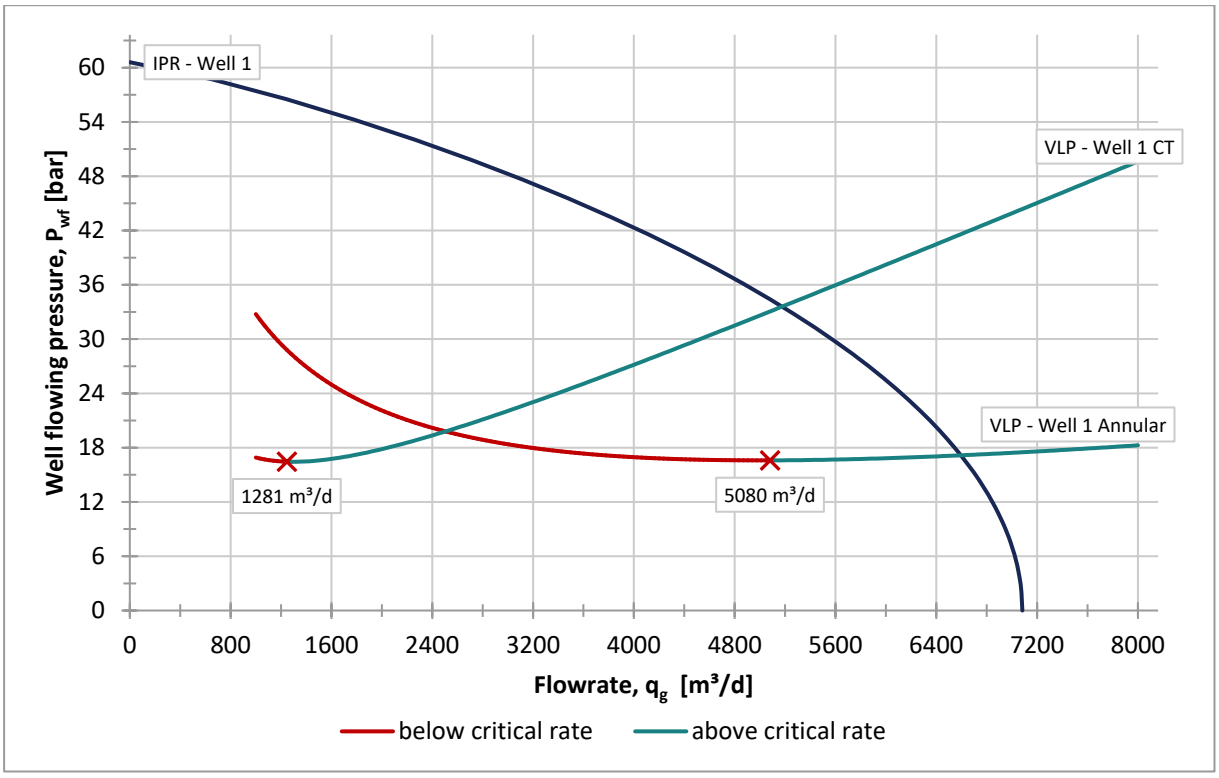

Figure 63: Velocity string nodal analysis Well 1

Well 1 is currently and always has been producing in the CT-tubing annulus since the installation of the CT. The tubing has an OD of 2 3/8 in, the CT an OD of 1 1/ in and an ID of 19.86 mm. Figure 63 shows the nodal analysis of the velocity string in Well 1. Both cases,

production through annulus and production through CT, are plotted for comparison. This plot shows that there would be the opportunity to switch this well over to production through the CT and thus further reduce the critical production rate. This will prove very valuable in the future when the reservoir pressure and subsequently the productivity of the well decline. Due to this smart CT sizing the velocity string, which is generally considered a quite inflexible unloading method, becomes a rather flexible, adaptable unloading method.

However, such a design is not always possible, or at least only with a limited range depending on the interaction of the size of the already installed tubing and the expected performance of the well. Due to the high expectations toward the effectiveness of the added perforations and the large tubing ID of 2 7/8 ina rather large CT with OD of 1 ¾ in (ID 39 mm) was chosen. This had the side effect, that the annular- and CT cross-section areas were very similar. However, even if the poor inflow had been known, the only two options would have been: to size the CT even larger for annular production, or significantly smaller for CT production. In both cases, a switch of the production method in the future to adapt for declining rate would not have been possible either. This is simply and solely caused by the large ID of the 2 7/8 in tubing.

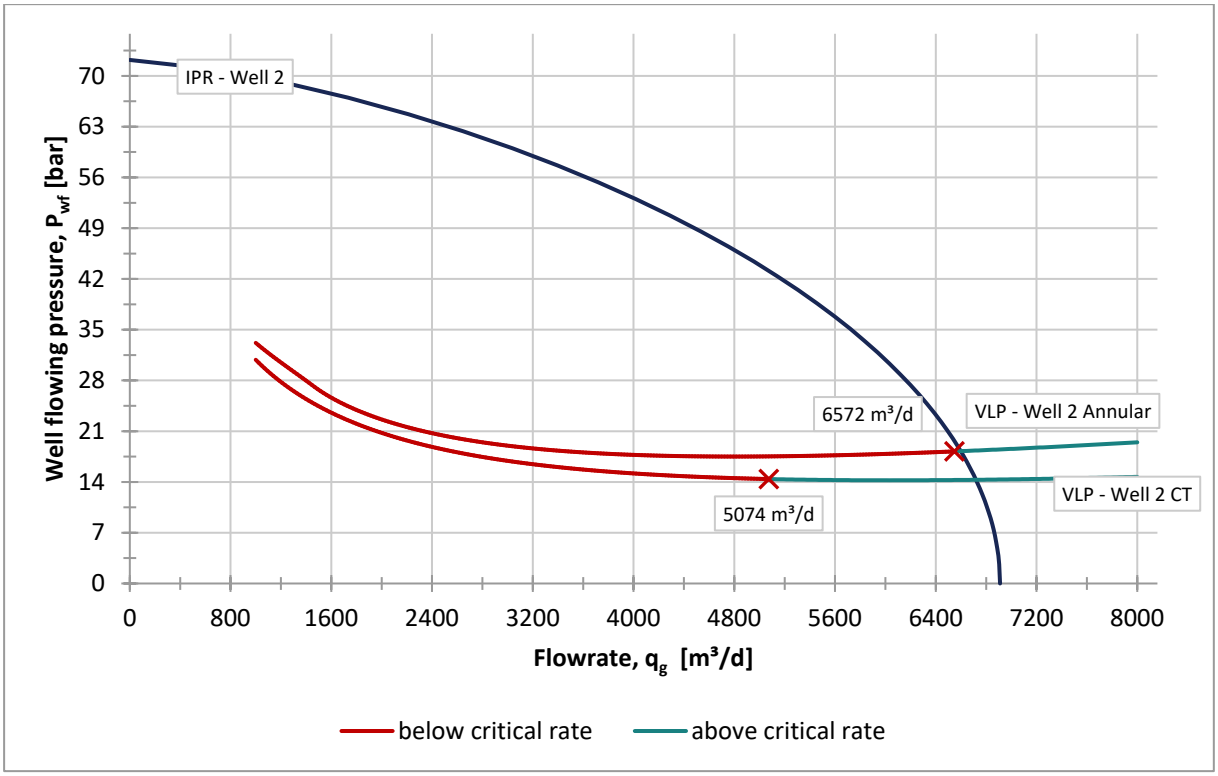

Figure 64: Velocity string nodal analysis Well 2

Figure 64 shows the nodal analysis output of the current installation in Well 2. Although the cross-section areas are similar there is some difference in critical production rate. Furthermore, it shows that despite the slightly larger cross-section area of the annulus the pressure losses are higher. This is due to the increased friction occurring with flow through an annulus. This is one of the main reasons justifying the implementation of the modification described in "*3.1.9 Flow in an annulus*". So switching to production through the coiled tubing has combined advantage that the critical rate is lowered due so smaller cross-section area and the actual

flow rate is likely to be increased due to reduced friction and thus lowered bottom hole flowing pressure.

Motivated by said results of the calculations illustrated in Figure 64 it was decided to try producing through the coiled tubing. The annular flow was shut-in in order to let the pressure build. Then the coiled tubing valve was opened to flow into the flow line. However, after a very short period of audible gas flow, the pressure fell and gas production seized. The well does not flow via the coiled tubing. This is most likely due to the fact that the end of the coiled tubing is 5 m below the last perforation. This was done on purpose with the idea to keep the entire perforated section liquid free to reduce problems with condensate banking which the Eger-sandstone horizon is prone to. Even if the flow velocity was high enough in the annulus between tubing and CT, it was certainly not in the section below the end of the tubing because of the large ID of the casing. There it is reasonable to assume that this section is mostly filled with 0.916 m³ liquid. As described in "*4.1.3 Velocity string implementation*", when the CT-valve is opened at the x-mas tree the pressure in the CT reduces. However, before any gas from the perforations can enter the CT the whole liquid volume has to be displaced or siphoned through the CT first. Due to the rather small ID of the CT, this causes a 767 m high liquid column in the CT, which is illustrated in Figure 65. This in combination with the wellhead pressure causes a back pressure of 62 to 82 bar depending on whether the liquid is condensate or water. The estimation of the liquid volume was taken rather conservatively. It is very likely that in reality also parts of the tubing-CT annulus contained some amounts of liquid. Since the estimated backpressures are close to (in case of condensate) or above (in case of water) the reservoir pressure of 72.2 bar there is a very high chance this is the reason why Well 2 cannot be produced via the CT.

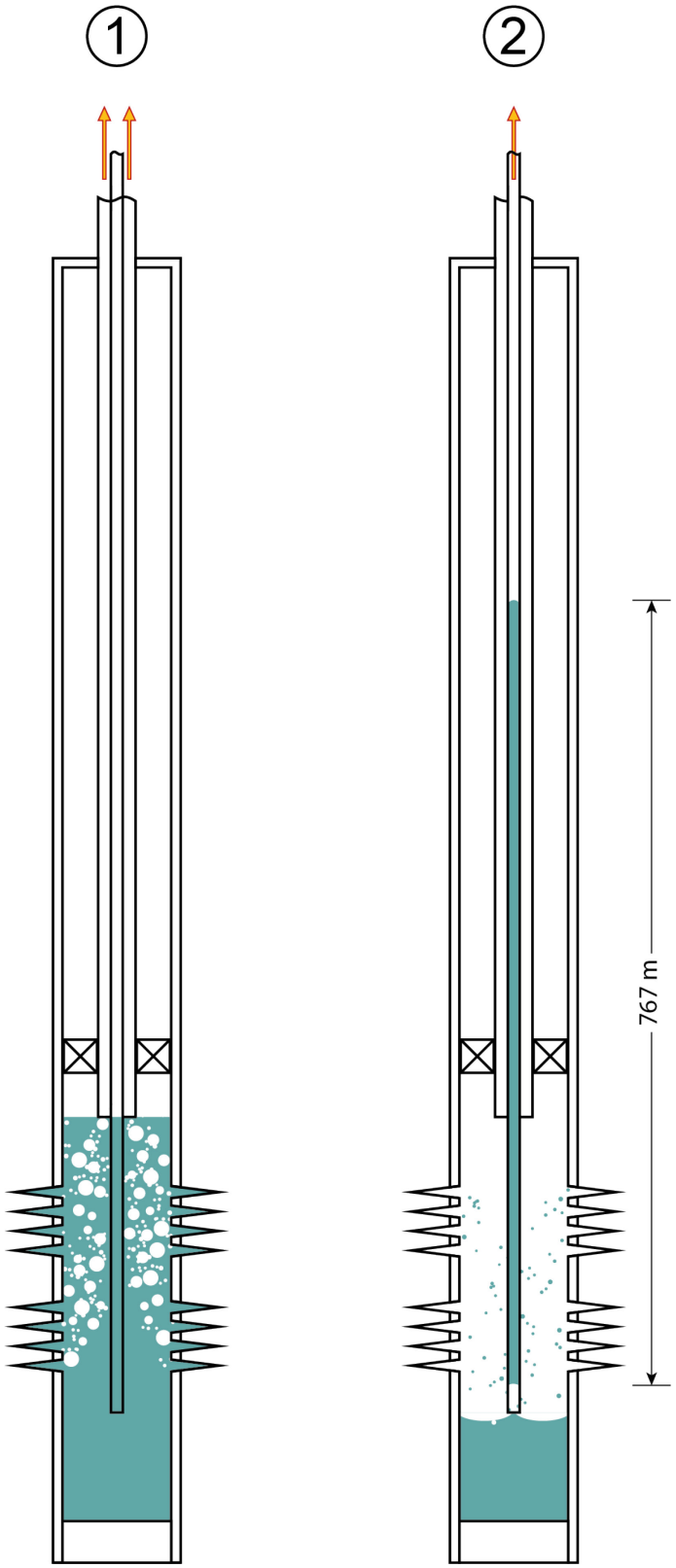

Figure 65: Problems when unloading through a CT set below the perforations

6.4 Lessons learned from foam lift application

Another well in Field 1, Well 3, has also liquid loading issues. The problems are worsened by a seized and stuck sand filter with a downhole choke with an initial ID of 3 mm. To improve the

well performance a small coiled tubing (OD ¼ in), often called capillary string, was run inside the 2 3/8 production tubing. This capillary string was used to pump down a foamer product (WSP 9655) by Weatherford. According to field personnel, however, a stable foam lift operation could not be established. Before the capillary string was installed the foamer product was tested by ICPT Campina with respect to its foaming capabilities. For the test, a total of 200 ml of sample fluid, containing the specified concentration of foamer, is transferred to a cylinder and brought up to the specified testing temperature. Then the liquid sample is purged with a constant stream of nitrogen for three minutes or until the foam reaches a volume of 1000 ml. The foam height (proportional to its volume) is measured every 15 seconds. When this part of the test is finished the time necessary, for the foam to decay to half of its volume is measured. This time duration is referred to as foam half-life. The test results are presented in Table 7. To judge these results, performance classification criteria were also included in the testing report by ICPT, which are presented in Table 8.

Table 7: Foaming capacity of WSP 9655 with Well 3 fluids

Condensate-water ratio	30:70						50:50					
Temperature, [°C]	70			90			70			90		
Foamer concentration, [ppm]	1000	2500	5000	1000	2500	5000	1000	2500	5000	1000	2500	5000
Time to form 1000 ml foam, [s]	105	45	45	115	40	30	-	-	39	-	-	-
Foam half-life time, [s]	30	95	285	28	80	100	-	-	80	-	-	-

Table 8: Performance classification of foamer performance

Foam build up time, [s]		Foam half-life, [s]	
< 80	good	> 180	good
80 < x < 120	moderate	60 < x < 180	moderate
> 120	poor	< 60	poor

Based on these measurement results the report by ICPT concluded that the foamer WSP 9655 can be used for deliquification of gas wells for condensate to water ratios lower than or equal

to 30:70 (0.43). The last well checker measurement done on Well 3 in 2010 is the only source to estimate the amount of produced liquids. The well was tested for two days and produced on average 0.203 m³ of condensate and 0.131 m³ of water per day. This translates to an average condensate to water ration of roughly 61:39 (1.55), which is significantly above the value of 0.43 recommend by the ICPT and thus explains the poor foamer performance.

As part of the same campaign, another capillary string was installed in Well 4, which was also known for its liquid loading problems. The results from the ICPT report for Well 4 are shown in Table 9. The recommended condensate to gas ratio is identical with 30:70 (0.43). There are no data available on the amount of produced liquids due to the way the wells in Field 2 are connected to the station. However, it is known that Well 4 produces only water and no condensate. So naturally, the foamer is working very well however the foam was very stable which is also indicated by the high foam half-life time in the ICPT testing results. This stable foam does not only create severe problems in the inlet separator of the Field 2 station but also significantly increases the friction pressure losses in the partially shared surface lines. This increased backpressure leads reduced production by the other wells and even reduced overall gas production although Well 4 gas production increased.

Table 9: Foaming capacity of WSP 9655 with Well 4 fluids

Condensate-water ratio	30:70						50:50					
Temperature, [°C]	50			90			50			90		
Foamer concentration, [ppm]	1000	2500	5000	1000	2500	5000	1000	2500	5000	1000	2500	5000
Time to form 1000 ml foam, [s]	>180	>180	75	>180	>180	>180	>180	180	150	>180	>180	>180
Foam half-life time, [s]	-	-	295	-	-	-	-	195	345	-	-	-

To deal with this problem the Gänserndorf laboratory (Fluid Analytics & Production Chemistry) performed similar tests to the ones described previously. According to their report, it is recommended to dilute the foamer 1:10 with Mono-Ethylenglycol (MEG) to reduce the effectiveness of the foamer and lower the foam stability subsequently.

On this note, it cannot be emphasized enough how important it is to check fluid compatibility when used through a capillary string. Furthermore, if fluids are exchanged it is very important to obey the recommended flush and spacer volumes. Capillary strings have been plugged and rendered useless due to unwanted fluid interactions on many occasions.

Additionally, the lab recommended the injection of a defoamer at the wellhead. Specifically, the product DFW82250 by Baker was tested. It was recommended to also dilute the defoamer 1:10 with MEG. This combination of foamer and defoamer did work in the field. However, there were still some operational issues like the limited precision of the dosing pump. After some time the diluted defoamer formed some high viscous sludge which was not pumpable by the dosing pump which also led to outages. It is important to keep in mind that the shutdown of Well 4 is always preferred over the reduced effectiveness of the whole Field 2 station due to foam entering the station.

6.5 Utilization of the well performance tool

Opposite to conventional approaches to the selection of deliquification methods like screening criteria, or decision trees the developed performance tools can provide an estimate of the produced gas. This is important since for a particular case technically multiple deliquification methods might be feasible and the goal is to select the one with the best economy or achieving the best recovery factor (RF). In this section, the current state of Well 2 is used as an example to evaluate different deliquification methods. Figure 66 shows the main results of the well performance tool applied to Well 2.

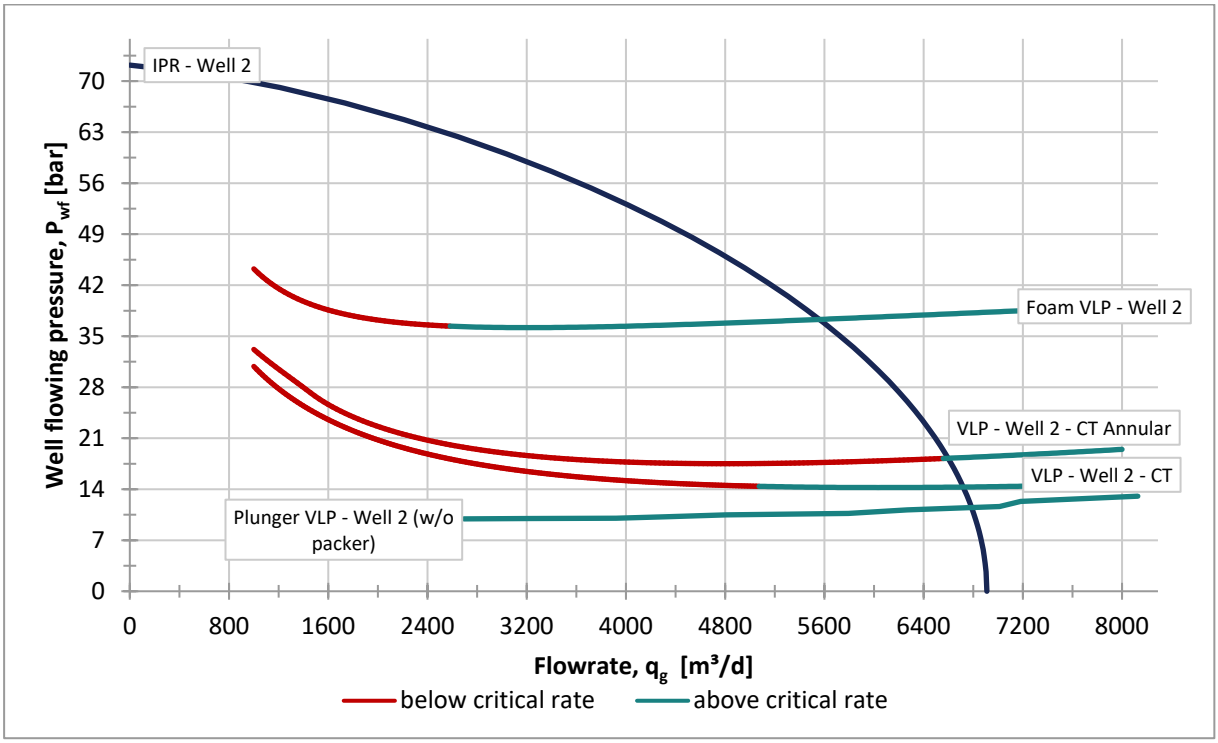

Figure 66: Comparison of different deliquification alternatives in a well based on Well 2

Firstly it rather accurately reflects reality in that the annular production with velocity string is at the point of loading. As already discussed it indicates that production through the coiled tubing itself would be favorable. However one can see that when the IPR changes the velocity string is rather inflexible. When the production falls below 5074 m³/d, even production through the coiled tubing would not be sustainable and another well intervention will be needed.

On the other hand, it shows that foam lift would successfully unload the well until very low rates. However, foam causes a much higher backpressure on the perforations than the dispersed mist flow in a velocity string which is reflected nicely in Figure 66. Naturally, the higher bottom hole flowing pressure causes a significantly reduced production rate. At the current situation with velocity string and flow through the annulus the well achieves roughly 6560 m³/d when it is about to load. The same well without CT with foam lift would only produce just shy of 5600 m³/d, that's a difference of 960 m³/d. It is important to note though that there are no pressure or IFT data available from the sometimes producing foamer wells like Well 4. Therefore, the VLP estimation for foam is associated with larger uncertainties which can be reduced in the future easily when the required data is available. If more accurate modeling is needed and a budget for detailed measurements is available there is the opportunity to implement more sophisticated foam flow models, which require more input data.

Thirdly Figure 66 shows that the plunger lift is very flexible and works down to very low rates. According to this model, it also does this with a very low average backpressure, assuming that no packer was installed. In principle, this tool could estimate also the average backpressure for a well with packer installed. However as previously discussed for Well 2 a plunger lift with installed packer is not feasible and thus an estimation of its performance is not possible. It is even possible to assess the influence of packers set at different depths relative to the mid perforation depth. The estimation presented in Figure 66 is also based on several assumptions since no plunger is currently operated within OMV Austria and the data that's left from the unsuccessful pilot is very limited.

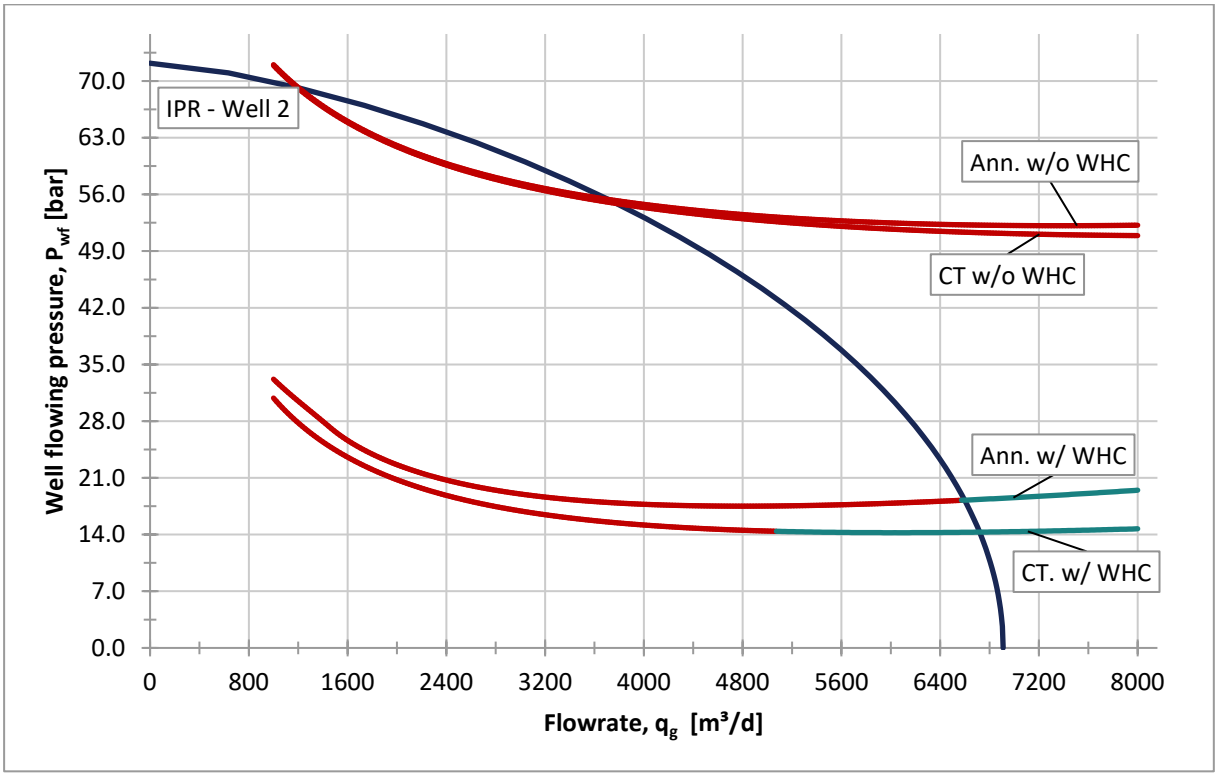

Figure 67: Effect of a wellhead compressor on the velocity string performance in Well 2

Finally, the effect a wellhead compressor (WHC) has on the performance of the well can be modeled with this tool. As a note, the performance of the compressor itself, meaning the achieved suction pressure for a particular flow rate is not modeled by this tool. The effect of the wellhead compressor is captured by simply changing the wellhead pressure to the lower one achieved by the compressor. Furthermore, this also allows for evaluation of the combined effect of the different deliquification methods with a wellhead compressor. It also can be used to evaluate to which value the wellhead pressure has to drop for a particular method to work. In fact Field 1 actually already facilitates a wellhead compressor although it is not situated next to particular wells but in the station. Before the WHC for Field 1 was installed the wellhead pressure of Well 2 was somewhere between 35 to 40 bar. Figure 67 shows that at a wellhead pressure of 35 bar Well 2, in its current state with velocity string, would produce only around 3600 m^3/d instead of 6560 m^3/d. Due to the overall higher pressure and the compressibility of gas, the gas velocity in all parts of the tubing would be significantly lower and thus always far below the critical velocity. This shows again the compound effect of a WHC on liquid loading or deliquification. Firstly, it reduces the average pressure and thus increases in-situ gas velocities for a particular production rate. Secondly, it also causes an increase in production rate due to a lowered bottom hole flowing pressure which increases the in situ gas velocities even further. It is important to note that at the time the WHC was installed in Field 1 the velocity string was not yet installed and also the reservoir pressure was still higher back then. As discussed in a previous chapter the reduction of pressure has an impact on the condensation of liquids and thus possibly on liquid loading and deliquification. This effect, however, is not captured or modeled in the well performance tool.

7 Conclusion and recommendations

In the following final chapter, the ideas, outcomes, lessons learned and recommendations for the future are grouped to the different deliquification methods.

The ***critical velocity criterion*** is very important in identifying liquid loading problems. The physical explanation of the Turner criterion and its derivatives is not sound and does probably not hold for most gas well scenarios. Nonetheless if applied correctly the results are accurate enough for practical decisions. Therefore, it should be seen more like an empirical relationship than a mechanistic model. This implicates that the results will be more accurate the closer the conditions met the ones from the original wells the criterion was based on. Furthermore, it suggests that modifications to the equation based on physical reasoning are rather questionable. Therefore, its applicability to foam flow by just using modified IFT and foam density is also rather limited. The Turner and Coleman models are the ones most recognized and respected by the industry, also in the studies of this Thesis, the Coleman model seemed to give good results. The Nosseir model seems to combine Turner and Coleman in a rather elegant way and thus it is the recommended choice. However also for the Nosseir model, the physical explanation is debatable. Finally to achieve the most accurate results the critical velocity criteria should be evaluated near to or at the wellhead. For wells with different IDs in the production string, the position with the biggest ID is decisive. This is generally agreed on in the literature and backed by limited data of this study. For the design of production tubing or velocity strings, it is recommended to take the more conservative approach of using the point in depth where the critical velocity is first undercut. This is the approach taken by PROSPER and probably leads to an overestimation of the critical rate. When using PROSPER it is important to choose the correct “Turner Constant” and not use the default one because it significantly overestimates the critical rate and can be considered too conservative. The liquid used for critical velocity estimation is usually water unless only or mostly condensate is produced which is rather rare. For designing purposes again the more conservative approach of using water properties is recommended.

Generally, ***velocity strings*** are more expensive due to high mobilization cost of a coiled tubing unit. However, this is very specific to Austria. Furthermore, they are rather inflexible, if one designs them too small, the friction pressure losses are high and the production rate is sacrificed. If one designs them rather big to keep the friction pressure low, it will be very inflexible and just a small decline in production rate will cause the well to have liquid loading problems again. It is recommended to use both the CT-tubing annulus and the CT itself and size the CT in a way that kind of a staged production is possible, similar to Well 1. However, this is only possible for certain combinations of well productivities and installed tubing sizes. For example, in Well 2 this approach is not possible. For Well 2, in particular, it is recommended to produce via the CT and not the CT-tubing annulus due to a slightly decreased cross-section area and simultaneously decreased friction losses. Unloading could be achieved by injecting nitrogen through the CT and trying to lift all liquids up the CT-tubing annulus. However, it is unclear whether high enough gas velocities can be achieved in the casing section below the tubing. Firstly because it depends on the nitrogen source used and secondly

because the critical unloading velocity is very likely to be different from the critical loading velocity. The reversed process of injecting nitrogen through the annulus is not recommended since it will cause downhole pressures around the reservoir pressure which will cause either the liquids or the nitrogen to enter the formation. In case liquids enter the formation the risk of significantly increasing the already substantial skin and thus damaging the formation is high. In case the nitrogen is lost to the formation the unloading procedure might fail. However, if it is possible to unload Well 2 and produce it in its current configuration through the CT it will be seen whether producing through the CT and setting the CT below the perforation has any advantageous effects. In case it indeed keeps all perforations liquid free there is the chance of reducing the skin over time and enhancing production. However, if the well loads up for any reason it has to be unloaded by nitrogen again. Pulling up the CT and setting it higher is technically not readily possible. So as a long-term solution it is recommended to cut or perforate the tubing somewhere around 1/3 from the top of the perforation interval, which is technically possible. It would also be possible to start perforating from the bottom of the perforation interval and move higher until unloading is possible.

The ***plunger lift*** pilot project was not the anticipated success because firstly one pilot is not enough for evaluating a technology completely new to the company. Although plunger lift is a rather simple, flexible and forgiving technology there are still many uncertainties involved when the experience with it is zero. One failed pilot does not allow for a well-grounded decision on whether this technology is worth investing in or not. The recommended size of a pilot project for plunger lift would be three to five pilots. In the case of Well 2, in particular, the combination of a closed completion with a packer in combination with the low reservoir productivity with high skin was with high probability the reason why it did not work as expected. Since most gas wells in Austria have a packer installed and a change of the completion is usually not economical the recommended option is to perforate the tubing above the packer and set the plunger stop above these perforations. This makes the annular volume accessible for pressure build up or in other words energy storage and thus significantly reduces the build pressure. Furthermore, it allows for a more sophisticated pressure controlled plunger lift operation which further increases the chance of success. Although under special circumstances a plunger lift might work in a well with an installed packer, without perforated tubing it is definitely not recommended for the next pilot wells. Plunger lift with packer could be revisited once several plunger lifts are operated successfully in wells without packer or at least with perforated tubing. Since changing the completion is not possible due to economics, plunger lift is not feasible for many wells in Austria, because they have complex completions with varying IDs. In many cases, the uppermost tubing single is of a larger ID, which was done to be able to reuse a x-mas tree with larger ID.

For the ***foam lift,*** it is generally very important to ensure compatibility of the foamer and produced liquids. For example, for Well 3 a different product has to be found which is able to generate foam even with high percentages of condensate. Since Well 3 is also producing some amount of water it should be possible achieve stable foam lift operation given the appropriate foamer product is used. The foamer system in Well 4 works in principle but offers some opportunities for optimization. Every chemical added to produced hydrocarbons can cause

problems or difficulties in some facilities downstream. Thus adding a foamer downhole and then adding a defoamer at the wellhead is not really optimal. Theoretically, it could be possible to reduce the amount of injected foamer until the foam is just stable enough to ensure sustained unloading but disintegrates near to the wellhead. This amount or injection rate can only be found by testing at the actual well. Therefore, defoamer installation is still needed because even during testing it is not acceptable for the foam to enter the surface line network and gas station subsequently. This could possibly take down the gas station and thus risk the production of the whole field. The recommended procedure is to start with sufficient foamer and defoamer and successively reducing both concentration until no defoamer is needed. One operational problem is that the currently installed dosing pumps are not precise enough to inject such small quantities of the chemicals. To remedy this, one could either install different dosing pumps suited for the purpose or further dilute the chemicals. Additionally, multiple products from different vendors could be compared to find the optimal solution.

Gas well deliquification is in principle very simple but there exist numerous different options which use different physical principles and thus differ profoundly. Therefore, one has to be very careful to implement deliquification methods based on simple screening criteria which are by their very nature using only scarce data input. The critical velocity criterion as discussed in contrary can be used as a screening criterion to highlight gas wells in danger of liquid loading problems. Further, it has been shown that evaluating the critical velocity criterion at wellhead conditions gives good results. Therefore, it should be possible to readily integrate this criterion into production databases, since all necessary data is usually contained in these databases. This would provide an efficient way to highlight between the many gas wells those which are about to load up or are currently loading. Once these wells are highlighted the different deliquification options should be evaluated for each well individually. For most gas wells, liquid loading occurs in the later stage of their lifetime, when production rates are already low and little gas is left in the reservoir. Therefore, usually, the economics of the implementation of any deliquification method are critical and one can consider the most economical, feasible method to be the best.

8 References

[1] C. U. Ikoku, Natural Gas Production Engineering, Malabar, Florida: Krieger Publishing Company, 1992.

[2] J. F. Lea, H. V. Nickens and M. R. Wells, Gas well deliquification, Burlington: Gulf Professional Publishing, 2008.

[3] A. L. Vitter, “Back Pressure Tests on Gas-Condensate Wells,” in *Drilling and Production Practice*, New York, 1942.

[4] J. O. Duggan, “Estimating Flow Rates Required To Keep Gas Wells Unloaded,” *Journal of Petroleum Technology,* vol. 13, no. 12, December 1961.

[5] A. E. Dukler, “Design of Multi-Phase flow Systems,” in *API Southwestern District Meeting*, Albuquerque, New Mexico, 1961.

[6] P. J. Jones, Petroleum Production, New York: Reinhold Publishing Corp., 1947.

[7] R. G. Turner, M. G. Hubbard and A. E. Dukler, “Analysis and Prediction of Minimum Flow Rate for the Continuous Removal of Liquids from Gas Wells,” *Journal of Petroleum Technology,* vol. 21, no. 11, pp. 1475-1482, November 1969.

[8] J. O. Hinze, “Fundamentals of the hydrodynamic mechanism of splitting in dispersion processes,” *AIChe Journal,* vol. 1, no. 3, pp. 289-295, 1955.

[9] S. B. Coleman, H. B. Clay, D. G. McCurdy and L. H. I. Norris, “A New Look at Predicting Gas-Well Load-Up,” *Journal of Petroleum Technology,* vol. 43, no. 3, pp. 329-333, March 1991.

[10] M. Li, L. Sun and S. Li, “New View on Continuous-removal Liquids from Gas Wells,” in *SPE Permian Basin Oil and Gas Recovery Conference*, Midland, Texas, 2001.

[11] J. E. McDonald, “The shape of raindrops,” *Scientific American,* vol. 190, no. 2, pp. 64-69, 1954.

[12] J. E. McDonald, “The Shape and Aerodynamics of large Raindrops,” *Journal of Meteorology,* p. 478–494, December 1954.

[13] M. A. Nosseir, T. A. Darwich, M. H. Sayyouh and M. El Sallaly, “A New Approach for Accurate Prediction of Loading in Gas Wells Under Different Flowing Conditions,” *SPE Production & Facilities,* vol. 15, no. 4, pp. 241-246, November 2000.

[14] G. G. Brown, Unit Operations, New York: John Wiley & Sons, 1950.

[15] J. M. C. Van't Westende, Droplets in annular-dispersed gas-liquid pipe-flows.

[16] T. W. F. Russell and D. E. Lamb, “Flow mechanism of two-phase annular flow,” *Can. J. Chem. Eng. (The Canadian Journal of Chemical Engineering),* p. 237–245, 1965.

[17] S. K. Friedlander and H. F. Johnstone, “Deposition of Suspended Particles from Turbulent Gas Streams,” *Ind. Eng. Chem. (Industrial & Engineering Chemistry),* p. 1151–1156, 1957.

[18] L. B. Cousins and G. F. Hewitt, “Liquid phase mass transfer in annular two-phase flow: droplet deposition and liquid entrainment,” Atomic Energy Research Establishment, 1968.

[19] L. B. Fore and A. E. Dukler, “Droplet deposition and momentum transfer in annular flow,” *AIChE J. (AIChE Journal),* p. 2040–2046, 1995.

[20] J. Young and A. Leeming, “A theory of particle deposition in turbulent pipe flow,” *J. Fluid Mech. (Journal of Fluid Mechanics),* p. 129–159, 1997.

[21] L. Pan and T. J. Hanratty, “Correlation of entrainment for annular flow in horizontal pipes,” *International Journal of Multiphase Flow,* p. 385–408, 2002.

[22] B. J. Azzopardi, “Drops in annular two-phase flow,” *International Journal of Multiphase Flow,* p. 1–53, 1997.

[23] P. Marmottant and E. Villermaux, “On spray formation,” *J. Fluid Mech. (Journal of Fluid Mechanics),* p. 73–111, 2004.

[24] G. Kocamustafaogullari, S. R. Smits and J. Razi, “Maximum and mean droplet sizes in annular two-phase flow,” *International Journal of Heat and Mass Transfer,* p. 955–965, 1994.

[25] S. T. Thoroddsen and K. Takehara, “The coalescence cascade of a drop,” *Physics of Fluids,* p. 1265–1267, 2000.

[26] J. C. B. Lopes and A. E. Dukler, “Droplet entrainment in vertical annular flow and its contribution to momentum transfer,” *AIChE J. (AIChE Journal),* p. 1500–1515, 1986.

[27] C.-A. Peng, L. A. Jurman and M. J. McCready, “Formation of solitary waves on gas-sheared liquid layers,” *International Journal of Multiphase Flow,* p. 767–782, 1991.

[28] R. J. Belt, On the liquid film in inclined annular flow, TU Delft, 2007.

[29] R. S. Darling and H. N. McManus, “Flow patterns in circular ducts with circumferential variation of roughness: a two-phase analog,” *Dev. Mech.,* vol. 5, p. 153–170, 1968.

[30] R. A. Gore and C. T. Crowe, “Effect of particle size on modulating turbulent intensity,” *International Journal of Multiphase Flow,* p. 279–285, 1989.

[31] G. Hetsroni, “Particles-turbulence interaction,” *International Journal of Multiphase Flow,* p. 735–746, 1989.

[32] S. Elghobashi and G. C. Truesdell, “On the two-way interaction between homogeneous turbulence and dispersed solid particles. I: Turbulence modification,” *Physics of Fluids A: Fluid Dynamics,* p. 1790–1801, 1993.

[33] B. Azzopardi, “Turbulence modification in annular gas/liquid flow,” *International Journal of Multiphase Flow,* p. 945–955, 1999.

[34] C. T. Crowe, “On models for turbulence modulation in fluid–particle flows,” *International Journal of Multiphase Flow,* p. 719–727, 2000.

[35] G. T. Csanady, “Turbulent Diffusion of Heavy Particles in the Atmosphere,” *J. Atmos. Sci. (Journal of the Atmospheric Sciences),* p. 201–208, 1963.

[36] G. C. Truesdell and S. Elghobashi, “On the two-way interaction between homogeneous turbulence and dispersed solid particles. II. Particle dispersion,” *Physics of Fluids,* p. 1405–1407, 1994.

[37] B. M. Mols, Particle dispersion and deposition in horizontal turbulent channel and tube flows, Delft: Delft University Press, 1999.

[38] B. J. Azzopardi and G. F. Hewitt, “Maximum drop sizes in gas-liquid flows,” *Multiphase Science and Technology,* vol. 9, no. 2, pp. 109-204, 1997.

[39] R. L. Christiansen, “Lifting Liquids from Natural Gas Wells by Aggressive Formation of Small Droplets,” in *SPE Production and Operations Symposium*, Oklahoma City, Oklahoma, 2003.

[40] K. Veeken, B. Hu and W. Schiferli, “Gas-Well Liquid-Loading-Field-Data Analysis and Multiphase-Flow Modeling,” *SPE Production & Operations,* vol. 25, no. 3, pp. 275-284, August 2010.

[41] T. S. Thrasher, “Well Performance Monitoring: Case Histories,” *SPE Production & Facilities,* vol. 10, no. 03, pp. 177-183, August 1995.

[42] W. E. Gilbert, “Flowing and gas-lift well performance,” in *Drilling and Production Practice*, New York, New York, 1954.

[43] J. N. McCoy, A. L. Podio, O. L. Rowlan and D. J. Becker, “Applications of Acoustic Liquid Level Measurements in Gas Wells,” in *SPE Annual Technical Conference and Exhibition*, San Antonio, Texas, 2006.

[44] H. D. Beggs, Production Optimization Using Nodal Analysis, Tulsa, Oklahoma: Society of Petroleum Engineers, 1980.

[45] H. U. Fuchs, The Dynamics of Heat - A Unified Approach to Thermodynamics and Heat Transfer, Springer Science & Business Media, 2010.

[46] T. E. W. Nind, Principles of oil well production, 1981.

[47] K. E. Brown and D. H. Beggs, The Technology of Artificial Lift Methods, 1977.

[48] H. E. Gray, *Vertical flow correlation in gas wells - User manual for API 14B, Subsurface controlled safety valve sizing computer program, App. B,* 1974.

[49] H. Duns and N. C. J. Ros, “Vertical flow of gas and liquid mixtures in wells,” in *World Petroleum Congress*, Frankfurt am Main, Germany, 1963.

[50] D. L. V. Katz, Handbook of natural gas engineering, New York: McGraw-Hill, 1959.

[51] N. Kumar and J. F. Lea, “Improvements for Flow Correlations for Gas Wells Experiencing Liquid Loading,” in *Proceedings of SPE Western Regional Meeting*, Irvine, California, 2005.

[52] J. L. Weisbach, Lehrbuch der Ingenieur- und Maschinen-Mechanik, Braunschweig, Germany: Vieweg und Sohn, 1845.

[53] C. F. Colebrook and C. M. White, “Experiments with fluid friction in roughened pipes,” *Proceedings of the Royal Socitey of London A,* vol. 161, pp. 367-381, 1937.

[54] P. Oudeman, “On the Flow Performance of Velocity Strings To Unload Wet Gas Wells,” in *Proceedings of SPE Middle East Oil and Gas Show and Conference*, Bahrain, 2007.

[55] T. Nymoen, Application of Backpressure Analysis to Gas Condensate Systems, Trondheim, Norway, 2017.

[56] Fekete Associates Inc., “fekete.com,” [Online]. Available: http://www.fekete.com/SAN/WebHelp/virtuwell/webhelp/c-te-pressdrop.htm. [Accessed 04 06 2018].

[57] Akadem Petroleum Technology Inc., “pengtools.com,” [Online]. Available: https://wiki.pengtools.com/index.php?title=Gray_correlation. [Accessed 04 06 2018].

[58] S. Soni and M. Kelkar, “Pressure-Drop Predictions in Tubing in the Presence of Surfactants,” in *SPE Production and Operations Symposium*, Oklahoma City, Oklahoma, 2009.

[59] T. Z. Harmathy, “Velocity of large drops and bubbles in media of infinite or restricted extent,” *AIChE Journal,* vol. 6, no. 2, pp. 281-288, 1960.

[60] N. Zuber and J. Hench, “Steady State and Transient Void Fraction of Bubbling System and Their Operating Limits. Part 1: Steady State Operation,” General Electric, Schenectady, New York, 1962.

[61] E. Hatchek, “Die Viskosität der Dispersoide,” *Kolloid-Zeitschrift,* pp. 34-39, 1911.

[62] B. J. Mitchell, *Viscosity of Foam,* University of Oklahoma, 1960.

[63] N. S. Deshpande and M. Barigou, “The flow of gas-liquid foams in vertical pipes,” *Chemical Engineering Science,* pp. 4297-4309, October 2000.

[64] D. J. Zigrang and N. D. Sylvester, “Explicit approximations to the solution of Colebrook's friction factor equation,” *AIChE Journal,* pp. 514-515, 1982.

[65] M. J. Economides, D. A. Hill, C. Ehlig-Economides and D. Zhu, Petroleum Production Systems, Upper Saddle River, New Jersey: Prentice-Hall, 1994.

[66] D. G. Russell, J. H. Goodrich, G. E. Perry and J. F. Bruskotter, “Methods of Predicting Gas Well Performance,” *Journal of Petroleum Technology,* vol. 18, no. 1, pp. 99-108, January 1966.

[67] E. L. Rawlins and M. A. Schellhardt, Back-pressure data on natural-gas wells and their application to production practices, Bartlesville, Oklahoma: Bureau of Mines, 1935.

[68] W. R. Greene, “Analyzing the Performance of Gas Wells,” *Journal of Petroleum Technology,* vol. 35, no. 7, pp. 1378-1384, July 1983.

[69] F. A. Thomas, “Low Pressure Compressor Applications,” in *49th Annual Liberal Gas Compressor Institute*, 2001.

[70] E. Ventura-Medina and J. J. Cilliers, “A model to describe flotation performance based on physiscs of foams and froth image analysis,” *International Journal of mineral processing,* pp. 79-99, 2002.

[71] J. T. G. Overbeek, *Colloids and Surface Chemistry - A Self-Study Subject - Study Guide Part 2, Lyophobic Colloids,* Cambridge Massechusetts: MIT Press, 1972.

[72] L. W. Lake, Enhanced Oil Recovery, Austin, Texas: Prentice Hall, Englewood Cliffs, New Jersey, 1989.

[73] W. J. Gibbs, “On the Equilibrium of Heterogeneous Substances,” *American Journal of Science and Arts,* p. 441, 1878.

[74] C. Marangoni, *On the expansion of a drop of liquid floating on the surface of another liquid.,* Pavia, Italy: Fratellli Fusi, 1869.

[75] T. Young, “An essay on the cohesion of fluids,” *Philosophical transactions of the royal society of London,* pp. 65-87, 1805.

[76] P.-S. Laplace, “Supplement to the tenth edition,” *Méchanique céleste,* 1806.

[77] W. Ostwald, “Über die vermeintliche Isomerie des roten und gelben Quecksilberoxyds und die Oberflächenspannung fester Körper,” *Zeitschrift für physikalische Chemie,* pp. 495-503, 1900.

[78] R. Lemlich, “Some Physical Aspects of Foam,” *Journal of the Society of Cosmetic Chemists,* pp. 299-311, 1972.

[79] J. Yang, V. Jovancicevic and S. Ramachandran, “Foam for gas well deliquification,” *Colloids and Surfaces A: Physicochemical and Engineering Aspects,* pp. 177-181, 2007.

[80] W. Schinagl, M. Caskie, S. R. Green, M. Docherty and A. C. Hodds, “Most Successful Batch Application of Surfactant in North Sea Gas Wells,” in *Offshore Europe*, Aberdeen, Scotland, 2007.

[81] W. Jelinek and L. L. Schramm, “Improved Production From Mature Gas Wells by Introducing Surfactants Into Wells,” in *International Petroleum Technology Conference*, Doha, Qatar, 2005.

[82] S. Campbell, S. Ramachandran and K. Bartrip, “Corrosion Inhibition/Foamer Combination Treatment to Enhance Gas Production,” in *SPE Production and Operations Symposium*, Oklahoma City, Oklahoma, 2001.

[83] H. Li, D. Yang and Q. Zhang, “A Theoretical Model for Optimizing Surfactant Usage in a Gas Well Dewatering Process,” in *Canadian International Petroleum Conference*, Calgary, Alberta, 2007.

[84] J. Yang and S. Siddiqui, “The Use Of Foam To Improve Liquid Lifting From Low-Pressure Gas Wells,” in *Technical Meeting / Petroleum Conference of The South Saskatchewan Sectio*, Regina, 1999.

[85] A. T. Van Nimwegen, L. M. Portela and R. A. W. M. Henkes, “A first look at the hydrodynamics of air-water-foam flow,” in *8th North American Conference on Multiphase Technology*, Banff, Alberta, 2012.

[86] A. Ajani, M. Kelkar, S. Cem and E. Pereyra, “Foam flow in vertical gas wells under liquid loading: Critical velocity and pressure drop prediction,” *International Journal of Multiphase Flow,* pp. 124-135, 2016.

[87] D. Barenea, “Transition from annular flow and from dispersed bubble flow - unified models for the whole range of pipe inclinations,” *International Journal of Multiphase Flow,* pp. 733-744, September-October 1986.

[88] A. A. Ajani, Experimental study and modeling of effect of surfactants on liquid loading in vertical pipes, Tulsa, Oklahoma: The University of Tulsa, 2014.

[89] S. D. Listiak and D. H. Philips, “Plunger Lift,” in *Petroleum Engineering Handbook, Volume IV: Production Operations Engineering*, Richardson, Texas, Society of Petroleum Engineers, 2007, pp. 839-885.

[90] C. M. Beeson, D. G. Knox and J. H. Stoddard, “Part 1: The Plunger Lift Method of Oil Production, Part 2: Constructing Nomographs to Simplify Calculations, Part 3: How to Use Nomographs to Estimate Performance, Part 4: Examples Demonstrate Use of Nomographs, Part 5: Well Selection and Applications,” *Petroleum Engineer,* 1957.

[91] Otis, *Plunger Lift Technical Manual,* 1991.

[92] J. F. Lea, “Plunger Lift Versus Velocity Strings,” *Journal of energy resources technology,* vol. 121, no. 4, pp. 234-240, 1999.

[93] L. N. Mower and J. F. Lea, “Defining the Characteristics and Performance of Gas-Lift Plungers,” in *SPE Annual Technical Conference and Exhibition*, Las Vegas, Nevada, 1985.

[94] D. Philips and S. Listiak, “How to optimize production from plunger lift systems,” *World oil,* pp. 110-116, 4 1998.

[95] J. McCoy and L. Rowlan, “Plunger-Lift Optimization by Monitoring and Analyzing Well High Frequency Acoustic Signals, Tubing Pressure and Casing Pressure,” in *SPE Rocky Mountain Petroleum Technology Conference*, May, Keystone, Colorado, 2001.

[96] L. O. Rowlan and J. N. McCoy, “Optimizing Plunger Lifted Wells By Acoustically Tracing The Plunger Fall,” in *48th Annual Southwestern Petroleum Short Course*, Lubbock, Texas, 2001.

[97] J. D. Hacksma, “Users guide to predict plunger lift performance,” in *Proceedings, Southwestern Petroleum Short Course*, Lubbock, Texas, 1972.

[98] S. J. Morrow and J. R. Rogers, “Increasing Production Using Microprocessors and Tracking Plunger-Lift Velocity,” in *SPE Mid-Continent Gas Symposium*, Amarillo, Texas, 1992.

[99] D. L. Foss and R. B. Gaul, “Plunger-life Performance Criteria with Operating Experience-Ventura Avenue Field,” in *Drilling and Production Practice*, New York, New York, 1965.

[100] J. F. Lea, “Dynamic Analysis of Plunger Lift Operations,” *Journal of Petroleum Technology,* vol. 34, no. 11, pp. 2617-2629, 1982 November 1982.

[101] L. N. Mower, J. F. Lea, E. Beauregard and P. L. Ferguson, “Defining the Characteristics and Performance of Gas-Lift Plungers,” in *SPE Annual Technical Conference and Exhibition*, Las Vegas, Nevada, 1985.

[102] B. A. Abercrombie, “Plunger Lift,” in *Technology of Artificial Lift Methods*, vol. 2b, Tulsa, Oklahoma, Petroleum Publishing Co., 1980, pp. 486-507.

[103] L. Rosina, “A Study of Plunger Lift Dynamics,” The University of Tulsa, Tulsa, Oklahoma, 1983.

[104] L. Marcano and J. Chacin, “Mechanistic Design of Conventional Plunger Lift Installations,” *SPE Advanced Technology Series,* pp. 15-24, March 1994.

[105] J. O. A. Baruzzi and F. J. S. Alhanati, “Optimum Plunger Lift Operation,” in *SPE Production Operations Symposium*, Oklahoma City, Oklahoma, 1995.

[106] S. Gasbarri and M. L. Wiggins, “A Dynamic Plunger Lift Model for Gas Wells,” in *SPE Production Operations Symposium*, Oklahoma City, Oklahoma, 1997.

[107] G. M. Hashmi, A. R. Hasan and C. S. Kabir, “Design of Plunger Lift for Gas Wells,” in *SPE North America Artificial Lift Conference and Exihibition*, The Woodlands, Texas, 2016.

[108] Artificial Lift R & D Council, “ALRDC Guidlines & Recommended Practices - Selection of Artificial Lift Systems for Deliquiying Gas Wells,” 2018. [Online]. Available: http://www.alrdc.com/recommendations/Gas%20Well%20Deliquification/New%20Documents%20in%202015/Section%204.1%20Tubing%20Plungers.docx. [Accessed 12 03 2018].

[109] Petroleum Experts Limited, “User Manual for Prosper Version 14,” 2016.

[110] Akadem Petroleum Technology Inc., “wiki.pengtools.com,” 2017. [Online]. Available: https://wiki.pengtools.com/index.php?title=Gray_correlation. [Accessed 1 04 2018].

[111] H. E. Gray, “Flowing Pressure calculations for Gas/Condensate Wells - EPR Report 855,” Shell Oil Corporation, 1955.

[112] R. P. Sutton, S. A. Cox, J. F. Lea and O. L. Rowlan, “Guidelines for the Proper Application of Critical Velocity Calculations,” in *SPE Production and Operations Symposium*, Oklahoma City, Oklahoma, 2010.

[113] G. G. Brown, D. L. Katz, G. G. Oberfell and R. C. Alden, “Natural gasoline and the volatile hydrocarbons,” *Natural Gasoline Association of America,* 1948.

[114] M. B. Standing, Volumetric and Phase Behavior of Oil Field Hydrocarbon Systems, Richardson, Texas: Society of Petroleum Engineers, 1977.

[115] A. Tarek, Equations of State and PVT Analysis, Houston, Texas: Gulf Publishing Company, 2013.

[116] J. Papay, “A Termelestechnologiai Parameterek Valtozasa a Gazelepk Muvelese Soran,” *OGIL MUSZ,* pp. 267-273, 1985.

[117] M. B. Standing and D. L. Katz, “Density of Natural Gases,” *Transactions of the AIME,* pp. 140-149.

[118] K. R. Hall and L. Yarborough, “A new equation of state for Z-factor calculations,” *Oil and Gas Journal,* pp. 82-92, 18 June 1973.

[119] J. R. Dempsey, “Computer Routine Treats Gas Viscosity as a Variable,” *Oil and Gas Journal,* pp. 141-143, 16 August 1965.

[120] A. L. Lee, M. H. Gonzalez and B. E. Eakin, “The Viscosity of Natural Gases,” *Journal of Petroleum Technology,* pp. 997-1000, August 1966.

[121] O. Glaso, “Generalized Pressure-Volume-Temperature Correlations,” *Journal of Petroleum Technology,* pp. 785-795, Mai 1980.

[122] M. Vazquez and H. D. Beggs, “Correlations for Fluid Physical Property Prediction,” in *SPE Annual Fall Technical Conference and Exhibition*, Denver, Colorado, 1977.

[123] G. H. Abdul-Majeed and N. B. Abu Al-Soof, “Estimation of gas-oil surface tension,” *Journal of Petroleum Science and Engineering,* pp. 197-200, September 200.

[124] A. M. Rowe and J. C. S. Chou, “Pressure-volume-temperature-concentration relation of aqueous sodium chloride solutions,” *J. Chem. Eng.,* pp. 61-66, January 1970.

[125] C. H. Whitson and M. R. Brulé, Phase behavior, Richardson, Texas: Society of Petroleum Engineers, 2000.

[126] J. H. Kestin, R. J. Correia and E. Khalifa, “Tables of the dynamic and kinematic viscosity of aqueous NaCl solutions in the temperature range 20-150°C and the pressure range 0.1-35 MPa,” *Journal of physical and chemical reference data,* pp. 71-88, 1981.

[127] R. P. Sutton, “An Improved Model for Water-Hydrocarbon Surface Tension at Reservoir Conditions,” in *SPE Annual Technical Conference and Exhibition*, New Orleans, Louisiana, 2009.

Appendices

Physical properties of fluids

To estimate any kind of pressure loss, naturally, it is necessary to estimate a multitude of physical properties at in situ pressure and temperature. Although fully compositional models exist, it is customary in the oil industry to use empirical correlations usually called black oil- or PVT correlations.

Critical and reduced gas properties

Since the exact composition is often unknown an estimation of the critical properties is given with **eq. 132** and **133** as a function of the gas gravity. In fact gas is a multicomponent mixture thus the critical properties are usually referred to as pseudo-critical properties.

$$T_{pc} = \frac{5}{9}\left(168 + 325\,\gamma_g - 12.5{\gamma_g}^2\right) \qquad (132)$$

$$p_{pc} = 6894.76\left(677 + 15.0\,\gamma_g - 37.5{\gamma_g}^2\right) \qquad (133)$$

T_{pc} pseudo critical temperature [K]
p_{pc} pseudo critical pressure [Pa]
γ_g specific gas gravity (relative to air = 1) [-]

Eq. 132 and **133** are based on graphical correlations developed by Brown et al. [113]. It was expressed in mathematical form by Standing [114] but converted to metric units by the author.

The term reduced pressure or temperature refers to pressure or temperature conditions that were normalized by the critical properties. Because oil field gases are mixtures also here they are referred to as pseudo reduced conditions. [115, p. 142]

$$T_{pr} = \frac{T}{T_{pc}} \qquad (134)$$

$$p_{pr} = \frac{p}{p_{pc}} \qquad (135)$$

T actual temperature [K]
p actual pressure [Pa]
T_{pr} pseudo reduced temperature [-]
p_{pr} pseudo reduced pressure [-]

It is important to recognize that (pseudo) critical properties are properties of the fluid and (pseudo) reduced conditions are the surrounding conditions of the gas.

Real gas factor (z-factor)

The real gas-, compressibility- or just z-factor is defined as the ratio of a real gas' volume to the volume of an ideal gas at the same pressure and temperature conditions, compare **eq. 136**. Since real gas- and ideal gas volume are functions of pressure and temperature also the z-factor is a function of pressure and temperature. [115, p. 142]

$$z(p,T) = \frac{V_{real}(p,T)}{V_{ideal}(p,T)} \qquad (136)$$

z z-factor [-]
V_{real} real gas volume [m³]
V_{ideal} volume of an ideal gas at same conditions [m³]

Using the z-factor the ideal gas law can be easily modified to be a real gas law, **eq. 137**. [115, p. 141]

$$pV = nRTz \qquad (137)$$

p pressure [Pa]
V volume [m³]
n amount of substance [mol]
T temperature [K]
R universal gas constant, 8.3144598 [J/(mol K)]

Papay [116] proposed a simple, explicit expression to estimate the z-factor with **eq. 138**.

$$z = 1 - \frac{5.53 p_{pr}}{10^{0.9813 T_{pr}}} + \frac{0.274 {p_{pr}}^2}{10^{0.8157 T_{pr}}} \qquad (138)$$

A more accurate mathematical representation of the original graphical Standing-Katz [117] correlations was presented by Hall and Yarborough [118] and is shown in **eq. 139-145**.

$$z = \left(\frac{0.06125 t\, p_{pr}}{Y}\right) e^{\left(-1.2(1-t)^2\right)} \qquad (139)$$

$$t = \frac{1}{T_{pr}} \qquad (140)$$

t inverse of the reduced temperature [-]
Y reduced density [-]

$$F(Y) = 0 = a_0 + \frac{Y + Y^2 + Y^3 - Y^4}{1-Y} - a_1 Y^2 + a_2 Y^{a_3} \qquad (141)$$

$$a_0 = -0.06125 p_{pr} t e^{-1.2(1-t)^2} \qquad (142)$$

$$a_1 = 14.76t - 9.76t^2 + 4.58t^3 \qquad (143)$$

$$a_2 = 90.7t - 242.2t^2 + 42.4t^3 \qquad (144)$$

$$a_3 = 2.18 + 2.82t \qquad (145)$$

The reduced density (Y) is defined with eq. 141 as a nonlinear, implicit function. Therefore, a numerical, iterative solution method should be used. The Newton-Raphson technique yields fast results reliably. The iteration step is defined in **eq. 146**, with **eq. 147** being the first derivative of **eq. 141** and **eq. 148** gives a good guess for the initial starting value. An acceptable preset error tolerance could be 10^{-12}. [115, p. 156]

$$Y^{k+1} = Y^k - \frac{F(Y^k)}{\acute{F}(Y^k)} \qquad (146)$$

$$\acute{F}(Y) = \frac{1+4Y+4Y^2-4Y^3+Y^4}{(1-Y)^4} - 2a_1 Y + a_2 a_3 Y^{a_3-1} \qquad (147)$$

$$Y^{k=0} = 0.0125 p_{pr} t e^{-1.2(1-t)^2} \qquad (148)$$

k number of iteration step [-]

Gas density

Once the z factor for the specific conditions has been found, the gas density can be calculated directly. **Eq. 137** can be transformed into **eq. 149** using the definition of molecular weight. Rearranging and separating the definition of density yields **eq. 150**. [115, p. 144] The apparent molecular weight (M_a) is another mixture property and is calculated as the mole-fraction-weighted average of the gas components' molecular weights.

$$pV = \left(\frac{m}{0.001 M_a}\right) RTz \qquad (149)$$

$$\rho_g = \frac{V}{m} = \frac{pM_a}{zRT} \qquad (150)$$

M_a apparent molecular weight [g/mol]
ρ_g density [kg/m³]

Gas specific gravity

In the oil and gas industry, the characteristics of a gas are specified using the specific gas gravity, which is the gas density relative to the density of air, both at standard conditions. Using **eq. 150** this results in the ratio of apparent molecular weights, **eq. 151**. [115, p. 139]

$$\gamma_g = \frac{\rho_{g,sc}}{\rho_{air,sc}} = \frac{\frac{p_{sc} M_a}{zRT_{sc}}}{\frac{p_{sc} M_{air}}{zRT_{sc}}} = \frac{M_a}{M_{air}} \qquad (151)$$

M_a apparent molecular weight of air, 28.96 [g/mol]
T_{sc} standard temperature, 288.71 [K]
p_{sc} standard pressure, 101353 [Pa]

Gas viscosity

The dynamic viscosity of a gas is generally a function of pressure, temperature, and specific gas gravity. Standing proposed a mathematical expression to estimate the gas viscosity at a specified temperature and standard pressure. It was adapted to metric units by the author and is presented in **eq. 152**. Corrections for impurities were also developed but not used in the work for this thesis.

$$\mu_{s.p.} = \left(8.118\ 10^{-3} - 6.15\ 10^{3} \log \gamma_g + \left(1.709\ 10^{-5} - 2.062\ 10^{-6}\gamma_g\right)\left(T\,\tfrac{9}{5} - 460\right)\right) 0.001 \qquad (152)$$

$\mu_{s.p.}$ dynamic gas viscosity at standard pressure [Pa s]

Dempsey expressed the ratio of gas viscosity at standard pressure to the gas viscosity at specified pressure with **eq. 153**. The necessary plethora of coefficients is listed in Table 10.

$$\ln\left(T_{pr}\frac{\mu_g}{\mu_{s.p.}}\right) = a_0 + a_1 p_{pr} + a_2 {p_{pr}}^3 + T_{pr}\left(a_1 + a_5 p_{pr} + a_6 {p_{pr}}^2 + a_7 {p_{pr}}^3\right) + {T_{pr}}^2\left(a_8 + a_9 p_{pr} + a_{10} {p_{pr}}^2 + a_{11} {p_{pr}}^3\right) + {T_{pr}}^3\left(a_{12} + a_{13} p_{pr} + a_{14} {p_{pr}}^2 + a_{15} {p_{pr}}^3\right) \qquad (153)$$

μ_g dynamic gas viscosity [Pa s]

Table 10: Coefficients for the Dempsey correlation [119]

a_0	–2.46211820	a_8	–7.93385648(10^{-1})
a_1	2.970547414	a_9	1.39643306
a_2	–2.86264054(10^{-1})	a_{10}	–1.49144925(10^{-1})
a_3	8.05420522(10^{-3})	a_{11}	4.41015512(10^{-3})
a_4	2.80860949	a_{12}	8.39387178(10^{-2})
a_5	–3.49803305	a_{13}	–1.86408848(10^{-1})
a_6	3.60373020(10^{-1})	a_{14}	2.03367881(10^{-2})
a_7	–1.044324(10^{-2})	a_{15}	–6.09579263(10^{-4})

Alternatively, a very popular gas viscosity correlation was presented by Lee, Gonzalez, and Eakin in 1966. The correlation was adapted to the metric system and is given by **eq. 154 - 157**. It is important to note that it doesn't hold for sour gases. [120]

$$\mu_g = 10^{-4} K\ exp\left[X\left(\frac{\rho_g(p,T)16.0185}{62.4}\right)^{Y}\right] \qquad (154)$$

$$K = \frac{(9.4+0.02M_a)\left(T\frac{9}{5}\right)^{1.5}}{209+19M_a+T\frac{9}{5}} \qquad (155)$$

$$X = 3.5 + \frac{986}{T\frac{9}{5}} + 0.01M_a \qquad (156)$$

$$Y = 2.4 - 0.2X \qquad (157)$$

$\rho_g(p,T)$ gas density at actual conditions [kg/m³]

API oil gravity

The equivalent for the gas specific gravity is the oil specific gravity which relates density at standard conditions to the density of water, compare **eq. 158**. [115, p. 182]

$$\gamma_o = \frac{\rho_{o,sc}}{\rho_{w,sc}} \qquad (158)$$

γ_o oil specific gravity [-]
$\rho_{o,sc}$ density at standard conditions [kg/m³]
$\rho_{w,sc}$ water density at standard conditions, 999.55 [kg/m³]

Eq. 159 relates specific oil gravity with API gravity. [115, p. 182]

$$API = \frac{141.5}{\gamma_o} - 131.5 \qquad (159)$$

API oil API gravity [API]

Gas solubility

The gas solubility (R_s) expresses how much volume gas is dissolved in one volume of oil. It can be estimated by a correlation which was proposed by Glaso in 1980, was adapted to the metric system by the author and is presented in **eq. 160**-**161**. [121] The original publication stated that the correlation can be easily adapted for volatile oils, which is more appropriate for the purposes in this thesis, by adjusting the temperature exponent from 0.171 to 0.130, which results in **eq. 162**. [121, p. 792]

$$R_s = 0.1781\gamma_g \left(\frac{API^{0.989}}{\left(T\frac{9}{5} - 459.67\right)^{0.171}} 10^X \right)^{1.22549} \qquad (160)$$

$$X = 2.8869 - \left(14.1811 - 3.3093 \log \frac{p}{6894.76}\right)^{0.5} \qquad (161)$$

$$R_s = 0.1781\gamma_g \left(\frac{API^{0.989}}{\left(T\frac{9}{5} - 459.67\right)^{0.13}} 10^X \right)^{1.22549} \qquad (162)$$

R_s gas solubility [Sm³/Sm³]
γ_g specific gas gravity of the dissolved gas [-]
T actual temperature [K]
p actual pressure [Pa]

Oil formation volume factor

The oil formation volume factor relates surface volumes to downhole volumes. More specifically it is the ratio of the volume of oil at downhole conditions, including dissolved gas, to its volume at standard conditions, given in **eq. 163**. [115, p. 213]

$$B_o = \frac{V_{o,p,T}}{V_{o,sc}} \qquad (163)$$

B_o oil formation volume factor [m³/Sm³]
$V_{o,sc}$ volume of oil at standard conditions [Sm³]
$V_{o,p,T}$ volume of oil at actual conditions [m³]

Also, a formation volume factor correlation was developed by Glaso, which is presented in **eq. 164-166** converted to metric units. [121]

$$B_o = 1.0 + 10^A \qquad (164)$$

$$A = -6.58511 + 2.91329\log(B_{ob}^*) - 0.27683(\log B_{ob}^*)^2 \qquad (165)$$

$$B_{ob}^* = R_s\left(\frac{\gamma_g}{\gamma_o}\right)^{0.526} + 0.968\left(T\frac{9}{5} - 460\right) \qquad (166)$$

B_o oil formation volume factor [m³/Sm³] or [-]

Oil density

The oil density can be readily derived from the definition of the oil formation volume factor, **eq. 163**. The derivation is given with **eq. 168-170**. It also uses the definition of specific oil and gas gravities (**eq. 158** and **eq. 150**) and the fact that one mole of any gas has a volume of 0.023685 m³ at standard conditions.

$$B_o = \frac{V_{o,p,T}}{V_{o,sc}} = \frac{\frac{m_o + m_g}{\rho_o}}{V_{o,sc}} \qquad (167)$$

$$m_g = R_s\gamma_g\frac{M_a}{1000} * 0.023685 = R_s\gamma_g M_{air} * 0.023685 \qquad (168)$$

$$m_o = \rho_{w,sc}\,\gamma_o \qquad (169)$$

$$\rho_o = \frac{\rho_{w,sc}\,\gamma_o + R_s\gamma_g\frac{M_a}{1000} * 0.023685}{B_o} = \frac{999.55\gamma_o + R_s\gamma_g 0.00068592}{B_o} \qquad (170)$$

m_g mass of gas dissolved in one m³ of oil [kg]
m_o mass oil in one m³ of oil [kg]

Oil viscosity

Considering the viscosity of oil one has to differentiate between dead oil viscosity, saturated oil viscosity, and undersaturated oil viscosity. Dead oil viscosity (μ_{od}) is the viscosity of oil at standard conditions with no dissolved gas in it. Saturated oil viscosity (μ_{ob}) is the viscosity of oil at and below the bubble point and undersaturated viscosity is the one above the bubble point. [115, p. 237]

Glaso found a correlation for the dead oil viscosity, which is given with **eq. 171-172** converted to metric/SI units. [121]

$$\mu_{od} = 3.141 * 10^{10} \left(T\frac{9}{5} - 460\right)^{-3.444} (\log API)^A \, 0.001 \qquad (171)$$

$$A = 10.313 \log\left(T\frac{9}{5} - 460\right) - 36.447 \qquad (172)$$

μ_{od} dead oil viscosity [Pa s]

A correlation for the saturated oil viscosity was found by Vazquez and Beggs, which was also adapted to metric/SI units and is given with **eq. 173-175**. [122]

$$\mu_o = a(\mu_{od} * 1000)^b \qquad (173)$$

$$a = 10.715(R_s 5.6146 + 100)^{-0.515} \qquad (174)$$

$$b = 5.44(R_s 5.6146 + 150)^{-0.338} \qquad (175)$$

μ_o saturated oil viscosity [Pa s]

Oil-gas interfacial tension

The oil-gas interfacial tension (IFT) also referred to as oil surface tension can be estimated by a model developed by Abdul-Majeed and Abu Al-Soof. A version of the model adapted to the metric/SI system is presented in **eq. 176-177**. Similarly to viscosity, there is a dead oil-gas IFT (σ_{od}), which is at standard conditions without dissolved gas and a live oil-gas IFT (σ_o) for oil with dissolved gas. [123]

$$\sigma_{od} = 0.001\left(1.17013 - 1.694 * 10^{-3}\left(T\frac{9}{5} + 460\right)\right)(38.085 - 0.259\gamma_{API}) \qquad (176)$$

$$\left(\frac{\sigma_o}{\sigma_{od}}\right) = 0.056379 + 0.94362e^{\left(-3.8491*10^{-3}R_s 5.6146\right)} \qquad (177)$$

σ_{od} dead oil-gas interfacial tension [N/m]
σ_o live oil-gas interfacial tension [N/m]

Water density

Oil field waters are often brines, therefore their density is influenced by the salinity of the water. The water density at standard pressure, specified temperature and salinity can be estimated with **eq. 178-181** according to Rowe and Chou. [124]

$$\rho_{w,sp} = \frac{1000}{a_0 + a_1 w_s + a_2 {w_s}^2} \qquad (178)$$

$$a_0 = 0.91635 - 0.01035794T + 0.9270048 * 10^{-5} T^2 - \frac{1127.522}{T} + \frac{100674.1}{T^2} \qquad (179)$$

$$a_1 = -2.5166 + 0.0111766T - (0.170552 + 10^{-4})T^2 \qquad (180)$$

$$a_2 = 2.84851 - 0.0154305T + (0.223982 * 10^{-4})T^2 \qquad (181)$$

$\rho_{w,sp}$ water density at standard pressure and specified temperature [kg/m³]
w_s water salinity as a mass fraction [-]

The correction for pressure can be done via the formation volume factor presented in the following under *0 Water formation volume factor"* and the definition of the formation volume factor itself. It has to be noted that **eq. 182** neglects the effect of the dissolved gas.

$$\rho_w = \frac{\rho_{w,sc}}{B_w} \qquad (182)$$

$\rho_{w,sc}$ water density at standard pressure and temperature [kg/m³]
ρ_w water density at a specified pressure and temperature [kg/m³]
B_w water formation volume factor at a specified pressure and temperature [-]

Water formation volume factor

The formation volume factor is estimated at two steps. First, it is evaluated for the relevant temperature at standard pressure in **eq. 183** using the density estimation in **eq. 178**. Again the effect of gas dissolving into the water is ignored. Then it is corrected for the effect of compressibility and pressure with **eq. 184-186**. [125, pp. 153-154]

$$B_{w,sp} = \frac{\rho_{w,sc}}{\rho_{w,sp}} \qquad (183)$$

$$B_w = B_{w,sp}\left[1 + \frac{a_1}{a_0}\left(\frac{p}{6894.76}\right)\right]^{1/a_1} \qquad (184)$$

$$a_0 = 10^6\left[0.314 + 0.58w_s + (1.9 * 10^{-4})\left(T\frac{9}{5} - 459.67\right) - (1.45 * 10^{-6})\left(T\frac{9}{5} - 459.67\right)^2\right] \qquad (185)$$

$$a_1 = 8 + 50w_s - 0.125w_s\left(T\frac{9}{5} - 459.67\right) \qquad (186)$$

$B_{w,sp}$ water formation volume factor at standard pressure and specified temperature [-]

Water viscosity

The viscosity of oilfield brine can be estimated with a set of correlations developed by Kestin et al. in 1981, presented in **eq. 187-192**. [126] The set of necessary coefficients is listed in Table 11.

$$\mu_w = (1 + a_0 p)\mu_w^* \quad (187)$$

$$\log \frac{\mu_w^*}{\mu_w^0} = a_1 + a_2 \log \frac{\mu_w^0}{\mu_{w20}^0} \quad (188)$$

$$a_0 = 10^{-3}[0.8 + 0.01(T - 273.15 - 90)e^{-0.25 c_{sw}}] \quad (189)$$

$$a_1 = \sum_{i=1}^{3} b_{1i}(c_{sw})^i \quad (190)$$

$$a_2 = \sum_{i=1}^{3} b_{2i}(c_{sw})^i \quad (191)$$

$$\log \frac{\mu_w^0}{\mu_{w20}^0} = \sum_{i=1}^{4} b_{3i} \frac{(20 - T + 273.15)^i}{96 + T - 273.15} \quad (192)$$

μ_w water viscosity at a specified pressure and temperature [Pa s]
c_{sw} water salt molality [mol/kg]

Table 11: Coefficients for the Kestin et al correlation [126]

b_{11}	3.324(10^{-2})	b_{21}	-3.96(10^{-2})
b_{12}	3.624(10^{-3})	b_{22}	1.02(10^{-2})
b_{13}	-1.879(10^{-4})	b_{23}	-7.02(10^{-4})
b_{31}	1.2378	b_{33}	3.060(10^{-6})
b_{32}	1.303(10^{-3})	b_{34}	2.550(10^{-8})
μ_{w20}^0	1.002(10^{-3})		

The salt molality in water which is needed as input for the Kestin et al model is defined with **eq. 182**. For a brine only containing sodium chloride (NaCl) with a molar weight of 58.4 g/mol, it can be estimated via **eq. 194**. [125, p. 150]194

$$c_{sw} = \frac{n_s}{m_w} \quad (193)$$

$$c_{sw} = \frac{17.1}{\frac{1}{w_s} - 1} \quad (194)$$

n_s amount of salt dissolved in water[mol]
m_w mass of water in which the salt is dissolved in [kg]

Water-gas interfacial tension

The water-gas interfacial tension is also called water surface tension the correlation for fresh water is given with **eq. 195** was developed by Sutton. The correction for salinity is provided by **eq. 196-197**. [127]

$$\sigma_w^0 = 0.001\left[\frac{\left(1.53988\left(\frac{\rho w-\rho g}{1000}\right)+2.08339\right)}{\left(\frac{T\frac{9}{5}}{302.881}\right)^{0.821976-0.00183785*T\frac{9}{5}+1.34016*10^{-6}*\left(T\frac{9}{5}\right)^2}}\right] \quad (195)$$

$$\sigma_{corr} = 3.44 * 10^{-5} w_s * 1000 \quad (196)$$

$$\sigma_w = \sigma_w^0 + \sigma_{corr} \quad (197)$$

σ_w^0 interfacial tension of sweet water and gas [N/m]
σ_{corr} salinity correction term [N/m]
σ_w interfacial tension of brine and gas [N/m]